Doklady Physics, Vol. 45, No. 6, 2000, pp. 241–244. Translated from Doklady Akademii Nauk, Vol. 372, No. 4, 2000, pp. 469–472.

PHYSICS

Drop Model for Formation of the Polyacenequinone Domain Structure

N. V. Afanas'ev, L. V. Mukhaeva, A. A. Maksimov, Academician M. G. Voronkov, and T. G. Ermakov

Received January 21, 2000

Studying the process of the formation of polymer semiconductors by the method of dielectric spectroscopy has considerable significance for developing materials of molecular electronics with prescribed electrophysical properties, in particular, materials synthesized from conducting molecular chains [1, 2]. With this purpose, we used the model of grains–interlayers [3], which was modified with allowance for the spherical shape of grains. This modified model was applied to determine the thickness h of high-resistance surface layers for conducting molecular domains of polyacenequinones [4] on the basis of their dielectric-spectra parameters. The corresponding structure model of the polymer represents the close packing of identical cubes with ribs of length L in which two-layer spherical domains are inscribed. In this case, the low-resistance part of a domain is a sphere with the radius $R = L/2 - h$ [5]. The permittivity ε' of both this sphere and its environment in the cube is assumed to be identical and equal to $\varepsilon'_\infty = 4$, i.e., to the value of ε' for polyacenequinones at sufficiently high frequencies of the applied electric field.

For calculating the low-frequency limit ε'_S of the permittivity for the proposed structure model in the region of dispersion associated with the interlayer polarization [6] of conducting spheres, we consider two neighboring cubes with a common face. The conducting spheres 1 and 2 in these cubes have charges Q_1 and Q_2 and potentials U_1 and $U_2 = -U_1$. In this case, the charges can be expressed in terms of the potentials for the conducting spheres by the equation $Q_i = c_{ik}U_k$, where i, $k = 1, 2$; k is the summation index; and the capacitance coefficients c_{ik} [7] are the functions of the structure-model parameter $\gamma = h/R$:

$$c_{11} = c_{22} = 2C_0\sum_{n=0}^{\infty}\frac{\sinh[f(\gamma)]}{\sinh[(2n+1)f(\gamma)]}, \qquad (1)$$

$$c_{12} = c_{21} = -2C_0\sum_{n=0}^{\infty}\frac{\sinh[f(\gamma)]}{\sinh[2(n+1)f(\gamma)]}. \qquad (2)$$

Here, $C_0 = 2\pi\varepsilon_0\varepsilon'_\infty R$, $\varepsilon_0 = 8.85 \times 10^{-12}$ F/m, n are integers, and $f(\gamma)$ is expressed by the formula

$$f(\gamma) = \frac{1}{2}\mathrm{Arccosh}(1 + 4\gamma + 2\gamma^2). \qquad (3)$$

Ignoring the surface capacitance of the conducting spheres, which is associated with the stray field outside the cubes, we can express the relation between their static capacitance C_s and C_0 by the formula

$$\frac{C_s(\gamma)}{C_0} = \frac{Q_1}{2U_1C_0} = \frac{c_{11} - c_{12}}{2C_0} = F(\gamma). \qquad (4)$$

For $\gamma \geq 10$, according to formula (4) with allowance for (1)–(3), C_s and C_0 virtually coincide, and the permittivity of the structure model approaches its high-frequency value ε'_∞. By this reason, the relationship between ε'_s and ε'_∞ must be similar to (4):

$$\frac{\varepsilon'_s(\gamma)}{\varepsilon'_\infty} = F(\gamma) = \sum_{n=0}^{\infty}\frac{\sinh[f(\gamma)]}{\sinh[(n+1)f(\gamma)]}. \qquad (5)$$

For $\gamma \leq 0.1$, the function $F(\gamma)$ virtually coincides with the logarithmic asymptote

$$F(\gamma) = a - k\log\gamma, \qquad (6)$$

where $a = 2.2$ and $k = 1.1$.

The contribution of the polarization mechanism under consideration to the permittivity of the polymer for the proposed model 1 is expressed by the formula

$$\frac{\Delta\varepsilon'}{\varepsilon'_\infty} = F(\gamma_1) - 1 = b - k\log\gamma_1. \qquad (7)$$

Here, $\Delta\varepsilon' = \varepsilon'_s - \varepsilon'_\infty$ is the increment of permittivity within the dispersion region and $b = 1.2$. In this case,

Irkutsk State University,
ul. Lermontova 126, Irkutsk, 664033 Russia
Institute of Organic Chemistry,
Siberian Division, Russian Academy of Sciences,
ul. Favorskogo 1, Irkutsk, 664033 Russia

1028-3358/00/4506-0241$20.00

Parameters of dielectric spectra and structure models for polyacenequinones.

Polymer	σ_0, 10^{-5} S m^{-1}	$\Delta\varepsilon'$	ε''_M	τ_p, 10^{-8} s	α	γ_2, 10^{-2}	γ_4, 10^{-2}
55JTK(2)	200	10	2.8	8	0.65	–	6.6
55JTK(3)	700	10	2.8	1.8	0.65	–	6.6
55JTK(5)	600	28	7.8	3.2	0.65	14	–
76EHE(3)	70	13	3.3	10	0.6	–	1.4
76EHE(5)	5	32	7.8	280	0.55	12	–
76EHE(8)	500	30	7.6	5.3	0.6	13	–
76EHE(10)	27	50	12	500	0.55	8	–
76EHE(20)	710	80	17		0.5	5	–
76EHE(24*)	2	27	5.3	1000	0.47	14	–

Note: σ_0 is the specific conductivity for the direct current. The 76EHE(24*) polymer is obtained with an interruption in the course of synthesis.

the values of the volume concentration for the conducting phase

$$v_1 = \frac{\pi}{6(1+\gamma_1)^3} \tag{8}$$

are assumed to be reasonably high: $\gamma_1 \longrightarrow 0$, $v_1 \longrightarrow \pi/6$.

A similar contribution for the grain–interlayer model [3] (model 2) can be calculated from the generalized Lorenz–Lorentz formula [8]:

$$\frac{\Delta\varepsilon'}{\varepsilon'_\infty} = \frac{v}{(1-v)N}. \tag{9}$$

Here, $0 \le N \le 1$ is the coefficient of the grain depolarization, which is equal to 1 for the extremely compressed conducting spheroids (or the close-packed two-layer cubes [3]) perpendicular to the applied electric field, while the volume concentration of the conducting phase is expressed by the relationship

$$v_2 = 1 - \frac{2h_2}{L} = \frac{1}{1+\gamma_2}, \tag{10}$$

where $\gamma_2 = \dfrac{2h_2}{L-2h_2}$. With decreasing thickness of insulating interlayers in such cubes ($h_2 \longrightarrow 0$, $v_2 \longrightarrow 1$), the increment of the permittivity for this model as $\Delta\varepsilon' \longrightarrow \infty$ is

$$\frac{\Delta\varepsilon'}{\varepsilon'_\infty} = \frac{v_2}{1-v_2} = \frac{1}{\gamma_2}. \tag{11}$$

For the structure model of the close-packed two-layer spheres, $\Delta\varepsilon'$ is calculated from formula (9) for $N = 1/3$ (model 3). In this case, the maximum value for the volume concentration v_3 of the conducting phase corresponding to $\gamma_3 = 0$ is 0.637.

In the proposed structure model of the close-packed cubes, the two-layer spheres form a cubic lattice. To fulfill the condition $v \longrightarrow 1$ as $\Delta\varepsilon' \longrightarrow \infty$, which is characteristic of the grain–interlayer model [3], we can determine the volume concentration of the conducting phase without taking into account the dielectric matrix outside these spheres:

$$v_0 = \frac{V_1}{V_1+V_2} = \frac{1}{(1+\gamma)^3} \approx \frac{1}{1+3\gamma}. \tag{12}$$

Here, V is the volume, and the subscripts 1 and 2 are referred to the conducting volume of the sphere and to the near-surface high-resistance layer, respectively. In this case, in the proposed variant of the model of spherical grains–interlayers (model 4), the following expression for $\Delta\varepsilon'$ follows from formula (7) with allowance for (12):

$$\frac{\Delta\varepsilon'}{\varepsilon'_\infty} = b + k\log\frac{3v_0}{1-v_0} = b + k\log\frac{1}{\gamma_4}. \tag{13}$$

The corresponding expression related to the model of two-layer spheres (model 5) follows from formula (9) for $N = 1/3$:

$$\frac{\Delta\varepsilon'}{\varepsilon'_\infty} = \frac{3v_0}{1-v_0} = \frac{1}{\gamma_5}. \tag{14}$$

In an alternating electric field with the circular frequency ω, the permittivity ε' and the loss factor ε'' for polyacenequinones within the radio-frequency range and in the absence of the barrier polarization mechanisms are described by the Debye equation [8]:

$$\varepsilon'(\omega) - j\varepsilon''(\omega) = \varepsilon'_\infty + \frac{\Delta\varepsilon'}{1+(j\omega\tau_p)^\alpha}. \tag{15}$$

Here, j is the imaginary unit, τ_p is the most probable value of the relaxation time τ in the statistical distribution being explained by the distribution of domains over the conductivity, and α ($0 \le \alpha \le 1$) is the parameter of this distribution.

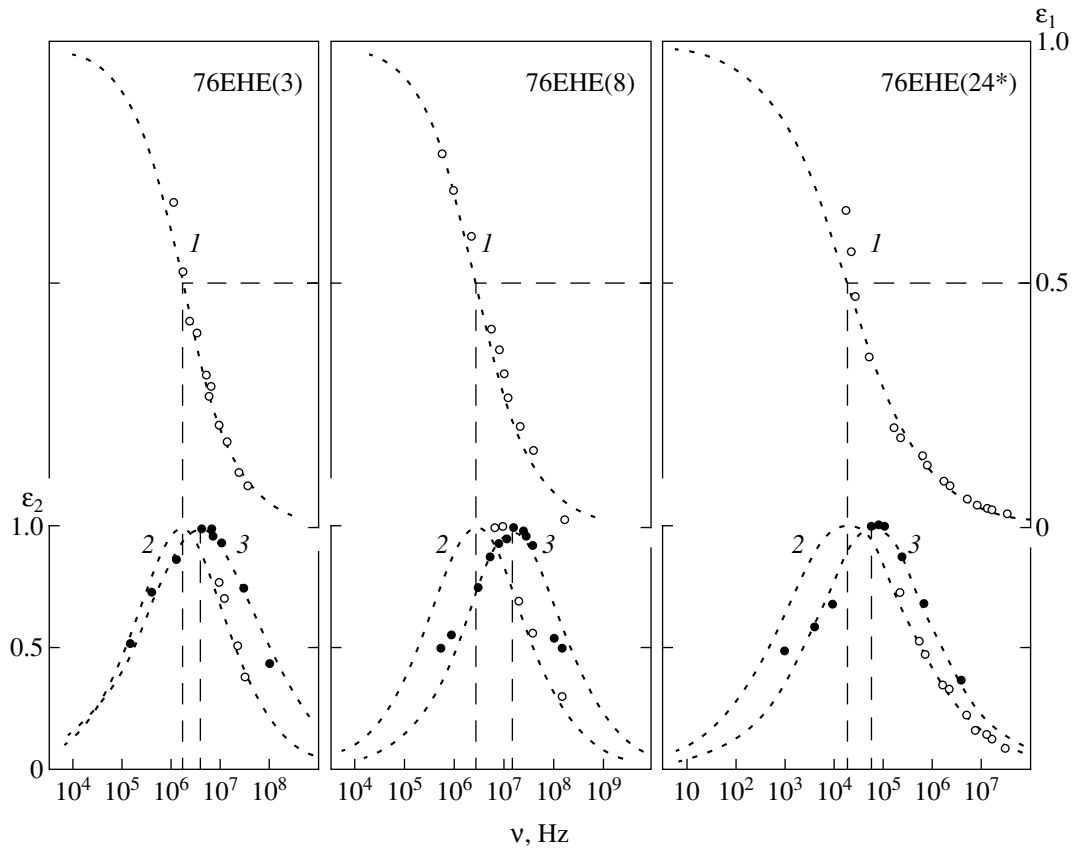

Dispersion plots for 76EHE(3), 76EHE(8), and 76EHE(24*) polyacenequinones: (*1*) ε_1; (*2*) ε_2. The sample diameter and thickness are 2.5 and 0.1 mm, respectively [11]. (*3*) ε_2 for the mixture of a polymer with paraffin for the polymer volume concentration of 0.1 [5] and $\varepsilon_M = 0.1$. Temperature is 293 K.

76EHE and 55JTK polyacenequinones on the basis of pyrene and dianhydride of pyromellitic acid, as well as of pyrene and 2-chlorbenzoic acid, respectively, were obtained according to the well-known method [9] of polycyclic condensation at 306°C in the presence of zinc chloride with the ratio 1 : 1 : 2 between the initial reactants. The duration of the reaction, which varied within the limits from 2 to 20 hours, is indicated in the parentheses near the name of a polymer in the notation of [9] (see table).

Parameters of dielectric spectra for the investigated polyacenequinones are determined by the method of dispersion plots [10] with allowance for the assumed spherical shape of domains [5]. In Fig. 1, we display the frequency dependences for reduced values of permittivity $\varepsilon_1 = \dfrac{\varepsilon' - \varepsilon'_\infty}{\Delta\varepsilon'}$ and the loss factor $\varepsilon_2 = \dfrac{\varepsilon''}{\varepsilon''_M}$, where ε''_M is the maximum of ε'' in the dispersion region.

The values of the parameter γ are also presented in the table. When estimating the thickness of surface layers in domains of size $L \le 1$ μm [11], model 5 admits $h \le 20$ nm for the largest observed values of $\Delta\varepsilon'$ on the order of 100. However, this model does not take into account mutual capacitance of neighboring conducting domains. The better substantiated model 4 makes it possible to explain only values of $\Delta\varepsilon'$ lower than in model 5 by an order of magnitude (see table) due to a low mutual capacitance of the neighboring spherical conductors. In this case, according to formula (13), the magnitude of h does not exceed 30 nm. For $\Delta\varepsilon' \gg 10$, better results are given by model 2 of close-packed conducting cubes separated by insulating interlayers (see table). For substantiating its applicability, it is possible to assume that the deformation of spherical domains in the region of their contacts with neighboring ones increases the mutual capacitance of conducting regions. In this case, we can expect an increase in the depolarization coefficient of domains from one-third for the conducting spheres to unity for conducting cubes. In principle, this fact admits experimental verification provided that the accuracy of measuring parameters for the dielectric spectra is improved.

In the case of determining $\Delta\varepsilon'$ by the method of the domain-pseudoisolation effect [5], the order of magnitude for the result obtained is independent of the depolarization coefficient when it varies in the above-indicated limits. Therefore, for estimating the parameter γ_2

according to formula (11), we used the values of $\Delta\varepsilon'$ corresponding to $N \approx 0.3$ [5] (see table).

We have assumed that the deformation of domains corresponding to the increase in N proceeds in the liquid state of the reacting mixture and is conserved after its solidification. An original drop of monomers is probably formed by means of a spontaneous dispersing in the melt of pyrene and dianhydride of pyromellitic acid and acquires the spherical shape owing to the surface tension in the liquid dispersion medium [13; 14, p. 162]. The cause of the domain deformation can be an increase in their volume concentration in the dispersion liquid. Such a mechanism for the formation of polymer semiconductors represents an interest for molecular electronics as a controlled method for fabricating molecular and submolecular heterogeneities at the microstructure and nanostructure levels.

The investigation carried out testifies to the possibility of using dielectric spectroscopy for studying the formation processes of polymeric semiconductors.

REFERENCES

1. K. A. Valiev, *Microelectronics: Achievements and Ways for Progress* (Nauka, Moscow, 1986).
2. J.-M. Lehn, Angew. Chem. **29**, 1304 (1990).
3. C. G. Koops, Phys. Rev. **83**, 121 (1951).
4. N. V. Afanas'ev, L. V. Mukhaeva, M. G. Voronkov, and T. G. Ermakova, Dokl. Akad. Nauk SSSR **323**, 452 (1992) [Sov. Phys.–Dokl. **37**, 135 (1992)].
5. N. V. Afanas'ev, L. V. Mukhaeva, L. Ya. Tsarik, *et al.*, Dokl. Akad. Nauk **367**, 179 (1999) [Dokl. Phys. **44**, 413 (1999)].
6. *Dielectrics. Handbook for Recommended Terms*, Ed. by B.M. Tareev (Akad. Nauk SSSR, Moscow, 1961).
7. N. N. Mirolyubov, M. V. Kostenko, M. L. Levinshteĭn, and N. N. Tikhodeev, *Methods for Calculation of Electrostatic Fields* (Vysshaya Shkola, Moscow, 1963).
8. A. V. Netushil, B. Ya. Zhukhovitskiĭ, V. N. Kudin, and E. P. Parini, *High-Frequency Heating of Dielectrics and Semiconductors* (Gosénergoizdat, Moscow, 1959).
9. H. A. Pohl and R. P. Chartoff, J. Polym. Sci. A **2**, 2787 (1964).
10. N. V. Afanas'ev, L. V. Mukhaeva, M. G. Voronkov, and T. G. Ermakova, Dokl. Akad. Nauk SSSR **319**, 858 (1991) [Sov. Phys.–Dokl. **36**, 580 (1991)].
11. N. V. Afanas'ev, L. N. Omel'chenko, L. V. Mukhaeva, *et al.*, Dokl. Akad. Nauk SSSR **289**, 596 (1986) [Sov. Phys.–Dokl. **31**, 572 (1986)].
12. N. V. Afanas'ev, L. V. Mukhaeva, M. G. Voronkov, and T. G. Ermakova, Dokl. Akad. Nauk **330**, 177 (1993) [Phys.–Dokl. **38**, 205 (1993)].
13. S. S. Medvedev, in *Kinetics and Mechanism of Formation and Transformation of Macromolecules* (Nauka, Moscow, 1968), pp. 5–24.
14. *Emulsion Polymerization and Its Industrial Application*, Ed. by V. I. Eliseeva, S. S. Ivanchev, S. I. Kuchanov, and A. V. Lebedev (Khimiya, Moscow, 1976).

Translated by V. Bukhanov

Doklady Physics, Vol. 45, No. 6, 2000, pp. 245–247. Translated from Doklady Akademii Nauk, Vol. 372, No. 4, 2000, pp. 473–475.

PHYSICS

A Model of a Crack in the Vicinity of Phase Transition

Chin' Van Khoa

Presented by Academician E.I. Shemyakin January 21, 2000

Received June 22, 1999

1. The block structure of a material arising in the course of its fracture was discussed in [1]. This problem can be formulated in the following way.

Let us consider a medium with particles x_i. Under loading, it transforms into a new structural state with blocks X_i. If $H(\alpha, \beta, e)$ and $H'(\alpha', \beta', e')$ are free energies of the initial and final states, respectively, the transition can be represented as the following transformation:

$$H(\alpha, \beta, e) \longrightarrow H'(\alpha', \beta', e').$$

Here, α and β are the coefficients of elasticity and e and e' are the strains corresponding to particles x_i and blocks X_i, respectively. The block state, referred to as the fracture state, is completely defined by coefficients α' and β'.

On the other hand, a local phase transition is observed in the vicinity of a crack tip. In ZrO_2, for example, the local phase transition manifests itself in the anomaly of the crack propagation rate [2]. Local phase transitions were also observed in the course of the hot pressing of boron nitride [3], at the surfaces of pores, and during the thermal fracture of diamonds [4]. Thus, the state close to fracture can be considered as that of the state of phase transition or the critical state. Based on an analogy between the (σ, e) diagrams and (P, V) or (P, ρ) diagrams, the authors of [5–8] analyzed the critical state of a strained medium. In this paper, we follow the same concept and use the renormalization group technique to determine coefficients α' and β' in the fracture state. These coefficients are assumed to depend on α and β according to the model discussed in [9]. Then, we derive the equation of the fracture surface in the parametric μ-space. This means that the criterion of fracture corresponds here to a surface in the parameter space.

2. Let us consider a close vicinity of the crack tip in an elastic medium. The free energy in this domain can be written in the momentum representation

$$F = \frac{1}{2}\lambda_{iklm}a_{iklm}\sum_p e_{ik}^2(p) - \frac{1}{2}\sum_p \rho p^2 e_{ik}^2(p)$$

$$+ \frac{1}{4}\beta_{iklm}^2 a_{iklm}^2 (e_{ik}(p))^4 + \sum_p e_{ik}(p)\sigma_{ik}.$$

We assume, of course, that only the second order transition occurs in the vicinity of the crack tip. Function F plays here the role of Hamiltonian H in the theory of phase transitions:

$$H = H_0 + H_1,$$

$$H_0 = \frac{1}{2}\lambda_{iklm}a_{iklm}\sum_p (e_{ik}(p))^2 - \frac{1}{2}\sum_p \rho p^2 e_{ik}^2(p), \quad (1)$$

$$H_1 = \frac{1}{4}\beta_{iklm}^2 a_{iklm}^2 \sum_p (e_{ik}(p))^2 + \sum_p e_{ik}\sigma_{ik}.$$

The parameter space is formed by the following μ points:

$$\mu = (\lambda_{iklm}a_{iklm}, \beta_{iklm}^2 a_{iklm}^2, \rho) \equiv (\lambda, \beta, \rho).$$

3. To determine the fixed point, we use the method of renormalization group R_s [10]. Under the effect of R_s, Hamiltonian H transforms according to the following rules:

$$e^{-H' - AL^d} = \left[\int \delta\hat{e} e^{-H}\right]_{e \to \lambda_s e(sp)}, \quad (2)$$

where $\delta\hat{e} = \prod_{\frac{\Lambda}{s} < p < \Lambda} \prod_i de_i(p)$. In the second-order approximation, we have

$$H' + AL^d = H_0' + A_0' L^d$$

$$+ \left[\langle H_1\rangle - \frac{1}{2}\langle (H_1 - \langle H_1\rangle)^2\rangle\right], \quad (3)$$

where AL is the additive constant, λ_s is the constant dependent on the transformation scale s, H_0' is the

Moscow State University,
Vorob'evy gory, Moscow, 119899 Russia

1028-3358/00/4506-0245$20.00

Hamiltonian H after transformation R_s, and $\langle H_1\rangle$ denotes the average over the Gaussian distribution $\exp(H_0')$.

Substituting (1) into (3), calculating the integral in (3), and replacing e_i by $\lambda_s e_i(sp)$, we find

$$H_0' = \frac{1}{2}\sum_{p'<\Lambda}(\lambda\lambda_s^2 + \rho\lambda_s^2 s^{-2}p'^2)e_i^2, \tag{4}$$

$$A'L^d = \frac{1}{2}\sum_{\frac{\Lambda}{s}<p<\Lambda} d^2 \ln\frac{2\pi}{\lambda + \rho p^2}. \tag{5}$$

Similarly to [12], we described here the state with strain e_i ($i = 1, 2, \ldots, 9$) in the E space. To calculate averages over $\hat{e}$, we separate $\hat{e}$ from e, assuming according to the definition that $e_{ik} = \hat{e}_{ik} + e'_{ik}$, $e'_{ik} = L^{-d/2}\sum_{p<\frac{\Lambda}{s}} e_{ik}e^{ipx}$, and $\hat{e} = L^{-d/2}\sum_{p>\frac{\Lambda}{s}} e_{ik}e^{ipx}$. As a result, we find

$$\langle \hat{e}_i^2\rangle = nB(1 - s^{-2+\epsilon}) - nC\ln s, \tag{6}$$

$$\langle (e_i'\hat{e}_i)^2\rangle = \frac{1}{n^2}e_i'^2 B(1 - s^{-2+\epsilon}) - nC\ln s, \tag{7}$$

$$\langle \hat{e}_i^4\rangle = (n^2 + 2n)B^2(1 - s^{-2+\epsilon}) - (n^2 + 2n)C\ln s,$$

where

$$B = \frac{k_4\Lambda^4}{2\rho} - \frac{\lambda}{\rho\Lambda^2}, \quad C = k_4\lambda, \quad k_4 = 2^{-d+1}\frac{\Gamma^{-d/2}}{\Gamma(d/2)},$$

and n is the strain space dimension ($n = 1, 2, \ldots, 9$).

Let us calculate the expression

$$\begin{aligned} H_1 - \langle H_1\rangle &= Q[\hat{e}_i^4 - \langle \hat{e}_i^4\rangle] \\ &+ 2Q[e_i^2(\hat{e}_i^2 - \langle \hat{e}_i^2\rangle) + 4((e_i'\hat{e}_i)^2 - \langle (e_i'\hat{e}_i)^2\rangle)] \\ &+ 4Qe_i'\hat{e}_i(e_i'^2 + \hat{e}_i^2) + \frac{1}{2}\hat{e}_i\sigma_i, \end{aligned} \tag{8}$$

where $Q = \beta/4$. Note that, according to the Wick theorem, the average of an odd function is equal to zero. Then, we consider the approximation $e'(y) \approx e'(x) + \delta e'(x)$. In the zeroth-order approximation, we have $e'(y) \approx e'(x)$ (see [11]), and (11) can be reduced to the following form:

$$\begin{aligned} &(\hat{e}^4(x) - \langle \hat{e}^4(x)\rangle)(\hat{e}^4(x) - \langle \hat{e}^4(x)\rangle) \\ &+ Q^2 48n^2(n^2 + 2)e'^2(x)G^2(r)G(0) \\ &+ Q^2(72n^2e'^4(x)G^2(r) + 16e'^6(x)G(x)) \\ &+ Q^2(16(n^2 + 2)e'^4(x)G(r)G(0) + 2e'^3(x)\sigma G(x)) \\ &+ Q^2 \times 16(n^2(n^2 + 2)e'^4(x)G(r)G(0) \\ &+ n^2(n^4 + 3n^2 + 5)e'^2G(r)G(0)) \\ &+ Q^2(32n^2(n^2 + 2)e'^2(x)G^3(r) \\ &+ 2n^2(n^2 + 2)e'(x)\sigma G(x)G(0)) + 2Qe'^3(x)\sigma G(x) \\ &+ 2Qn^2(n^2 + 2)e'(x)\sigma G(x)G(0) + \frac{n^2}{4}\sigma^2 G(x), \end{aligned} \tag{9}$$

where $G(r) = (2\pi)^{-2}r^{-2}\rho^{-1}(J_0(\Lambda r/s) - J_0(\Lambda r))$, $d = 4$, and J_0 is the Bessel function. We limit ourselves to the case when both λ and β are of the order of $o(\epsilon)$ and calculate (9) accurate to the order of $o(\epsilon^2)$. If components (λ^*, β^*) of the fixed point are actually of the order of $o(\epsilon)$, we may implement the obtained results to determine these components. According to [10], expression (9) already contains $\beta^2 = o(\epsilon^2)$ as a factor; hence, it is sufficient to calculate the corresponding integral only at $d = 4 - \epsilon$, and it is possible to neglect λ. It is known that

$$\int d^d r G(r) = 0, \quad \int d^4 r G^2(r) = \frac{n^2 k_4}{\rho^2}\ln s.$$

As a result, we find

$$\begin{aligned} &Q^2\int d^d x 2e'^2(x) \\ &\times [48n^2(n^2 + 2)G^2(x)G(0) \qquad \text{(a)} \\ &+ 32n^2(n^2 + 2)G^3(r)] \qquad (10) \\ &+ Q^2\int d^d x[(\hat{e}^4(x) - \langle \hat{e}^4(x)\rangle)(\hat{e}^4(y) - \langle \hat{e}^4(y)\rangle)] \quad \text{(b)} \\ &+ \int d^d x 72Q^2n^2e'^2(x)G^2(r). \qquad \text{(c)} \end{aligned}$$

Term (b) in (10) is a constant depending on $e'(x)$ and contributes to the additive quantity $A'L^d$ involved in (3). Term (a) has the form $e'^2(x)$, and it contributes to λ. The other terms in (10) contain $e'^4(x)$. Relationship (10) can be represented as

$$\frac{1}{2}\int d^d x\left(e'^2(x)D\lambda' + \frac{1}{4}e'^4(x)D\beta'\right), \tag{11}$$

where

$$\begin{aligned} D\lambda' &= -Q^2\int d^d dr[48n^2(n^2 + 2)G^2(r)G(0) \\ &+ 32n^2(n^2 + 2)G^3(r)], \qquad (12) \\ D\beta' &= -Q^2\int d^d dr 72n^2G^2(r). \end{aligned}$$

Substitutions $e'(x') \longrightarrow \lambda_s e(x')$, $x' \longrightarrow x/s$, and $\int d^d x \longrightarrow s^d\int d^d x'$ in (11) and (12) lead to the following expressions:

$$D\lambda' = -Q^2 s^d \int d^d dr[48n^2(n^2+2)G^2(r)G(0) + 32n^2(n^2+2)G^3(r)], \quad (13)$$
$$D\beta' = -Q^2 s^d \int 72n^2 G^2(r) d^d dr.$$

Here, we consider the critical state as the fracture state. Therefore, the critical character of a region adjacent to the crack tip determines the properties of the crack. Let us discuss the features of the fixed point in the course of phase transition. Fixed point (λ^*, β^*) described above is stable, since $y_2 = -\epsilon < 0$. Under condition $\lim_{s\to\infty} R_s^L \mu = \mu^*$, the equation

$$\lambda + \frac{1}{2\rho}\beta\left(\frac{n^2}{2}+1\right)\Lambda^2 k_4 = 0$$

describes the critical surface accurate to $O(\epsilon)$.

4. Features of the model that describes the development of a crack in a continuous medium are summarized below. Under the effect of external forces, the system involving the medium with the crack turns out to be in the state of fracture (in the state of phase transition). Since stresses are concentrated at the crack tip, the phase transition occurs precisely in this region. This phase transition of the second order reduces the strength of the medium and promotes propagation of the crack. Paper [13] puts forward the scaling law, according to which the defect formation process is self-similar in the course of multiple fracture. In fact, our model allows a similar interpretation. However, in the modern theory of critical phenomena, the scaling has a more fundamental physical meaning than simply the geometric similarity of a crack. It is related to the fluctuation behavior of stress and strain fields accompanying the plastic deformation. As a result, each point μ of the parameter space determines the distribution of the probability density for the state under study. The change in the character of strains in the medium determines the new point μ'. We described this change by the renormalization group transformation R_s,

$$\mu' = R_s\mu.$$

We constructed the renormalization group in two stages. The first stage involves the coarse-grain partitioning $H''[e] = K_s H[e]$, where K_s is the Kadanoff transformation. At the second stage, we reduced the system by a factor of s down to the initial dimension $H'[e] = (H''[e])_{e_x \to \lambda_s e_{x'}}$, $x' = x/s$. The scaling parameter s reflects the correlation length of fluctuations and, consequently, the block dimension in the fractured state.

REFERENCES

1. A. P. Bobryakov, A. F. Revuzhenko, and E. I. Shemyakin, Fiz.-Tekh. Probl. Razrab. Polezn. Iskop., No. 5 (1983).
2. V. A. Pesin, N. N. Pachenko, and L. I. Fel'dchuk, ÉPFKh **53**, 2794 (1979).
3. V. G. Gargin, Sverkhtverd. Mater., No. 2, 17 (1982).
4. Li-Shing Li and R. J. Pabst, Mater. Sci. **15**, 2861 (1980).
5. D. Sornette, Phys. Rev. B **36**, 8847 (1987).
6. M. Ausloos, Solid State Commun. **59**, 401 (1986).
7. K. Sieradzki and Rong Li, Phys. Rev. Lett. **56**, 2509 (1986).
8. L. de Arcangelis, A. Hansen, H. J. Herrmann, and S. Roux, Phys. Rev. B **40**, 877 (1989).
9. Chin' Van Khoa, Candidate's Dissertation in Chemistry (Mosk. Gos. Univ., Moscow, 1993).
10. S. Ma, *Modern Theory of Critical Phenomena* (Benjamin, Reading, Mass., 1976; Mir, Moscow, 1980).
11. Yu. I. Sirotin and M. P. Shaskol'skaya, *Fundamentals of Crystal Physics* (Nauka, Moscow, 1975).
12. A. A. Il'yushin, *Mechanics of Continuous Media* (Moscow, 1986).
13. G. I. Barenblatt and L. R. Botvina, Fiz.-Khim. Mekh. Mater. **21** (1) (1986).

Translated by Yu. Verevochkin

Doklady Physics, Vol. 45, No. 6, 2000, pp. 248–251. Translated from Doklady Akademii Nauk, Vol. 372, No. 5, 2000, pp. 608–611.

PHYSICS

Imaging of Filtration Channels in Track Membranes by the Schwarzschild X-ray Microscope

I. A. Artyukov*, V. E. Asadchikov, A. I. Vilenskiĭ**, A. V. Vinogradov*, D. L. Zagorskiĭ**, V. E. Levashov*, B. V. Mchedlishvili**, A. V. Popov***, A. A. Postnov**, and I. I. Struk***

Presented by Academician N.G. Basov June 2, 1999

Received July 28, 1999

Nowadays, one of the most widespread technological processes for separation of complex mixtures is membrane filtration. Among the materials used in this process, an important role is played by track membranes (nuclear filters) manufactured by means of irradiating polymeric films by high-energy ion beams with the subsequent etching tracks until pores have been obtained [1]. The distinctive features of track membranes compared to traditional ones are their high selectivity with respect to particles to be filtered, low adhesion ability, and inertial behavior with respect to a large number of compounds—including also biological objects. The track membranes are used in the processes of purification, concentration, and filtration of viruses, for purging vaccines of medicine solutions [2], etc. These membranes are also promising in developing means for protecting respiratory organs against unfavorable actions.

Determining the geometrical dimensions of filtration channels in track membranes is rather significant for using them efficiently. Meanwhile, the solution of this problem is not evident in the case of pore diameters smaller than 0.5 μm. Standard methods of optical microscopy make it impossible to resolve such sizes, while electron and X-ray microscopy (wavelengths of 0.05 to 0.3 nm) require additional processing of the surface for materials under study.

* *Lebedev Physical Institute, Russian Academy of Sciences, Leninskiĭ pr. 53, Moscow, 117924 Russia*

** *Shubnikov Institute of Crystallography, Russian Academy of Sciences, Leninskiĭ pr. 59, Moscow, 117333 Russia*

*** *Institute of Terrestrial Magnetism, Ionosphere, and Radio-Wave Propagation, Russian Academy of Sciences, Troitsk, Moscow oblast, 142092 Russia*

EXPERIMENTAL SETUP AND SCHEMATIC DIAGRAM OF THE EXPERIMENT

For investigating properties of track membranes, we used a microscope operating with soft X-rays and having a Schwarzschild lens. The microscope magnification attained 20× at a wavelength of 20 nm [3, 4] (Fig. 1). The Schwarzschild lens was composed of two spherical mirrors (a concave mirror with R = 100 mm and a convex one with r = 35 mm) with an aperture of 0.17 and a common center of curvature. The object under investigation was situated at a point where the third-order spherical aberrations were compensated. The theoretical spatial resolution of the lens was 0.1 μm. The mirrors had multilayer Mo/Si coatings providing a reflection factor of ~20% at a wavelength of 20 nm. A thin aluminum filter cut off the visible-range radiation. Plasma was formed as a result of focusing the YAG-laser radiation (λ = 1.06 μm, τ = 5 ns, E = 0.1 J) upon the surface of a solid-state target onto a spot 0.1 mm in diameter. The object was illuminated by the laser-plasma source with the help of an optical condenser. The lens, the source, and the photographic film were placed into a vacuum chamber with a pressure on the order of 10^{-3} mm Hg. The image was recorded for 1 to 10 laser bursts by UF-4 film (NIIKhIMFOTOPROEKT, Russia).

In contrast to the previous versions of the Schwarzschild microscope operating with a unique intense laser in the single-pulse mode (the pulse energy attained 20 J), the new microscope uses a low-power pulse-frequency laser. The exposure of the film is regulated by the number of pulses of the solid-state laser and is unlimited. The construction of the device provides sufficient stability so that no adjustment is necessary during the time interval between laser pulses.

IMAGE FOR THE SET OF TRACK MEMBRANES

Track membranes can be investigated by X-ray microscopes because they provide a good contrast in the wavelength region near 20 nm, which is difficult to

1028-3358/00/4506-0248$20.00

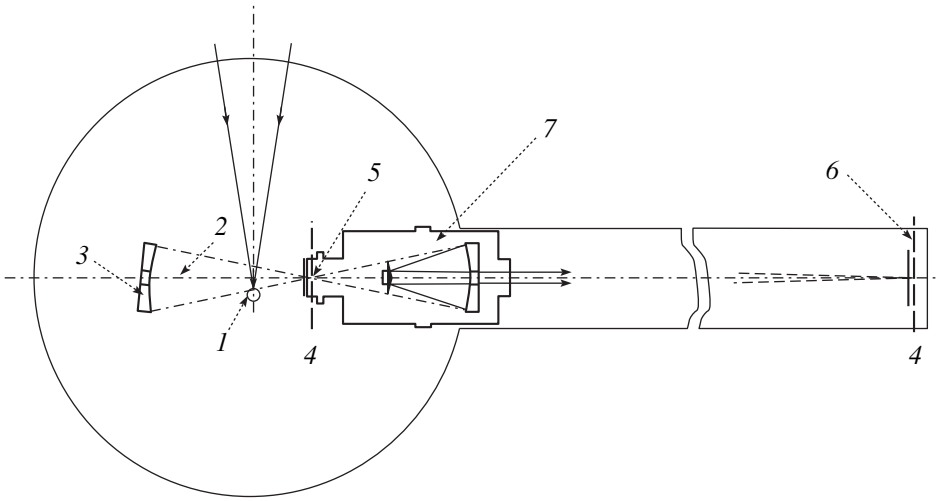

Fig. 1. Schematic diagram of the X-ray microscope operating at a wavelength of 20 nm: (*1*) massive tungsten target, (*2*) laser plasma, (*3*) optical condenser, (*4*) aluminum filters 0.4–0.5-μm thick, (*5*) test object, (*6*) UF-4 photosensitive film, and (*7*) Schwarzschild lens.

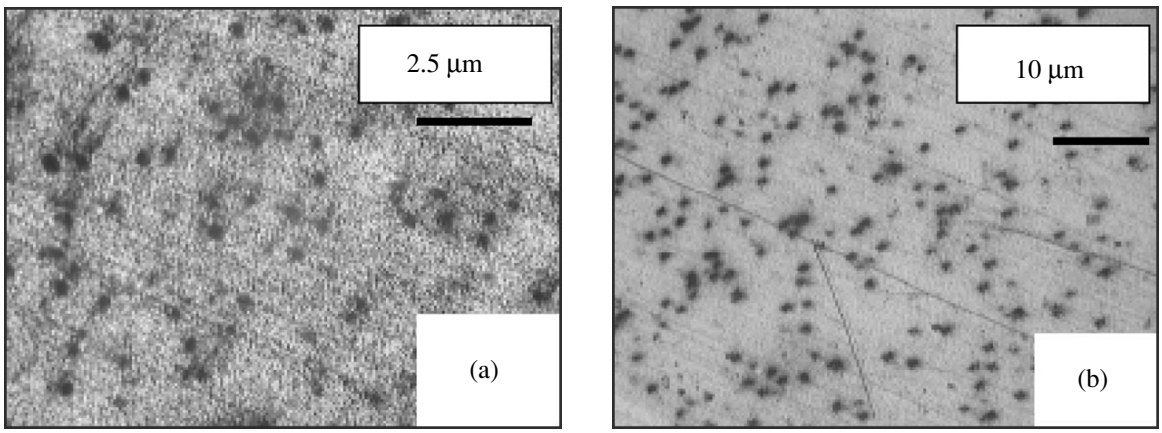

Fig. 2. Images of nuclear filters with pore diameters of (a) 0.2 and (b) 1 μm. The images were obtained by means of an X-ray microscope with an operating wavelength of 20 nm.

attain in the visible range or harder X-ray (the wavelength $\lambda < 0.3$ nm) spectral range.

As samples, we used irregular track membranes fabricated from polyethylene terephthalate (lavsan, i.e., a Russian equivalent of Dacron) with a pore diameter of 1 μm (a matrix thickness of 20 μm) and 0.2 μm (a matrix thickness of 10 μm) [5]. Moreover, we investigated regular track membranes with a pore diameter of 0.5 μm and a period of 1 μm.

In Fig. 2, the shape of pores in the irregular track membranes with orifice diameters of 1 μm is well seen. The density of the orifices measured on photographs amounted to 6.28×10^7 cm^{-2}.

In order to attain the highest possible resolution, we investigated membranes with small orifices. In this case, it turned out that for orifice diameters smaller than 0.15 μm, the membranes became virtually opaque owing to the diffraction inside the pore channels. The minimum diameter of pores that we managed to investigate was 0.2 μm. Figure 2 presents the photograph of such a membrane, which exhibits the shape of channels and density of orifices. This density amounted to 1.35×10^8 cm^{-2}. In both cases, the measured densities coincided with those found in the independent electron-microscopic investigations.

In addition to membranes with irregularly disposed pores, we also obtained images of track membranes with a regular set of pores (a mean diameter of orifices was 0.5 μm). In Fig. 3, we show the photographs obtained with the help of the electron microscope and Schwarzschild microscope. Using such photographs, it is easy to estimate the magnification of the microscope and to compare the imaging properties of the Schwarzschild microscope with a standard image obtained by the

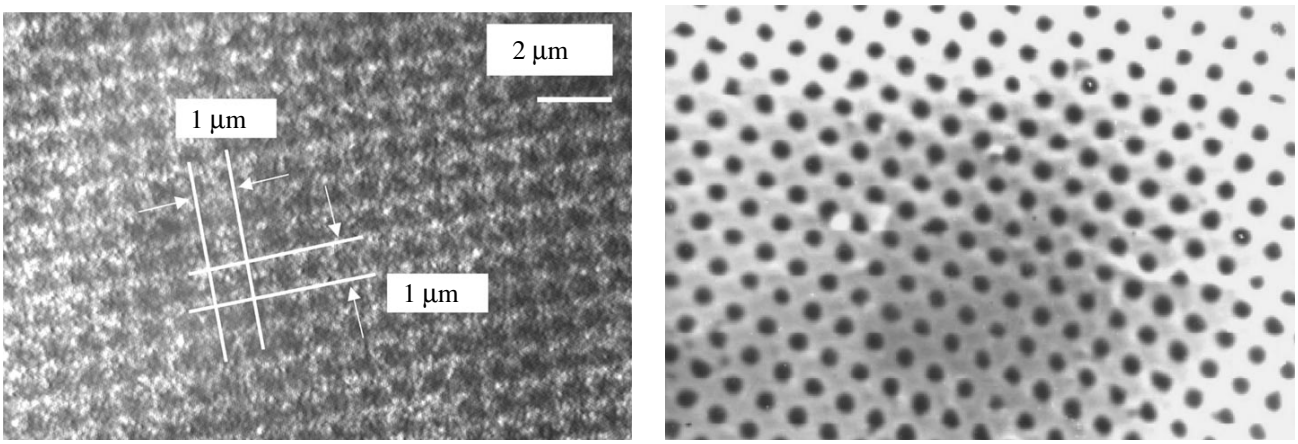

Fig. 3. Images of a regular track membrane with channel diameters of 0.5 μm. The images were obtained by means of an X-ray microscope with a wavelength of 20 nm and by an electron microscope.

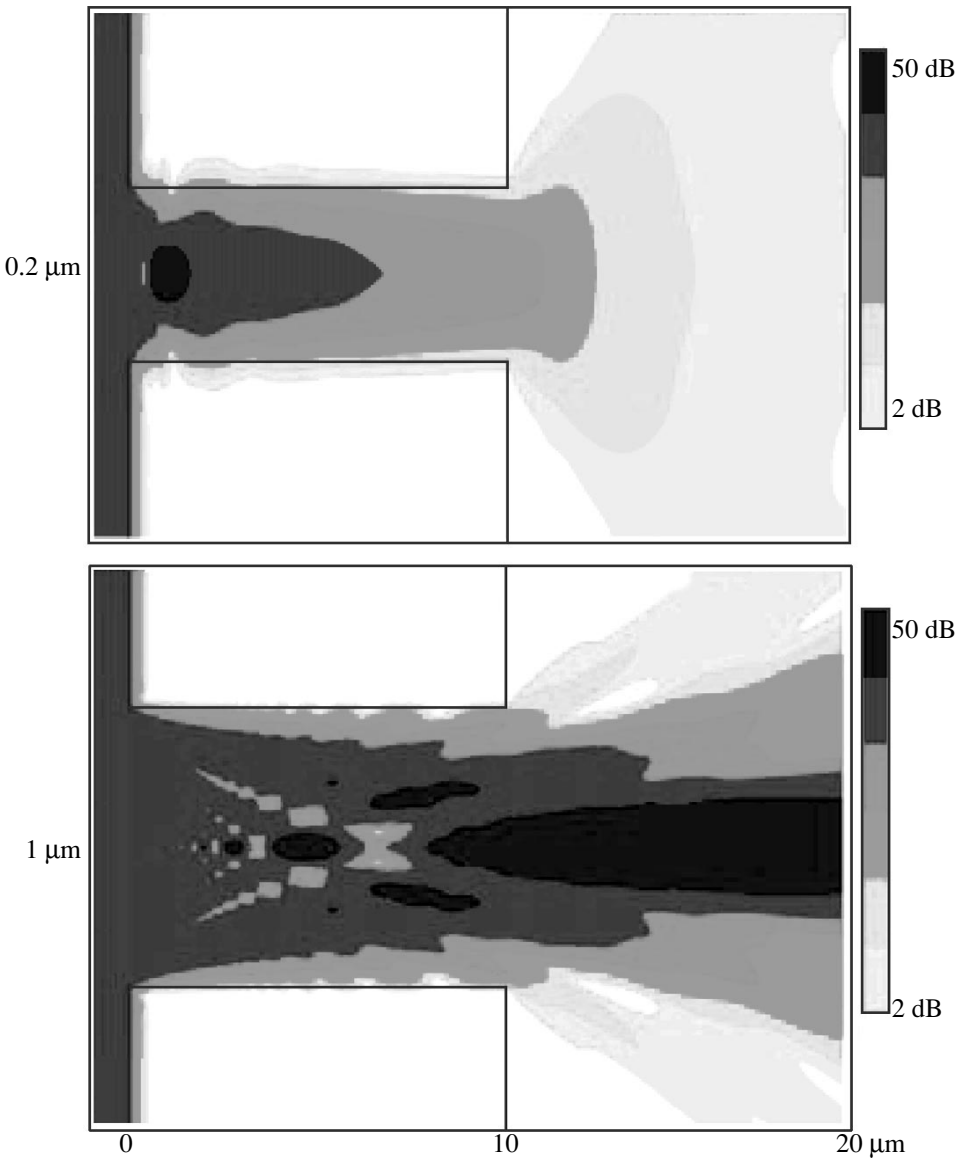

Fig. 4. Numerical simulation of the field inside and beyond a pore of 0.2 and 1 μm in diameter.

electron microscope. The Schwarzschild microscope reproduces the periodic structure well. It is also seen that the dimension of the orifices is not markedly distorted by diffraction effects.

The visualization of pores with a small diameter of ~0.2 μm required a considerable increase in the exposure time compared to pores with a diameter of ~1 μm, and, as has been noted, for pore diameters of ~0.15 μm the pores became virtually opaque. In order to investigate the dependence of the transparency of pores on their diameter, we performed numerical simulation of the interaction between an electromagnetic wave and small orifices.

NUMERICAL CALCULATION OF A FIELD BEYOND THE TRACK MEMBRANE

A field beyond the membrane filter was calculated theoretically by the numerical solution of the parabolic wave equation under the assumption that the plane monochromatic wave is incident to the filter [6]. The permittivity of the track membrane involved the real and imaginary parts according to known constants for a wavelength of 20 nm.

The field distribution for various distances from the membrane plane can be seen in Fig. 4. The exposure time for photographic materials is determined experimentally, and the complete blackening can be attained when the radiation passed corresponds to an arbitrary color, thereby inducing either an increase or decrease in the orifice size compared to the actual one.

The calculation results for the field beyond pores of 0.2 μm in diameter show a considerable decrease in the membrane transmission for X-ray radiation, which corresponds to experimental observations.

Thus, using the Schwarzschild microscope, we managed to observe the structure of track membranes, with the resolution being higher than that of the optical microscope without additionally processing the membrane surface. We succeeded in measuring the density of tracks and in studying their shape. The resolution of 0.2 μm obtained for an actual object is close to the theoretical ultimate resolution.

By the method of the parabolic equation, we performed numerical simulation of the X-ray transmission through pores with allowance for the diffraction as well as for the refraction and absorption in the membrane material.

In contrast to electron microscopy, the method described for investigating track membranes is nondestructive and makes it possible to obtain information about the entire track, not just about the part of the membrane adjacent to this track.

ACKNOWLEDGMENTS

The authors are grateful G.N. Kulipanov, V.F. Pendyurin, and V.A. Brovkov. This work was supported by the ISTC, project no. 918.

REFERENCES

1. G. N. Flerov, Vestn. Akad. Nauk SSSR, No. 4, 35 (1984).
2. T. Brock, *Membrane Filtration: A User's Guide and Reference Manual* (Science Technical Incorporation, Madison, 1983; Mir, Moscow, 1987).
3. I. A. Artyukov, V. E. Asadchikov, A. V. Vinogradov, *et al.*, Kvantovaya Élektron. **22**, 951 (1995).
4. I. A. Artyukov and K. M. Krymskiĭ, *Analysis of Optical Properties of a Schwarzschild Lens*, Preprint No. 30, FIAN (Lebedev Physical Institute, Russian Academy of Sciences, Moscow, 1998).
5. A. I. Vilenskiĭ and G. S. Zhdanov, Khim. Vys. Énerg. **32**, 112 (1998).
6. Yu. V. Kopylov, A. V. Popov, and A. V. Vinogradov, Opt. Commun. **118**, 619 (1995).

Translated by V. Bukhanov

Doklady Physics, Vol. 45, No. 6, 2000, pp. 252–254. Translated from Doklady Akademii Nauk, Vol. 372, No. 5, 2000, pp. 612–614.

PHYSICS

Slightly Ionized Gas-Discharge Plasma as a Two-Phase Medium

G. I. Mishin

Presented by Academician A.M. Prokhorov August 23, 1999

Received September 7, 1999

In contrast to thermally ionized gas, gas-discharge plasma has unusual dynamic properties discovered during the period from the late sixties to the early seventies [1–3]. In such plasma, the measured sound velocity turned out to be lower than that in the nonionized gas at the same temperature. Moreover, amplitudes of sound waves in gas-discharge plasma turned out to be larger than those in the nonionized gas at the same external parameters and was seen to increase by several times while cooling plasma [3].

In 1978, it was also found that a spherical model body moving in air gas-discharge plasma began to generate a head shock wave at a Mach number smaller than that for the body moving in air at the same gas parameters [4].

Theoretical analysis of this phenomenon [5–7] failed to explain both unusual effects of cooling plasma under the action of sound waves [8] and the considerable decrease of the heat flow at the frontal surface of a spherical model body moving in plasma compared to those in air (at the same velocity, temperature, and static pressure) [9].

These experimental results suggest that, apart from the conventional kinetic energy of random motion, there exists an additional potential energy of intermolecular interaction in plasmas.

On the basis of this assumption, the following two-term equation of state for gas-discharge plasma was proposed [10, 11]:

$$P = nkT + \alpha(n^2 - n_0^2). \tag{1}$$

Here, P and T are pressure and temperature; n is the current particle density (concentration); n_0 is the density of plasma originating in the process of gas discharge at the initial values P_0 and T_0; α is a coefficient of the interparticle interaction; and $k = 1.38 \times 10^{-16}$ erg/K is the Boltzmann constant.

John Hopkins University, Lowrell, Maryland, USA

Using equation (1) and the first law of thermodynamics, which is written in a differential form, we obtain the expression for the sound velocity squared

$$W^2 = \frac{C_V + R}{C_V}\frac{RT_0}{\mu} + \frac{2\alpha N n_0}{\mu} = \left(\frac{C_V + R}{C_V} + \frac{2\alpha N n_0}{RT_0}\right)\frac{RT_0}{\mu} = \gamma_P \frac{RT_0}{\mu}, \tag{2}$$

where C_V is the molar heat capacity at a constant volume and constant plasma temperature, and μ is the molecular mass. As is seen from formula (2), the sound velocity in plasma and Poisson's ratio γ_P are higher than the corresponding experimental values for ideal gas.

It should be noted that vibrational degrees of freedom for molecules turn out to be excited in gas discharge and, therefore, the distribution function of the electron energy becomes nonequilibrium. However, all these effects result in the increase of the internal molecular energy, which must be accompanied by a decrease in the ratio γ_P for specific heat capacities of plasma, i.e., contradictory to available experimental data. Thus, the increase of γ_P cannot be explained by intramolecular processes but is a result of intermolecular interaction.

Measurements of the drag force acting upon a spherical model body moving either in slightly ionized gas-discharge plasma or, for comparison, in nonionized air [12] have led to the discovery of three effects.

Firstly, the sound velocity W in gas-discharge plasma turned out to be equal to 840 m/s (a point of inflection for the velocity dependence of the drag coefficient C_x, which occurs due to the change from the subsonic to supersonic motion), while the gas-kinetic (thermal) value at $T = 1140$ K is 660 m/s.

Secondly, for subsonic velocities, the value of C_x in plasma turned out to be considerably smaller than that in nonionized air. This fact is explained by the decrease in C_x with an increasing Mach number for subsonic velocities. Since the sound velocity in plasma is always higher than that in air, the Mach number in plasma (for equal velocities) is smaller than that in air.

1028-3358/00/4506-0252$20.00

The third effect is the most important and surprising. Namely, a significant rise of C_x can be expected in plasma for supersonic velocities compared to that in nonionized air, which is, naturally, impossible.

From various explanations of this phenomenon, only one turned out to be consistent with experimental data. Namely, there is a small amount of additional "hidden" mass of metastable molecules bound with each other in gas-discharge plasma consisting of molecules of slightly ionized ideal gas [13]. The molecules of the hidden mass are integrated into a volume structure, i.e., a certain "skeleton," with large bonding energies and, therefore, have no translational degrees of freedom. This implies that these molecules do not produce the external pressure. Therefore, when measuring pressure, their presence in plasma remains unobservable. Moreover, the motion of optical electrons in the particles forming the skeleton is unaffected by the action of the electromagnetic field within the visible-light range. Thus, the presence of bound particles in gas-discharge plasma cannot be detected by interferometers.

We denote the densities of free and bound molecules (atoms) by n_f and n_b, respectively. Then, the total particle density in plasma is $n = n_f + n_b$. Since the relative concentrations of free and bound molecules are independent of the density, then, we can write $\psi = n_{f0}/n_0 = n_f/n$ for the former, and $1 - \psi = n_{b0}/n_0 = n_b/n$ for the latter. Therefore, the external (measured) pressure is

$$P_f = n_f kT = \psi nkT, \tag{3}$$

and the additional internal pressure (potential energy) of bound particles in plasma is given by

$$P_b = \alpha(1-\psi)(n^2 - n_0^2). \tag{4}$$

Thus, the equation of state for gas-discharge plasma takes the form

$$P = P_f + P_b = \psi nkT + \alpha(1-\psi)(n^2 - n_0^2). \tag{5}$$

In this case, the specific factor $(1 - \psi)$ appears in the expression for the molar bonding energy in plasma [11]:

$$U_b = 2\alpha N(1-\psi)n_0. \tag{6}$$

In turn, the equation for the sound velocity squared changes:

$$W^2 = \psi\frac{C_V + R}{C_V}\frac{RT_0}{\mu} + \frac{2\alpha N(1-\psi)n_0}{\mu}$$
$$= \left(\psi\frac{C_V + R}{C_V} + \frac{2\alpha N(1-\psi)n_0}{RT_0}\right)\frac{RT_0}{\mu} = \gamma_P\frac{RT_0}{\mu}. \tag{7}$$

The energy equation for a mole of gas-discharge plasma flow having the velocity v (and the initial velocity v_0) is also modified:

$$\psi(C_V + R)T_0 + 2\alpha N(1-\psi)n_0 + \frac{1}{2}\mu v_0^2$$
$$= \psi(C_V + R)T + \alpha N(1-\psi)\left(n + \frac{n_0^2}{n}\right) + \frac{1}{2}\mu\frac{(n_0 v_0)^2}{n}. \tag{8}$$

Using the system of equations (5)–(8), the equations for conservation of the mass and momentum,

$$n_0 v_0 = nv, \tag{9}$$

$$\psi n_0 kT_0 + \frac{\mu}{N}n_0 v_0^2 = \psi nkT + \frac{\mu}{N}nv^2, \tag{10}$$

and the experimental data of [12], we can find the characteristics of the plasma structure [13]. Namely, it turned out that $\alpha = 3.608 \times 10^{-30}$ erg cm^3, $U_b = 0.974 \times 10^4$ J/mol, $n_{b0} = 0.224 \times 10^{17}$ cm^{-3}, and the molar bonding energy is equal to 10.8×10^{-13} erg. Under the conditions of this specific plasma, $\psi = 0.85$.

Our calculations have shown that, in the stagnation zone at the frontal surface of a spherical model body moving with the velocity of 1320 m/s, the relative compression of plasma was 4.42 (in contrast to 3.12 in ideal air), and the stagnation temperature was $T_s = 1573$ K (smaller by 319 K than T_s in nonionized air for identical gas-dynamic parameters).

Since the external pressure is determined only by free molecules, the stagnation pressure is $P_s = \psi n_s kT_s = 12.21 \times 10^4$ dyne/cm^2, which corresponds to the drag coefficient $C_x = 0.974$. Without allowance for a contribution of bound molecules, the value of C_x is found to be overestimated by 19%.

The results of two more experiments performed in air plasma [4, 14], in which the sound velocity was reliably measured, showed that structures originating in air plasma had the same bonding energy even though the values of P_0 and T_0, as well as methods of the ionization production, had been quite different. This is an important indication for the existence of a skeleton. In fact, there must exist a standard type of structure in plasmas having an identical physical character (gas discharge and molecular mass) because molecules of slightly ionized ideal gas are only its "filler."

For $n_{b0} = 0.224 \times 10^{17}$ cm^{-3}, the average intermolecular distance is 3.5×10^{-6} cm. Molecules are able to interact with each other at such large distances only if their valence electrons form a common collective system; i.e., a Rydberg state of the gas excited by the electron impact is originated. Such an unusual state of matter is appropriately referred to as a "gas crystal."

Highly excited metastable molecules forming the skeleton are generated as a result of the gas-discharge process and then are deactivated in a decomposing plasma at a temperature of about 1400 K with a time constant of 0.02 s.

Thus, the existence of the strong interaction between particles, despite a low average density of the structure under consideration, is explained.

REFERENCES

1. U. Ingard, Phys. Rev. **145**, 41 (1966).
2. Y. Ishida and T. Idehara, J. Phys. Soc. Jpn. **35**, 1747 (1973).
3. M. Hasegawa, J. Phys. Soc. Jpn. **37**, 193 (1974).
4. G. I. Mishin, Yu. P. Serov, and I. P. Yavor, Pis'ma Zh. Tekh. Fiz. **17** (11), 65 (1991) [Sov. Tech. Phys. Lett. **17**, 413 (1991)].
5. G. I. Mishin, *Sonic and Shock Wave Propagation in Weakly Ionized Plasma in Gas Dynamics* (Nova Science, Commack, New York, 1992), p. 81.
6. Ya. B. Zel'dovich and Yu. P. Raizer, *Physics of Shock Waves and High-Temperature Hydrodynamic Phenomena* (Nauka, Moscow, 1963; Academic Press, New York, 1966, 1967), Vols. 1, 2.
7. F. G. Baksht and G. I. Mishin, Zh. Tekh. Fiz. **53**, 854 (1983) [Sov. Phys. Tech. Phys. **28**, 547 (1983)].
8. M. A. Antinyan, G. A. Galechyan, and L. B. Tavakalyan, Teplofiz. Vys. Temp. **29**, 1081 (1991).
9. Yu. L. Serov and I. P. Yavor, Zh. Tekh. Fiz. **65** (3), 38 (1995) [Tech. Phys. **40**, 248 (1995)].
10. G. I. Mishin, Pis'ma Zh. Tekh. Fiz. **23**, 81 (1997) [Tech. Phys. Lett. **23**, 570 (1997)].
11. G. I. Mishin, Appl. Phys. Lett. **71**, 49 (1997).
12. A. P. Bedin and G. I. Mishin, Pis'ma Zh. Tekh. Fiz. **21**, 14 (1995) [Tech. Phys. Lett. **21**, 5 (1995)].
13. G. I. Mishin, Pis'ma Zh. Tekh. Fiz. **24**, 80 (1998) [Tech. Phys. Lett. **24**, 448 (1998)].
14. A. I. Klimov, G. I. Mishin, A. B. Fedotov, *et al.*, Pis'ma Zh. Tekh. Fiz. **15**, 31 (1989) [Sov. Tech. Phys. Lett. **15**, 800 (1989)].
15. I. V. Basargin and G. I. Mishin, Zh. Tekh. Fiz. **66**, 198 (1996) [Tech. Phys. **41**, 742 (1996)].

Translated by V. Chechin

Doklady Physics, Vol. 45, No. 6, 2000, pp. 255–258. Translated from Doklady Akademii Nauk, Vol. 372, No. 6, 2000, pp. 749–752.

PHYSICS

Surface Tension of Elemental Substances at the Melting Curve

Academician V. P. Skripov and M. Z. Faizullin

Received February 10, 2000

1. The data on the values of specific free energy σ of the crystal–liquid interface[1] are few and rather unreliable. In contrast to the surface tension at the equilibrium liquid–vapor boundary, there is no simple method for measuring σ at the melting curve at certain temperatures and corresponding pressures [1]. The theoretical estimates of σ for the crystal–melt boundary are highly questionable. The scatter in the different calculated values of σ in metals [2] ranges within an order of magnitude, and this does not allow us to draw any definite conclusion concerning the temperature dependence of σ.

The surface tension plays the dominant role in the spontaneous nucleation of the crystal phase, and it significantly affects the formation of the polycrystalline structure in solids. Basically, the theory of homogeneous nucleation is universal as far as mechanisms underlying the coexistence and metastability of the involved phases are concerned [3, 4]. A systematic study of homogeneous nucleation for boiling [5] and crystallization [6] of different substances definitely suggests that such experiments can provide certain information on the surface tension at the interphase boundary. This technique was successively and widely implemented for vapor bubbles nucleating in overheated liquids [5, 7]. Independent measurements of σ by the capillary technique at the same temperatures allowed us to compare the data and to estimate the correction related to the curvature of the interface. Usually, this correction does not exceed 2–6% if critical radius r_* of the nucleating bubbles is about 5 nm, $r_* \approx 5$ nm.

For the crystal–liquid interface, the authors of [8] used the following relationship,

$$G = \frac{W_*}{kT} \approx 62, \tag{1}$$

as a condition of the homogeneous nucleation. Based on (1), they found the values of σ for a series of organic substances using the attained degree of overheating $T_0 - T$. Here, W_* is the work needed to nucleate a bubble of critical size and k is the Boltzmann constant. Within the thermodynamic approximation, it is possible to use one of the following expressions for work W_* needed to form a spherical nucleus with radius r_*:

$$W_* = \frac{4\pi}{3}\sigma r_*^2 = \frac{16\pi}{3}\frac{\sigma^3 v_S^2}{(\mu_L - \mu_S)^2} = \frac{16\pi}{3}\frac{\sigma^3 v_S^2}{(\Delta s)^2 (T_0 - T)^2}. \tag{2}$$

Here, v_S is a specific volume of the crystalline phase, and μ_L and μ_S are the chemical potentials of the liquid and crystal at given pressure p_0 and temperature $T < T_0$ of the experiment. Parameters p_0 and T_0 correspond to a point chosen in the equilibrium melting curve $\mu_L(T_0, p_0) = \mu_S(T_0, p_0)$. The heat of melting ΔH is related to the entropy jump Δs at the melting curve by the conventional relation $\Delta H = T_0 \Delta s$.

Based on condition (1), the authors of [8] calculated the surface tension using the values of v_S, Δs, T_0, and T (known from the experiment) at the crystal–melt interface at atmospheric pressure. A similar approach to the estimations of σ for a number of metals was employed by Hollomon and Turnbull [9]. A more detailed experimental study in the kinetics of spontaneous crystallization [6] allowed us to refine and extend the set of existing data on the surface tension of metals, water, and organic compounds. Similar to previous experiments, supercooling was performed under atmospheric or lower pressures.

The aim of this paper is to determine the temperature dependence of the surface tension at the boundary between the crystal and its melt for a large portion of the melting curve. We are unaware of any such data. This situation is in striking contrast with the large body of information on the behavior of σ at the phase boundary between liquid and vapor in pure substances. In the latter case, the surface tension gradually decreases with

[1] The term “surface tension” will be used as another equivalent for σ.

Institute of Thermal Physics, Ural Division, Russian Academy of Sciences, ul. Pervomaĭskaya 91, Yekaterinburg, 620219 Russia

1028-3358/00/4506-0255$20.00

increasing of temperature and vanishes at the critical point obeying the power law, $\sigma \sim (T_c - T)^{1.25}$. Such behavior is also confirmed by an analysis of experimental data on the kinetics of spontaneous boiling in liquids.

We want to show that despite the narrow range of available data on the kinetics of spontaneous crystallization ($p \approx p_{atm}$) range, it is possible to formulate a scaling rule allowing us to extend our predictions of the σ values to a wider range in the equilibrium melting curve $p_{SL} = f(T)$. In a differential form, the latter relationship is given by the Clapeyron–Clausius equation

$$\frac{dp}{dT} = \frac{\Delta s}{\Delta v}, \tag{3}$$

where $\Delta v = v_L - v_S$ is the specific volume jump at melting. It is convenient to approximate the melting curve itself by the Simon equation

$$1 + \frac{p}{p_*} = \left(\frac{T}{T_0}\right)^c, \tag{4}$$

which allows the extrapolation of the melting curve to the negative pressure range [10] with the asymptote $p \longrightarrow -p_*$ at $T \longrightarrow 0$; c and p_* are the constants characterizing a specific substance; and T_0 is the melting temperature at $p = 0$.

2. Now we turn to the methodological background of the discussed estimates for the $\sigma(T)$ dependence at the melting curve. In the experiments reported in book [6], it was possible to observe the spontaneous crystallization of the supercooled liquids either at atmospheric pressure or in vacuum for a broad range of nucleation rates J from $J \approx 10^2$ s^{-1} cm^{-3} up to $J \approx 10^{20}$ s^{-1} cm^{-3}. The temperature dependence of J agrees well with the theory of homogeneous nucleation. For a steady-state process, we have

$$J = N_1 B \exp\left(-\frac{W_*}{kT}\right), \tag{5}$$

where N_1 is the number of molecules in the unit volume of a liquid at temperature T of the experiment. For the low-viscosity liquids, the kinetic factor B varies only slightly with an increasing degree of supercooling $\Delta T = T_0 - T$. Factor B is of the order of 10^{10}–10^{11} s^{-1}. The exponential factor in (5) provides the main contribution to the change of J; this factor involves work W_* needed to form a critical nucleus. The latter expression in (2) is derived in the framework of the linear approximation for the expansion in terms of ΔT of chemical potentials $\mu_L(T, p)$ and $\mu_S(T, p)$ near the point of the phase equilibrium between the liquid and crystal at $T = T_0$, $p =$ const. Employing this form of work W_*, we obtain the following expression for exponent $G = -W_*/kT$ in (5):

$$G = \frac{16\pi}{3}\frac{\sigma^3 v_S^2}{kT(\Delta s)^2(T_0 - T)^2}. \tag{6}$$

Expression (6) implies the applicability of condition (1). This condition itself corresponds to a fixed (accurate to an order of magnitude) nucleation rate, $\log J \approx 6$. The processing of experimental data [6] revealed a certain linearization of the $J(T)$ curve plotted in coordinates $\ln J$ versus $[T(T_0 - T)^2]^{-1}$. Since $\ln J \approx \text{const} - G$, the combination

$$\frac{\sigma^3 v_S^2}{k(\Delta s)^2} = Z_1 \tag{7}$$

remains constant for a specified deeply supercooled liquid. If the jump in entropy Δs is fixed in relation to the reference point $\{T_0, p_0\}$ in the melting curve, we get a constant value of σ from the experimental data on the homogeneous nucleation at various degrees supercooling. This was the behavior observed in [6]. On the other hand, when comparison with predictions (5) and (6) suggests pronounced changes in σ with increasing degree of supercooling by several Kelvins, we get an indication of the inhomogeneous character of the nucleation.

However, the constant value of combination (7) can be also understood in a different way, as the correlation between the changes of σ, Δs, and v_S at the melting curve. Then, we can use this condition to estimate σ based on the known values of Δs and v_S. Here, we accept this point of view. It is suggested by the experiments on the homogeneous nucleation; however, essentially, it is an assumption, since it was not verified in experiment that the linearity and the slope of the $\ln J$ versus $[T(\Delta T)^2]^{-1}$ curve remain unchanged at different pressures. We reduce expression (7) to a dimensionless form, dividing it by T_0^3 (T_0 is the temperature corresponding to the melting curve of a given substance for $p = 0$):

$$\mathrm{Nc} = \frac{\sigma^3 v_S^2}{kT_0^3(\Delta s)^2}. \tag{8}$$

We assume number Nc to be independent of temperature. It is convenient to fit the melting curve choosing the reference point at $T_0, p = 0$. The corresponding value $\sigma = \sigma_0$ can be taken from the experiments on the nucleation kinetics [6], where σ_0 is a single important fitting parameter of the theory.

Number $\mathrm{Nc}^{1/3}$ for the normally melting substances is close to 0.5. Actually, combinations (7) and (8) introduced to determine the surface tension at the crystal–liquid phase boundary imply the applicability of a phe-

nomenological approach based on thermodynamical scaling. The surface tension is assumed to be an explicit function of temperature only, whereas the pressure corresponds to this temperature at the melting curve or at its metastable continuation, according to approximation (4), toward the $p < 0$ range. Similar to the case of vapor nuclei in an overheated liquid, we will neglect the correction to σ_0 due to the curved surface of the crystalline nuclei.

3. The values of parameters determining number Nc for several substances at similar points of melting curves under zero (atmospheric) pressure are presented in the table. Surface tension σ_0 is taken from [6], except for the values for sodium [2] and argon. For argon, σ_0 is determined using condition $\mathrm{Nc}^{1/3} = 0.5$ with the values of T_0, v_S, and ΔH taken from [11].

Condition Nc = const allows us to estimate for each of the substances under discussion how the surface tension changes throughout the melting curve and its metastable continuation to the region $T < T_0$, $p < 0$. To calculate $\sigma(T)$ based on (7), we should know entropy jump Δs and the specific volume of the crystal phase at different points of the $p_{SL} = f(T)$ curve. These values are taken from the published data for $p_{SL} > 0$ and through the use of approximations consistent with the Simon equation for $p_{SL} < 0$ [10]. The calculations of $\sigma(T)$ are illustrated in Fig. 1 for mercury and argon and in Fig. 2 for tin, lead, and sodium. The values of σ are denoted by squares in the temperature range where the kinetics of nucleation was experimentally studied [6]. The points corresponding to the calculations using condition Nc = const and the published experimental data on

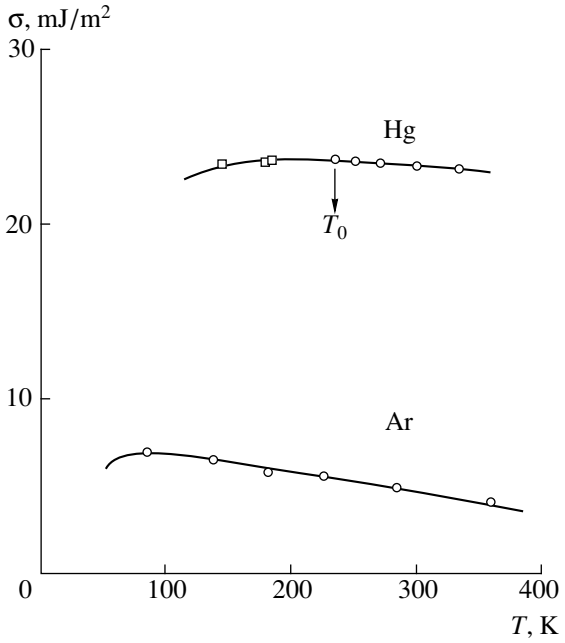

Fig. 1. Temperature dependence of the surface tension of argon and mercury at the melting curve.

ΔH and v_S are denoted by circles. To plot the continuous curves, we used the extrapolation for the ΔH and v_S values. Temperatures T_0 for mercury and tin are indicated by arrows. For the other substances in Figs. 1 and 2, temperature T_0 corresponds to the last left point (circle). The values of σ marked by squares correspond to negative pressures, since the spontaneous crystallization was observed [6] for a finite supercooling of the

Parameters characterizing the crystal–liquid equilibrium in a number of substances at atmospheric pressure; Nc is dimensionless combination (8)

Substance	T_0, K	v_S, 10^{-3} m^3/kg	ΔH, kJ/kg	σ_0, mJ/m^2	$\mathrm{Nc}^{1/3}$
Sodium	370.8	1.019	115.2	20	0.50
Copper	1356	0.119	203.1	200	0.54
Silver	1235	0.102	104.7	143	0.55
Indium	429.8	0.139	28.4	31	0.49
Tin	505.0	0.139	60.7	60	0.54
Mercury	234.3	0.070	11.5	23	0.51
Lead	600.0	0.091	22.6	40	0.50
Argon	83.8	0.608	29.8	7	0.5
Tetrachloromethane	250.6	0.570	16.4	6.7	0.47
Benzene	278.6	0.990	128.2	21.7	0.54
Gallium	302.9	0.175	80.3	40	0.41
Antimony	903.7	0.152	163.9	101	0.41
Bismuth	544.5	0.103	52.6	69	0.55
Water	273.2	1.090	334.4	28.7	0.41

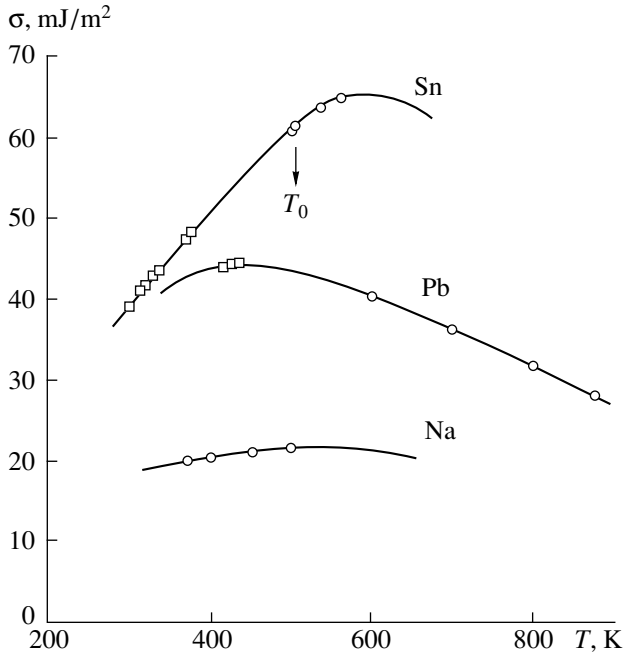

Fig. 2. Temperature dependence of the surface tension of tin, lead, and mercury at the melting curve.

liquid, $T < T_0$. Here, the projection mapping the points at given T falls within the portion of the melting curve where $p < 0$. This does not disagree with the fact that the σ_0 values were determined from the experiments on the nucleation kinetics at fixed ΔH and v_S taken at T_0.

The width of the temperature range corresponding to the variation of σ in Figs. 1 and 2 depends on the available data for ΔH and v_S at high pressures. For argon, the extreme right point corresponds to a pressure of 1770 MPa [11]; for mercury, 2000 MPa [12]; for Sn, 2600 MPa [13]; for Pb, 5000 MPa [14]; and for Na, 2200 MPa [15]. A conventional method used for estimating $\sigma(T)$ at the melting curve results in a decrease of the surface tension with temperature increase at $p > 0$. In addition, we observe a peak in σ and reveal a tendency to the decrease of σ with temperature within the negative pressure range.

Nonmonotonic behavior of $\sigma(T)$ at the melting curve is caused by specific features characterizing changes in the states of a coexisting crystal and liquid. Although the difference of densities $\rho_S - \rho_L$ decreases with an increase in temperature, the densities ρ_S and ρ_L themselves increase. The elasticity $\left(\frac{\partial p}{\partial \rho}\right)_T$ of both phases characterizing their thermodynamic stability also increases. On the contrary, approaching the spinodal state $\left(\frac{\partial p}{\partial \rho}\right)_T = 0$ along the melting curve, the crystal and liquid turn out to be stretched, i.e., at $T/T_0 \ll 1$ [10].

The values of σ_0 for substances presented in the table are determined from the experiments on spontaneous crystallization using the theory of homogeneous nucleation. This method is sufficiently reliable, and the estimates of different authors lend support to it. However, the surface tension at the crystal–liquid boundary was determined based on condition Nc = const [see (8)]. This condition following from experiments on the nucleation kinetics requires, nevertheless, further verification.

REFERENCES

1. *Physics and Chemistry of the Organic Solid State* (Wiley, New York, 1965; Mir, Moscow, 1967), Vol. 1.
2. M. P. Dokhov, Metally, No. 4, 28 (1999).
3. J. W. Gibbs, *Thermodynamics*, in *The Collected Works of J. Willard Gibbs* (Yale Univ. Press, New Haven, 1948; Gostekhteorizdat, Moscow, 1950).
4. Ya. B. Zel'dovich, Zh. Éksp. Teor. Fiz. **12**, 525 (1942).
5. V. P. Skripov, *Metastable Liquids* (Nauka, Moscow, 1972; Wiley, New York, 1974).
6. V. P. Skripov and V. P. Koverda, *Spontaneous Crystallization of Supercooled Liquids* (Nauka, Moscow, 1984).
7. V. G. Baĭdakov, *Superheating of Cryogenic Fluids* (Ural. Otd. Ross. Akad. Nauk, Yekaterinburg, 1995).
8. D. G. Thomas and L. A. K. Staveley, J. Chem. Soc., No. 12, 4569 (1952).
9. H. Hollomon and D. Turnbull, in *Nucleation. Progress in Metal Physics* (Pergamon, London, 1953; Moscow, 1956), Vols. 3–4.
10. V. P. Skripov and M. Z. Faĭzullin, Teplofiz. Vys. Temp. **37**, 814 (1999) [High Temp. **37**, 784 (1999)].
11. P. H. Lahr and W. G. Eversole, J. Chem. Eng. Data **7**, 42 (1962).
12. M. P. Vukalovich, A. I. Ivanov, L. A. Fokin, and A. T. Yakovlev, *Thermal Characteristics of Mercury* (Izd. Standartov, Moscow, 1971).
13. M. E. Cavalery, T. G. Plymate, and J. H. Stout, J. Phys. Chem. Solids **49**, 945 (1988).
14. V. D. Urlin, Zh. Éksp. Teor. Fiz. **49**, 485 (1965) [Sov. Phys. JETP **22**, 341 (1965)].
15. V. A. Ivanov, I. N. Makarenko, A. M. Nikolaenko, and S. M. Stishov, Phys. Lett. A **47**, 75 (1974).

Translated by T. Galkina

Doklady Physics, Vol. 45, No. 6, 2000, pp. 259–264. Translated from Doklady Akademii Nauk, Vol. 372, No. 6, 2000, pp. 753–758.

PHYSICS

Excitation of Singlet Levels for a Magnesium Atom by Electron Impact

Yu. M. Smirnov

Presented by Academician V.V. Osiko September 27, 1999

Received September 7, 1999

1. Although studies of excitations of singlet levels for a magnesium atom have been undertaken repeatedly, the authors of the majority of publications restricted their investigations to transitions from the lowest levels, primarily from the resonance $3p\,^1P_1^0$-level. This is true for both earlier experimental papers [1, 2] and much more recent ones [3]. In the theoretical papers [4–6], excitation of the same level was also studied. Moreover, excitation of the $4s^1S_0$- and $3d^1D_2$-levels was investigated only in the recent paper [7].

Only in two papers [8, 9], the excitation of higher singlet levels of a magnesium atom was studied. In [8], the cross sections and optical excitation functions (OEFs) for 17 spectral lines relevant to transitions between singlet levels have been measured. For the *S*-series, the measurements were carried out up to the value of the principal quantum number $n = 9$, and for the *D*-series, even up to $n = 13$. The most intense lines were studied by the method of intersecting beams, while a vapor-filled cell was employed for investigating less intense ones. For the main part of the experiment, the current density of the electron beam was as much as 3–7 mA/cm^2, and the width of the energy distribution was 0.8–1.0 eV (for 90% of the electrons). For studying the structure of the OEF, an electrostatic velocity selector was used, which allowed one to reduce the width of the electron-energy distribution to 0.3–0.4 eV at the expense of simultaneously decreasing the beam current to ~1 μA.

The primary objective of the subsequent study [9] was to investigate the OEF structure within the energy range from the excitation threshold to 11 eV. This was done with the purpose of studying the formation mechanisms for such a structure. Owing to usage of a trochoidal electron monochromator, the full width at the half-maximum for the electron energy distribution function amounted to 0.1 eV. Ten OEFs were recorded, four of them belonging to the singlet-term system. In [9], the spectral resolution was rather poor. As a consequence, for example, the 470.299-nm and 473.003-nm lines were not resolved. However, the overall OEF obtained can be considered completely related to the 470.299-nm line, the excitation cross section of which is larger by approximately an order of magnitude than that for the 473.003-nm line.

2. From the above discussion, it follows that the excitation of the lowest singlet levels for a magnesium atom has been studied rather thoroughly, whereas the excitation of higher levels for the singlet-term system had been investigated only in experimental paper [8] and was not treated theoretically. In the present study, the method of extended intersecting beams is employed for investigating the excitation of singlet levels of a magnesium atom. The technique and experimental procedure, as well as control experiments and analysis of experimental errors, have been covered many times in the author's papers (see, e.g., [10]). Therefore, there is no reason for repeatedly describing them in the present paper. Only the main experimental parameters defining the conditions for performing this study are briefly outlined.

Throughout the entire operating range of electron energies, the current density of the electron beam did not exceed 1.0 mA/cm^2, with the width of the electron-energy distribution function being 0.9–1.0 eV (for 90% of the electrons). For the main part of the 250- to 600-nm spectral range, the spectral resolution was about 0.1 nm and about 0.2 nm outside this range. At a crucible temperature of 750 K, the atomic concentration in the beam-intersection region was 1.0×10^{11} cm^{-3} for the main part of the experiment, and it was reduced to $(1–2) \times 10^9$ cm^{-3} in studies of the head line for the resonance series.

It is well known [2] that, at low electron energies, the radiation relevant to the head line (with a wavelength of 285.213 nm) of the resonance series for MgI possesses a high degree of polarization, which approaches 100% near the threshold. Special measurements of the monochromator spectral transmission for linearly polarized radiation have shown that the MDP-3 diffractometer used in this study introduced an error not exceeding ±10% throughout the entire spectral range

Moscow Institute of Power Engineering (Technical University), ul. Krasnokazarmennaya 14, Moscow, 111250 Russia

1028-3358/00/4506-0259$20.00

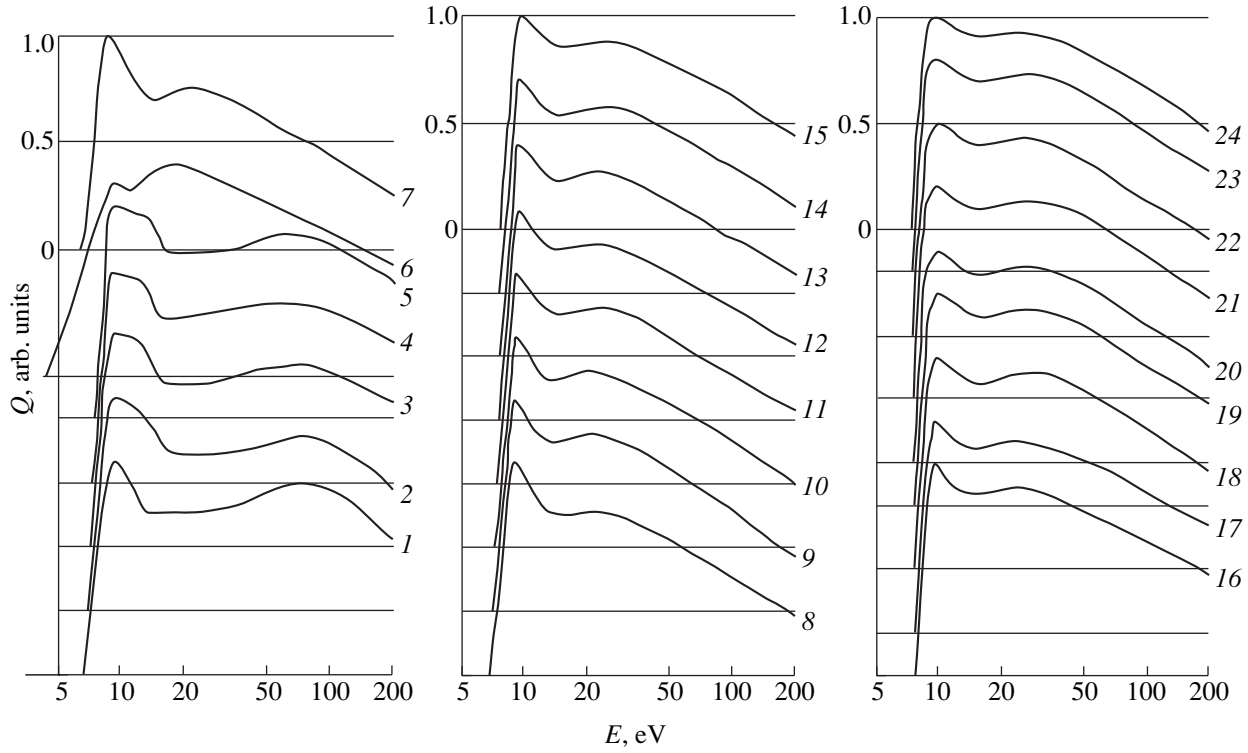

Fig. 1. Optical-excitation functions for a magnesium atom.

even in the case of completely polarized radiation. Therefore, in this study, we introduced no corrections for possible linear polarization of the radiation.

3. For an electron-exciting energy of 30 eV, the values of 46 excitation cross sections were measured for the MgI spectral lines belonging to the singlet-term system and lying within the spectral range between 202 and 822 nm. Twenty-four OEFs were recorded within the electron energy range from the excitation threshold to 200 eV. The experimental results are presented in Table 1. There, along with the transitions and the number of an OEF according to the sequence of the curves in Fig. 1, the values for the following quantities are given: the wavelength λ; the internal quantum number J; the energies of the lower (E_l) and upper (E_u) levels; the cross sections for an electron energy of 30 eV (Q_{30}) and at the OEF maximum (Q_{max}); and, finally, the position of the maximum for the energy E(max).

In [8], for ^1S- and ^1D-series of MgI, the dependence of the spectral-line excitation cross section Q on the principal quantum number for the upper level n was found to be of the form

$$Q = A_i n^{-\alpha_i}, \quad (1)$$

where A_i and α_i are constants with characteristic values for each of the spectral series. However, it is worth noting that deviations from this dependence for some experimental points were found in [8] to be rather large. This is true for initial portions of both series as well as for certain higher terms of the D-series.

The dependence $Q = f(n)$ plotted according to the results of the present study is shown in Fig. 2 in a logarithmic scale. The choice of the coordinate system is dictated by the fact that in this system power-law

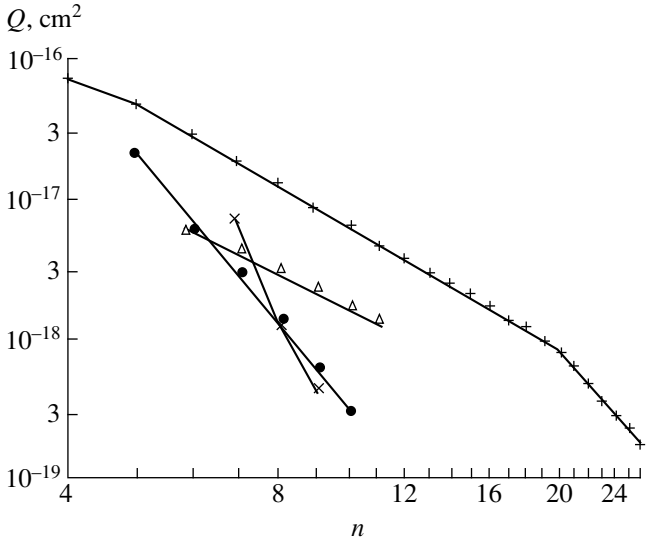

Fig. 2. Dependence $Q = f(n)$ for singlet spectral series of MgI: (•) $3p\,^1P_1^0 - ns\,^1S_0$; (×) $3d\,^1D_2 - np\,^1P_1^0$; (+) $3p\,^1P_1^0 - nd\,^1D_2$; (△) $3d\,^1D_2 - nf\,^1F_3^0$.

Table 1. Excitation cross sections for a magnesium atom

λ, Nm	Transition	J	E_l, cm^{-1}	E_u, cm^{-1}	Q_{30}, 10^{-18} cm^{-2}	Q_{max}, 10^{-18} cm^{-2}	E(max), eV	OEF
202.582	$3s^2\,^1S$–$4p\,^1P^0$	0–1	0	49346	6.66	–	–	–
269.245	$3p\,^3P^0$–$7d\,^1D$	2–2	21911	59041	0.27	0.35	9.0	10
276.522	$3p\,^3P^0$–$6d\,^1D$	1–2	21870	58023	0.82	1.02	9.0	9
276.834	$3p\,^3P^0$–$6d\,^1D$	2–2	21911	58023	1.77	2.22	9.0	9
285.166	$3p\,^3P^0$–$5d\,^3D$	2–1, 2, 3	21911	56968	1320.	1450.	–	–
285.213	$3s^2\,^1S$–$3p\,^1P^0$	0–1	0	35051			18	6
291.545	$3d\,^1D$–$3p3d\,^1D^0$	2–2	46403	80693	0.28	–	–	–
377.983	$3p\,^1P^0$–$26d\,^1D$	1–2	53051	61500	0.18	–	–	–
378.169	$3p\,^1P^0$–$25d\,^1D$	1–2	35051	61487	0.24	–	–	–
378.398	$3p\,^1P^0$–$24d\,^1D$	1–2	35051	61471	0.30	–	–	–
378.670	$3p\,^1P^0$–$23d\,^1D$	1–2	35051	61452	0.38	–	–	–
378.957	$3p\,^1P^0$–$22d\,^1D$	1–2	35051	61432	0.49	0.53	10.0	24
379.316	$3p\,^1P^0$–$21d\,^1D$	1–2	35051	61407	0.65	0.69	10.0	23
379.717	$3p\,^1P^0$–$20d\,^1D$	1–2	35051	61379	0.79	0.85	10.0	22
380.180	$3p\,^1P^0$–$19d\,^1D$	1–2	35051	61346	0.96	1.02	10.0	21
380.741	$3p\,^1P^0$–$18d\,^1D$	1–2	35051	61308	1.25	1.34	10.0	20
381.412	$3p\,^1P^0$–$17d\,^1D$	1–2	35051	61262	1.39	1.51	9.8	19
382.200	$3p\,^1P^0$–$16d\,^1D$	1–2	35051	61208	1.75	1.90	9.8	18
383.168	$3p\,^1P^0$–$15d\,^1D$	1–2	35051	61142	2.14	–	–	–
384.370	$3p\,^1P^0$–$14d\,^1D$	1–2	35051	61060	2.56	2.88	9.5	17
385.886	$3p\,^1P^0$–$13d\,^1D$	1–2	35051	60958	2.95	3.39	9.5	16
387.831	$3p\,^1P^0$–$12d\,^1D$	1–2	35051	60828	3.68	4.28	9.5	15
390.386	$3p\,^1P^0$–$11d\,^1D$	1–2	35051	60659	4.68	5.44	9.2	14
393.840	$3p\,^1P^0$–$10d\,^1D$	1–2	35051	60435	6.55	7.90	9.2	13
398.421	$3p\,^1P^0$–$10s\,^1S$	1–0	35051	60143	0.32	–	–	–
398.675	$3p\,^1P^0$–$9d\,^1D$	1–2	35051	60127	8.30	10.5	9.0	12
405.469	$3p\,^1P^0$–$9s\,^1S$	1–0	35051	59707	0.61	0.77	9.0	5
405.751	$3p\,^1P^0$–$8d\,^1D$	1–2	35051	59689	12.9	16.1	9.0	11
407.506	$3p\,^3P^0$–$3d\,^1D$	1–2	21870	46403	0.165	–	–	–
408.133	$3p\,^3P^0$–$3d\,^1D$	2–2	21911	46403	0.22	–	–	–
416.510	$3p\,^1P^0$–$8s\,^1S$	1–0	35051	59053	1.32	1.65	9.0	4
416.727	$3p\,^1P^0$–$7d\,^1D$	1–2	35051	59041	17.9	23.3	9.0	10
435.191	$3p\,^1P^0$–$6d\,^1D$	1–2	35051	58023	28.7	35.9	9.0	9
435.453	$3p\,^1P^0$–$7s\,^1S$	1–0	35051	58009	2.74	3.47	9.0	3
470.299	$3p\,^1P^0$–$5d\,^1D$	1–2	35051	56308	46.2	63.3	8.8	8
473.003	$3p\,^1P^0$–$6s\,^1S$	1–0	35051	56186	6.20	8.38	9.0	2
552.840	$3p\,^1P^0$–$4d\,^1D$	1–2	35051	53134	66.8	94.1	8.5	7
571.109	$3p\,^1P^0$–$5s\,^1S$	1–0	35051	52556	21.7	28.2	9.0	1
696.540	$3d\,^1D$–$11f\,^1F^0$	2–3	46403	60755	1.35	–	–	–
706.040	$3d\,^1D$–$10f\,^1F^0$	2–3	46403	60562	1.67	–	–	–
719.317	$3d\,^1D$–$9f\,^1F^0$	2–3	46403	60301	2.23	–	–	–
738.700	$3d\,^1D$–$9p\,^1P^0$	2–1	46403	59936	3.39	–	–	–
738.768	$3d\,^1D$–$8f\,^1F^0$	2–3	46403	59935				

Table 2. Values of A_i and α_i for singlet series of a magnesium atom

Series	n		α_i		A_i, cm^2	
	this study	[8]	this study	[8]	this study	[8]
$3p^1P_1^0$–ns^1S_0	5–10	5–9	6.12	6	4.00×10^{-13}	2.6×10^{-14}
$3p^1P_1^0$–nd^1D_2	5–20	4–13	2.91	4.5	2.64×10^{-15}	8.8×10^{-15}
	20–26		5.88		3.75×10^{-10}	
$3d^1D_2$–$np^1P_1^0$	7–8		13.2		9.85×10^{-7}	
	8–9		8.74		9.30×10^{-11}	
$3d^1D_2$–$nf^1F_3^0$	6–11		2.49		5.13×10^{-16}	

dependence (1) is represented by straight lines. This allows the power-law dependence, as well as possible deviations from it, to be more clearly revealed. The numerical values of the constants A_i and α_i are given in Table 2.

As is shown in [11], the singlet terms for the 3*snl*-configurations ($l = s, p, d$), corresponding to a single-electron excitation of a magnesium atom, are perturbed by the action of the shifted terms of the 3*pnl*-configuration. Only for the $nf^1F_3^0$ terms is the quantum effect small in its absolute value and changes within a narrow range as the principle quantum number varies within the interval n = 4–12. Thus, the $^1F^0$-series may be considered as unperturbed, and the dependence $Q = f(n)$ must be exactly consistent with power law (1). From Table 1, it is seen that two pairs of lines in the red part of the spectrum, which are associated with transitions from the $^1F^0$- and $^1P^0$-levels, could not be experimentally resolved. Therefore, we can isolate the values of the cross sections for the lines of the $^1F^0$-series with n = 7 and 8 from the total cross sections for the unresolved pairs of lines by interpolating the power-law dependence in Fig. 2. The remaining values of the cross sections are assigned to the lines of the $3d^1D_2$–$np^1P_1^0$-series with n = 8 and 9 (by the way, the triplet transition contributes about 1% to one additional unresolved pair of lines with wavelengths of 285.166 and 285.213 nm).

The quantum defect for the ns^1S_0, $np^1P_1^0$, and nd^1D_2 terms is equal to 1.5, 1.0, and 0.5, respectively, and varies rather markedly as the principle quantum number changes from 3 to 10. Sizable perturbations are also observed for similar terms of a calcium atom [11]. However, for the terms under consideration for a magnesium atom, the quantum defect varies monotonically, whereas for a calcium atom the monotonicity is essentially broken for all three perturbed series. As a consequence, the behavior of the cross sections for the $^1S_0$-, $^1P_1^0$-, and $^1D_2$-series of a calcium atom substantially deviates from the power-law dependence [12], whereas for a magnesium atom, such deviations are extremely small and exceed experimental errors only for $^1D_2$-series.

Firstly, such deviation exists at the beginning of the series at n = 4; similar deviation in this series has been previously discovered for a calcium atom [12]. Secondly, the rate of the decrease of the cross section with increasing n for a magnesium atom changes at about n = 20, which is also seen from Table 2. However, an alternative explanation for this deviation can be put forward which is not associated with the excitation of levels. It was shown in [13] that, in the experiments with extended intersecting beams, radiating transitions from levels having rather large lifetimes can be recorded. In particular, the lifetime of the bismuth levels was found to exceed 10^{-2} s [13]. Since the time of flight for atoms through the collision region is about 10^{-5} s, a major portion of excited atoms do not radiate in the field of view of the optical system but undergo nonradiating relaxation at the surface of the atomic collector. This fact can be taken into account by multiplying the measured cross section Q^* by the factor

$$\kappa = \frac{1}{1 - \frac{v\tau}{L}(1 - e^{-L/v\tau})}, \qquad (2)$$

where v is the average velocity of atoms, L is the flight distance, and τ is the proper lifetime for atoms in the excited state.

Up to now, experimental data concerning values for the lifetimes of high-lying $^1D_2$-levels of a magnesium atom are not known. Correct extrapolation of available data for low-lying levels towards higher n-values cannot be performed, as far as it was established in [14] that for low-lying $^1D_2$-levels of a magnesium atom, experimental values for the lifetimes behave irregularly and differ significantly (by one or two orders of magnitude!) from theoretical ones. This situation was confirmed later in [15], where it was also shown that the

Table 3. Comparison of values for Q_{max}, which are obtained in the present study and of those from [8]

Series	n	λ, nm	Q_{max}, 10^{-18} cm^2		Q[this study]/Q[8]
			this study	[8]	
$3s^1S_0$–$np^1P_1^0$	3	285.213	1450	860	1.69
$3p^1P_1^0$–ns^1S_0	5	571.109	28.2	5.2	5.43
	6	473.003	8.38	0.64	13.1
	7	435.453	3.47	0.24	14.5
	8	416.510	1.65	0.09	18.3
	9	405.469	0.77	0.04	19.2
$3p^1P_1^0$–nd^1D_2	4	552.840	94.1	15.0	6.26
	5	470.299	63.3	6.9	9.18
	6	435.191	35.9	2.5	14.4
	7	416.727	23.3	1.6	14.6
	8	405.751	16.1	0.68	23.6
	9	398.675	10.5	0.45	23.4
	10	393.840	7.90	0.37	21.3
	11	390.386	5.44	0.16	34.0
	12	387.831	4.28	0.11	38.9
	13	385.886	3.39	0.075	45.2

discrepancy between experimental and theoretical values of lifetimes for $^1D_2$-levels of magnesium atoms could be eliminated if the perturbance caused by the terms of the 3*pnl*-configuration was taken into account. From the above considerations, it appears that currently, due to the lack of reliable data on lifetimes for low-lying levels of a magnesium atom, we cannot quantitatively examine the conjectured reason for the deviation of the dependence $Q = f(n)$ from the power law for $^1D_2$-series of MgI at $n \geq 20$.

We now turn to the comparison of the absolute values for the cross sections and consider the data presented in Table 3. The values of the cross sections for a resonance line obtained in the present study are 1.7 times as large as those obtained in [8]. For the lowest investigated transitions of the $^1S_0$- and $^1D_2$-series, this factor ranges up to 5.4 and 6.3, respectively. The discrepancy factor increases respectively to 13.1 and 9.2 for the next terms of the same series, and 19.2 and 45.2 for the highest terms recorded in [8]. If we extrapolate the serial dependence found in [8] for the $^1D_2$-series to the cross-section value for $n = 26$, which was studied in the present paper, then we would find for the cross section $Q(26)$ a value of 2.5×10^{-21} cm^2. This value is by about two orders of magnitude lower than that measured in the present study, and recording it is unfeasible with the available sensitivity of our setup. On the other hand, the straightforward correlation of the results of the present study and of paper [8] with theoretical values of the cross sections for the lowest excited singlet $4s^1S_0$-, $3p^1P_1^0$-, and $3d^1D_2$-levels of a magnesium atom is incorrect. Firstly, in both experiments, the cross sections for the excitation of spectral lines, but not levels, were measured. Secondly, in both experimental studies, the cross sections for the allowed infrared transitions from the $4s^1S_0$- and $3d^1D_2$-levels with corresponding wavelengths of 1183 and 881 nm, respectively, were not measured.

However, it should be borne in mind that the contribution of the cascade transitions for the three levels under discussion cannot be too large and, according to our estimate, comprises 10–20% of the total excitation cross section. On the other hand, the cross sections for the head lines of the *S*- and *D*-series can be obtained by extrapolating the above-discussed serial regularities. Allowing for these considerations, we can obtain the following values of the cross sections (expressed in units of 10^{-16} cm^2) for head lines at the electron energy of 30 eV (according to the present study, [8], and [7], respectively): 0.88, 0.43, and 1.03 for the $4s^1S_0$-level; 1.32, 0.79, and 1.58 for the $3p^1P_1^0$-level; and 1.07, 0.28, and 1.70 for the $3d^1D_2$-level. Thus, the results of the present study are by 15, 16, and 37%, respectively, lower than the theoretical values for the three levels under discussion. The results of [8] are 2.4, 2.0, and 6.1 times as large as the theoretical values, respectively.

At the same time, it is worth noting that the OEFs recorded in the present study coincide, within the experimental errors, with those obtained previously in [8] but substantially differ from the theoretical OEFs [7] by the general behavior of the energy dependence. Apparently, this discrepancy cannot be completely explained by the contribution of cascade population.

REFERENCES

1. F. Karstensen and H. Koster, Astron. Astrophys. **13**, 116 (1971).
2. D. Leep and A. Gallagher, Phys. Rev. A **13**, 148 (1976).
3. M. J. Brunger, J. L. Riley, R. E. Scholten, and P. J. O. Teubner, J. Phys. B **21**, 1639 (1988); **22**, 1431 (1989).
4. J. Mitroy and I. E. McCarthy, J. Phys. B **22**, 641 (1989).
5. I. E. McCarthy, K. Ratnavelu, and Y. Zhou, J. Phys. B **22**, 2597 (1989).
6. G. D. Meneses, C. B. Pagan, and L. E. Machado, Phys. Rev. A **41**, 4740 (1990).
7. R. E. H. Clarc, G. Csanak, and J. Abdallah, Jr., Phys. Rev. A **44**, 2874 (1991).
8. I. S. Aleksakhin, I. P. Zapesochnyĭ, I. I. Garga, *et al.*, Opt. Spektrosk. **34**, 1053 (1973).
9. O. B. Shpenik, I. P. Zapesochnyĭ, E. É. Kontrosh, *et al.*, Zh. Éksp. Teor. Fiz. **76**, 846 (1979) [Sov. Phys. JETP **49**, 426 (1979)].
10. Yu. M. Smirnov, J. Phys. II France **4**, 23 (1994).
11. G. Risberg, Ark. Fys. **28**, 381 (1965); **37**, 231 (1968).
12. A. N. Kuchenev and Yu. M. Smirnov, Phys. Scr. **51**, 578 (1995).
13. Yu. M. Smirnov, Pis'ma Zh. Tekh. Fiz. **11**, 689 (1985) [Sov. Tech. Phys. Lett. **11**, 287 (1985)].
14. L. Liljeby, A. Lindgard, S. Mannervik, *et al.*, Phys. Scr. **21**, 805 (1980).
15. T. N. Chang, Phys. Rev. A **41**, 4922 (1990).

Translated by V. Tsarev

Doklady Physics, Vol. 45, No. 6, 2000, pp. 265–268. Translated from Doklady Akademii Nauk, Vol. 372, No. 4, 2000, pp. 476–479.

TECHNICAL PHYSICS

Solution to the Transport Equation of Geometrical Optics for Arbitrary Wave Fields in Nonhomogeneous Media

V. D. Gusev and V. E. Kunitsyn

Presented by Academician V.V. Migulin June 26, 1999

Received July 5, 1999

The propagation of waves—independently of their nature—is a subject of investigation in various fields of physics. Wave processes whose general theory is determined by conditions of geometrical optics are of special interest. There exist two basic relations in geometrical optics: the eikonal equation and the transport equation. In this paper, we concentrate our attention on the transport equation, which is associated with logical incompleteness of its solution.

As is well known, the transport equation for a scalar field exhibits the form

$$2\nabla A\nabla\phi + A\Delta\phi = 0. \quad (1)$$

Here, A and ϕ are the amplitude and phase of a wave, respectively. Since, within geometrical optics

$$\nabla\phi = \mathbf{p} = n\mathbf{S}, \quad (2)$$

where n is the refractive index and $\mathbf{S}$ is the unit vector of the normal to the wave front, then (1) transforms into

$$n\frac{dA^2}{d\sigma} + A^2\mathrm{div}\mathbf{p} = 0. \quad (3)$$

Here, $\boldsymbol{\sigma}$ is directed along the normal to the wave-surface front. With allowance for (2), expression (3) transforms into

$$\frac{d}{d\sigma}(A^2n) + A^2n\mathrm{div}\mathbf{S} = 0. \quad (4)$$

The solution to equation (4) can be written in the form

$$A^2(\sigma)n(\sigma) = (A^2n)_{\sigma=\sigma_0}\exp\left(-\int_{\sigma_0}^{\sigma}\mathrm{div}\mathbf{S}\,d\sigma\right), \quad (5)$$

where $(A^2n)_{\sigma=\sigma_0}$ corresponds to the initial value of relevant variables. Thus, the solution to the transport equation written out in the form (1), (3), or (4) is reduced to finding a possibility for explicitly representing div$\mathbf{S}$ and performing relevant integration in (5). Explicit representation of div$\mathbf{S}$ appears to be a rather intricate problem. The general representation of div$\mathbf{S}$ is outlined in the well-known course of higher mathematics by V.I. Smirnov (see [2, vol. 4]):

$$\mathrm{div}\mathbf{S} = \frac{d}{d\boldsymbol{\sigma}}\ln D, \quad (6)$$

where

$$D(\sigma) = \frac{\partial(x, y, z)}{\partial(\xi, \eta, \sigma)} \quad (7)$$

represents the Jacobian for the conversion from the Cartesian coordinates (x, y, z) to the ray coordinates (ξ, η, σ) for an arbitrary point belonging to the wave-front surface:

$$\phi(x, y, z) = \mathrm{const}. \quad (8)$$

The solution to the transport equation given in the from (5)–(7) was included into one of the latest monographs devoted to this subject [3]. The monographs [2] and [3] are separated in time by approximately 30 years. To our knowledge, any new results in this field have not been obtained until now. The complicated form of the expression for div$\mathbf{S}$ (6), (7) makes it impossible to derive an explicit solution for A in a majority of problems important for practice. The simplest solution to the transport equation corresponds to the case of wave propagation through plane-laminated media [4].

Another representation for div$\mathbf{S}$ is also known [5]:

$$\mathrm{div}\mathbf{S} = 2H, \quad (9)$$

where H corresponds to the average curvature of the wave-front surface. However, this representation is still sufficiently complicated, since it is necessary to determine principal radii of curvature at each point of the surface (8), with allowance for its various possible orientations in space.

Below, we present a new solution to the problem of determining div$\mathbf{S}$, which enables us to perform an integration in (5) in the simplest way.

Moscow State University,
Vorob'evy gory, Moscow, 119899 Russia

1028-3358/00/4506-0265$20.00

As is well known [6], the general integral definition for div**S** is given in the form

$$\mathrm{div}\mathbf{S} = \lim_{V\to 0}\frac{\iint_\Sigma \mathbf{S}\mathbf{N}d\Sigma}{V}, \tag{10}$$

where Σ is a surface bounding the volume V and **N** is an external normal to this surface. Since the surface Σ is arbitrary, it can be chosen to have a cylindrical shape, with the lateral walls being parallel to the **S** rays, while the bases of the cylinder are the cross sections for the ray tubes by planes parallel to the (x, y)-plane, and the z-axis is considered as the polar axis. Since **SN** = 0 on the lateral walls, the integral in (10) is calculated only over the bases. As a result, this integral can be presented, with an accuracy to the second-order terms, in the form

$$\int_\Sigma S_z d\Sigma = \int_{\Sigma_2} S_z(\sigma+\delta\sigma)d\Sigma - \int_{\Sigma_1} S_z(\sigma)d\Sigma \simeq \delta S_z \delta\Sigma, \tag{11}$$
$$\delta S_z = S_z(\sigma+\delta\sigma) - S_z(\sigma) \approx \frac{dS_z}{d\sigma}\delta\sigma.$$

Within the same approximation, simple considerations yield the obvious result

$$V \simeq S_z \delta\sigma\, \delta\Sigma. \tag{12}$$

Substituting (11) and (12) into (10) and passing to the limit, we obtain the following rather simple expression for div**S**:

$$\mathrm{div}\mathbf{S} = \frac{d}{d\sigma}\ln S_z. \tag{13}$$

A similar expression for the divergence of the unit-vector field could be derived on the basis of general concepts of differential geometry. In [6], the expression is presented for the difference between the ray-tube areas that relate to two close wave fronts (8) separated by the distance $\delta\sigma$:

$$\delta\Sigma = -2Hg\,\delta\sigma\,\delta\xi\,\delta\eta, \tag{14}$$

Here, $g = \sqrt{g_{11}g_{22} - g_{12}^2}$ represents the first quadratic form, while H is the average curvature of the wave-front surface (8). In this case, evidently,

$$\delta\Sigma = \delta g\,\delta\xi\,\delta\eta. \tag{15}$$

It follows from (14) and (15) that, in the limiting case,

$$2H = -\frac{d}{d\sigma}\ln g. \tag{16}$$

Combining (16) and (9), we obtain

$$\mathrm{div}\mathbf{S} = -\frac{d}{d\sigma}\ln g. \tag{17}$$

It is well known that for the wave-front surface written out in the form (8), the relation

$$gS_z = 1 \tag{18}$$

is valid [7], which confirms the identity of (13) and (17).

The explicit expression obtained for div**S** (13) enables us to perform integrating transport equation (4). As a result, we obtain

$$A = \frac{A_0\sqrt{n(x_0, y_0, z_0)}S_z(x_0, y_0, z_0)}{\sqrt{n(x, y, z)S_z(x, y, z)}} = \frac{A_0\sqrt{p_{z_0}(x_0, y_0, z_0)}}{\sqrt{p_{z_0}(x, y, z)}}. \tag{19}$$

A particular case (19) for the plane-laminated medium was presented in [4].

The normal vector **p** is known to be determined from the differential equation [7]

$$\frac{d\mathbf{p}}{d\sigma} = \nabla n. \tag{20}$$

Therefore, we obtain from (20)

$$p_z = p_{z_0}(x_0, y_0, z_0) + \int_{\sigma_0}\frac{\partial n}{\partial z}d\sigma, \tag{21}$$

where $p_{z_0}(x_0, y_0, z_0)$ are specified for the initial step of integration in (21) when $\sigma = \sigma_0$.

Thus, expression (19) provides the complete solution to the problem under consideration. Practical application of (19) is restricted only by the possibility of performing an integration in (21), which presents a rather trivial problem.

It should be emphasized that solution (19) to the transport equation is valid under the following conditions:

(i) The wave-front surface (8) is free of singular points.

(ii) The field of the unit vectors **S** has no intersecting points.

To illustrate the possibility of the practical application for the result obtained (19), we present a solution to one of the simplest problems for the wave propagation through a scattering medium.

We consider fluctuations of signal amplitudes in the course of wave propagation through a statistically homogeneous medium featuring the isotropic spatial correlation function. This presents a particular interest, since a similar problem was analyzed previously in [7].

According to the definition of the level χ, we obtain from (19)

$$\chi = \ln\frac{A}{A_0} = -\frac{1}{2}\ln\left(1+\frac{p_{z_1}}{p_{z_0}}\right) = -\frac{1}{2}\left(\frac{p_{z_1}}{p_{z_0}} - \frac{1}{2}\frac{p_{z_1}^2}{p_{z_0}^2} + \ldots\right). \quad (22)$$

This is valid provided that fluctuations of the level are small, i.e., $|p_{z_1}| \ll |p_{z_0}|$, where

$$p_{z_1} = \int_{\sigma_0}^{\sigma}\frac{\partial n}{\partial z}d\sigma = \int_{\sigma_0}^{\sigma}\frac{\partial n_1}{\partial z}d\sigma, \quad (23)$$

since $n = 1 + n_1$.

It is evident from (22) and (23) that, within accuracy to the second-order terms, $\langle\chi\rangle = 0$.

For the given particular problem, the basic goal is calculating the variance $\langle\chi^2\rangle$ of level fluctuations.

While performing a relevant procedure for the determining the value of $\langle\chi^2\rangle$, it is necessary to take into account that the argument $n_1(\mathbf{r})$ in the integrand (23) has the form

$$\mathbf{r} = \int_{\sigma_0}^{\sigma}\frac{\mathbf{p}d\sigma}{1+n_1}. \quad (24)$$

Thus, for determining $\langle\chi^2\rangle$ in accordance with (22)–(24), we need detailed analysis for all terms of the second-order with respect to $\sqrt{\langle n_1^2\rangle}$. Let the path of the propagating wave lie in the (x, z) plane, with ϑ_0 being the polar angle for this path. Then,

$$p_{z_1} = \int\left(\frac{\partial n}{\partial x'}S_0 + \frac{\partial n}{\partial z'}C_0\right)d\sigma, \quad (25)$$

where $S_0 = \sin\vartheta_0$, $C_0 = \cos\vartheta_0$, while (x', z') are the coordinates of a point in the new coordinate system.

According to (21), in this coordinate system, the projections of the ray deviation have the forms

$$x' \sim \vartheta_1(\sigma - \sigma_0), \quad y' \sim \vartheta_1(\sigma - \sigma_0),$$
$$z' \sim \left[(\sigma - \sigma_0) - \frac{1}{2}\int_{\sigma_0}^{\sigma}\vartheta_1^2 d\sigma + \ldots\right]. \quad (26)$$

Here, ϑ_1 is the scattering angle. We can show that $\langle p_{z_1}^2\rangle = 0$ within accuracy to the second-order terms in $\sqrt{\langle n_1^2\rangle}$. In the case of the small-angle scattering, $\langle\vartheta_1^2\rangle \ll 1$. For isotropic scattering, the correlation function $R(\mathbf{r})$ has the form

$$R = \exp\left\{-\frac{(x_1-x_2)^2 + (y_1-y_2)^2 + (z_1-z_2)^2}{a^2}\right\}. \quad (27)$$

The result obtained indicates the necessity of allowance for the next terms in the expansion in series with respect to χ (22). Then,

$$\langle\chi^2\rangle = \frac{1}{16}\left\langle\left(\frac{p_{z_1}}{p_{z_0}}\right)^4\right\rangle. \quad (28)$$

When n corresponds to the Gaussian random process, it follows from (28) that

$$\langle\chi^2\rangle = \frac{3}{16}\left[\left\langle\left(\frac{p_{z_1}}{p_{z_0}}\right)^2\right\rangle\right]^2 = \frac{3}{16}(\langle\vartheta_1^2\rangle)^2.$$

In [7], for a similar problem, it was obtained that

$$\langle\chi_2^2\rangle = \frac{4}{3}\langle\vartheta_1^2\rangle\left(\frac{L}{a}\right)^2.$$

It is evident that in the case of small-angle scattering, with the conventional relation $\frac{a}{L} \ll 1$ being true, we have

$$\frac{\langle\chi^2\rangle}{\langle\chi_2^2\rangle} = \frac{9}{64}\langle\vartheta_1^2\rangle\left(\frac{a}{L}\right)^2 \ll 1. \quad (29)$$

The considerable discrepancy of the values for $\langle\chi^2\rangle$ could be related to the following arguments. When calculating

$$\mathrm{div}\mathbf{S} \simeq \mathrm{div}\mathbf{S}_1,$$

where

$$\mathbf{S}_1 = \int\nabla n_1 d\sigma, \quad (30)$$

it was assumed in [7] that

$$\mathrm{div}\mathbf{S}_1 = \int\Delta n_1 d\sigma. \quad (31)$$

In other words, the differentiation operator had been introduced into the integrand. However, such a procedure is incorrect, since the ray's trajectory in the integrand and, consequently, arbitrary points of the ray do depend on σ. Moreover, expression (30) follows from the solution to the variational problem. Hence, with the help of the relevant procedure [9], the left-hand side in (31) must naturally be associated with the variational derivative.

A considerable difference between the exact value of $\langle\chi^2\rangle$ and $\langle\chi_2^2\rangle$ presented in [7] indicates the importance of the solution obtained for the transport equa-

tion. Thus, solution (19) to the transport equation exhibits the complete form, which enables us to solve arbitrary problems, in particular, those of great practical importance. It should be emphasized that the solution is based on the proven theorem (17) having its own significance for determining the variation of the field of unit-vectors.

Thus, we have considered the phenomenon of diverging rays in the framework of geometrical optics. The exact expression for the divergence of the rays as a function of their angular components is determined. This result makes it possible to represent the solution to the transport equation in the form of an algebraic function for direction cosines of rays.

REFERENCES

1. M. B. Vinogradova, O. V. Rudenko, and A. P. Sukhorukov, *Theory of Waves* (Nauka, Moscow, 1979).
2. V. I. Smirnov, *A Course of Higher Mathematics* (Nauka, Moscow, 1957; Addison-Wesley, Reading, Mass., 1964), Vol. 4.
3. Yu. A. Kravtsov and Yu. A. Orlov, *Geometrical Optics of Inhomogeneous Media* (Nauka, Moscow, 1980).
4. V. L. Ginzburg, *Propagation of Electromagnetic Waves in Plasmas* (Nauka, Moscow, 1967; Pergamon Press, Oxford, 1970).
5. M. Lagally, *Mathematik und ihre Anwendungen in Monographien und Lehrbüchern. Vorlesungen über Vektor-Rechnung* (Akademic Verlag Gesellschaft, Leipzig, 1928; Moscow, 1936).
6. V. I. Smirnov, *A Course of Higher Mathematics* (Nauka, Moscow, 1967; Addison-Wesley, Reading, Mass., 1964), Vol. 2.
7. L. A. Chernov, *Wave Propagation in Randomly Inhomogeneous Media* (Nauka, Moscow, 1977; McGraw-Hill, New York, 1960).
8. B. D. Budak and S. V. Fomin, *Multiple Integrals and Series* (Moscow, 1967).
9. S. M. Rytov, Yu. A. Kravtsov, and V. I. Tatarskiĭ, *Introduction to Statistical Radio Physics* (Nauka, Moscow, 1978), Part 2.

Translated by O. Chernavskaya

Doklady Physics, Vol. 45, No. 6, 2000, pp. 269–272. Translated from Doklady Akademii Nauk, Vol. 372, No. 4, 2000, pp. 480–483.

TECHNICAL PHYSICS

A Method of Auxiliary Spline Currents for Wave-Diffraction Problems

A. G. Kyurkchan* and A. I. Stukov**

Presented by Academician A.L. Mikaélyan July 14, 1999

Received July 22, 1999

The method of discrete (or auxiliary) sources (MDS) proposed by V.D. Kupradze [1] and somewhat later by K. Yasuura [2], which was advanced further in a number of papers (see, e.g., [3, 4]), is one of the most efficient methods in solving boundary value problems for the Helmholtz equation. The method has been applied to a wide range of problems, although in some cases, the algorithms developed on the basis of the method were found to be unstable. This fact is explained in [5, 6], where a linkage between the method of auxiliary sources and the problem of analytic continuation for a wave field is established.

We consider, for definiteness, a two-dimensional external problem of diffraction, when the uniform Dirichlet boundary condition (for the total, i.e., incident and scattered fields) holds at the boundary S of a scatterer.

In this case, in accordance with the method of auxiliary sources, the initial boundary value problem reduces to the following algebraic system:

$$\sum_{m=1}^{N} I_m H_0^{(2)}(k|\mathbf{r}_n - \mathbf{r}_m|) = -U^0(\mathbf{r}_n), \quad n = 1, \ldots, N. \tag{1}$$

In this system, $U^0(\mathbf{r})$ is the initial (incident) field, $H_0^{(2)}(k|\mathbf{r} - \mathbf{r}'|)$ is the fundamental solution to the Helmholtz equation, I_m are coefficients to be determined, $\mathbf{r}_n$ are the radii vectors of the collocation points at the boundary S, and $\mathbf{r}_m$ are the radii vectores for coordinates of sources on a certain carrier Σ entirely residing inside S.

System (1) can be derived from the following Fredholm integral equation of the first kind [5, 6]

$$\int_\Sigma H_0^{(2)}(k|\mathbf{r}_S - \mathbf{r}_\Sigma|) I(\mathbf{r}_\Sigma) d\sigma = -U^0(\mathbf{r}_S), \quad \mathbf{r}_S \in S, \tag{2}$$

by substituting the Riemannian sum for the integral in the left-hand side of (2) and equating the left- and right-hand sides at discrete points of the boundary S.

Equation (2) is naturally derived by employing representation for the secondary (diffraction) field $U^1(\mathbf{r})$ in terms of wave potentials with densities, whose carrier is Σ. Then, this representation should be substituted into the boundary condition [in the case under consideration, it is $(U^1 + U^0)|_{S=0}$].

The method for solving diffraction problems by reducing them to an integral equation of type (2) with respect to the auxiliary current $I(\mathbf{r}_\Sigma)$ is referred to as the method of auxiliary currents.

The following theorem providing a basis for the method of auxiliary currents was proved in [5, 6] (see, also, [7, 8]).

Let a simple closed curve Σ be such that k^2 is not an eigenvalue of the internal uniform Dirichlet problem for the domain inside Σ (in this case, Σ is said to be nonresonance). Then, equation (2) is solvable if and only if Σ encloses all singularities of the wave field $U^1(\mathbf{r})$ inside S.

It is easy to show that equation (2) has a unique solution if the conditions of the theorem are met.

The order N of an algebraic system in the method of auxiliary sources is determined, in particular, by the desired accuracy of the solution to the initial boundary-value problem. As N increases, the sources become more and more closely situated in Σ. Therefore, it is clear that in the method of auxiliary sources, the carrier Σ must also enclose singularities of the field $U^1(\mathbf{r})$. Ignorance of this fact causes deterioration of the corresponding calculation algorithms.

In this paper, we propose to employ for solving equations of type (2) the linear or spline approximation of the auxiliary current $I(\mathbf{r}_\Sigma)$. Such an approach must ensure an appreciable increase in the accuracy of calcu-

* *Moscow Technical University of Communication and Informatics, Aviamotornaya ul. 8a, Moscow, 111024 Russia*

** *Moscow State Technological University "Stankin," Vadkovskiĭ per. 3a, Moscow, 101472 Russia*

1028-3358/00/4506-0269$20.00

lations compared to the method of auxiliary sources, the order N of the algebraic system being retained. Moreover, the method of auxiliary sources must be stabler to various variations (within the admissible limits) for the carrier Σ of the auxiliary current.

For definiteness, we assume that the boundary S and carrier Σ of the auxiliary current are specified by the parametric equations

$$x = x(t), \quad y = y(t), \quad t \in [0, 2\pi],$$

and

$$x = x_0(t'), \quad y = y_0(t'), \quad t' \in [0, 2\pi]$$

for the boundary S and for the carrier Σ, respectively.

Then, equation (2) takes the form

$$\int_0^{2\pi} H_0^{(2)}[kR(t, t')]I(t')dt' = -U^0(t), \tag{3}$$

where

$$R(t, t') = \sqrt{[x(t) - x_0(t')]^2 + [y(t) - y_0(t')]^2}.$$

We now divide the interval $[0, 2\pi]$ into N equal parts and replace the desired auxiliary current on the partial arc Σ_k from t'_{k-1} to t'_k by a polynomial in terms of t' with indeterminate coefficients. Performing the integration and equating the left- and right-hand sides in (3) at N collocation points, we reduce the problem to an algebraic system in these coefficients.

For example, in the case of linear approximation, we have

$$I(t') = \frac{N}{2\pi}[I_m(t' - t'_{m-1}) + I_{m-1}(t'_m - t')], \quad m = 1, 2, \ldots, N, \tag{4}$$

where $I_m = I(t'_m)$ and $I_0 = I_N$.

In line with the presented logic pattern, we have the following algebraic system for finding the coefficients I_m:

$$\sum_{m=0}^{N-1} (\alpha_{n,m} + \beta_{n,m+1})I_m = -U_n^0, \quad n = 0, 1, \ldots, N-1. \tag{5}$$

Here, $U_n^0 = U^0(t_n)$,

$$\alpha_{n,m} = \frac{N}{2\pi}\int_{t'_{m-1}}^{t'_m} H_0^{(2)}[kR(t_n, t')](t' - t'_{m-1})dt',$$

$$\alpha_{n,0} = \alpha_{n,N};$$

$$\beta_{n,m} = \frac{N}{2\pi}\int_{t'_{m-1}}^{t'_m} H_0^{(2)}[kR(t_n, t')](t'_m - t')dt'.$$

In a similar manner, quadratic splines can be used for approximating the auxiliary current:

$$I(t') = \frac{N}{2\pi}[I_m(t' - t'_{m-1}) + I_{m-1}(t'_m - t')] + a_m(t' - t'_{m-1})(t' - t'_m). \tag{6}$$

Here, by virtue of the continuity for the first derivatives of $I(t')$ at the nodes $t' = t'_m$, we have

$$a_m + a_{m+1} = \left(\frac{N}{2\pi}\right)^2 [I_{m+1} - 2I_m + I_{m-1}], \quad m = 1, 2, \ldots, N-1,$$
$$a_1 + a_N = \left(\frac{N}{2\pi}\right)^2 [I_1 - 2I_0 + I_{N-1}]. \tag{7}$$

In this case, for indeterminate coefficients I_m, we have the system of equations

$$\sum_{m=0}^{N-1} (\alpha_{n,m} + \beta_{n,m+1})I_m = -U_m^0 - \sum_{m=1}^{N} a_m\gamma_{n,m}, \quad n = 0, 1, \ldots, N-1, \tag{8}$$

where

$$\gamma_{n,m} = \int_{t'_{m-1}}^{t'_m} H_0^{(2)}[kR(t_n, t')](t' - t'_{m-1})(t' - t'_m)dt'. \tag{9}$$

We can see that the solution to the system of algebraic equations (8) is essentially the perturbed solution to system (5). Therefore, for sufficiently large values of N, we should expect a high degree of consistency between the corresponding solutions $\{I_m\}$ to both the systems.

A similar procedure may be employed while approximating auxiliary current by higher-order splines. Moreover, for algebraization of equation (2), instead of the collocation method, we can use, e.g., the projection method. However, this gives rise to double integrals in calculating matrix elements for the corresponding algebraic systems.

We now consider examples for applying the method proposed for solving diffraction problems. We consider the diagram of scattering of the plane monochromatic electromagnetic wave

$$U_0 = \exp(-i(w_0 x - \nu_0 y))$$

by a perfectly conducting infinite cylinder, whose generatrix is parallel to the Oz-axis and the directrix of S is given in the parametric form. Here, $w_0 = k\sin\theta_0$, $\nu_0 =$

$k\cos\theta_0$, $k = 2\pi/\lambda$, λ is the wavelength, and θ_0 is the angle of incidence (see Fig. 1). The electric-field vector is taken to be parallel to the cylinder generatrix and perpendicular to the plane of incidence.

We assume that Σ belongs to the internal (with respect to S) region (Fig. 1) and satisfies all the above-listed conditions. Then, the expression for the scattering diagram in the polar coordinates (r, φ) takes the form

$$f(\varphi) = \int_0^{2\pi} \exp(ikr_0(t')\cos(\varphi_0(t') - \varphi))I(t')dt', \quad (10)$$

where $(r_0(t'); \varphi_0(t'))$ are the polar coordinates of points belonging to Σ. Starting from the relations obtained above, we calculate scattering diagrams corresponding to various cross-section shapes of the initial perfectly conducting infinite cylinder.

1. An elliptic cylinder. In this case, the directrix of S is specified in the form

$$x(t) = a\cos t, \quad y(t) = b\sin t, \quad t \in [0; 2\pi].$$

As an auxiliary surface, we choose a cylindrical one for which Σ can be represented as

$$x_0(t') = a_0\cos t', \quad y_0(t') = b_0\sin t', \quad t' \in [0; 2\pi].$$

Without loss of generality for the numerical experiment, we consider the case when the angle of incidence $\theta_0 = \pi/4$, $ka = 3$, and $kb = 1.2$. We vary the value of ka_0 assuming $kb_0 = 1.08$. The generatrix Σ of the auxiliary cylinder must enclose the interfocal segment $[2kf = 2\sqrt{(ka)^2 - (kb)^2} = 2 \times 2.7495\ldots; 2f$ is the interfocal distance] in which singularities of the analytic continuation are concentrated [9]. The restriction indicated is reduced to the inequality $ka_0 > kf$. Numerical experiments have shown that the scattering diagrams corresponding to all kinds of possible combinations of parameters and various approaches to the realization of the auxiliary-current method coincide within the limits of graphic accuracy for $ka_0 \in [2.72; 2.80]$ (i.e., for $ka_0 \lessgtr kf$) and $N = 70$ and 90. Thus, while calculating the scattering diagram, it is not evident whether the singularities for the analytic continuation of the wave field play a fundamental role in the choice of an auxiliary contour Σ.

However, it is worth noting that the reliability of the results obtained is primarily determined by the accuracy for the fulfillment of the boundary condition between collocation points. Therefore, we choose the maximum (in the absolute value) difference δ between the left- and right-hand sides of (5) and (8), which are obtained in the method of auxiliary sources, as a measure of an error of the numerical solution obtained when the values of t vary from 0 to 2π. Figure 2 shows the ka_0-dependence of the residual δ for various realizations of the auxiliary-current method at $N = 90$. It is

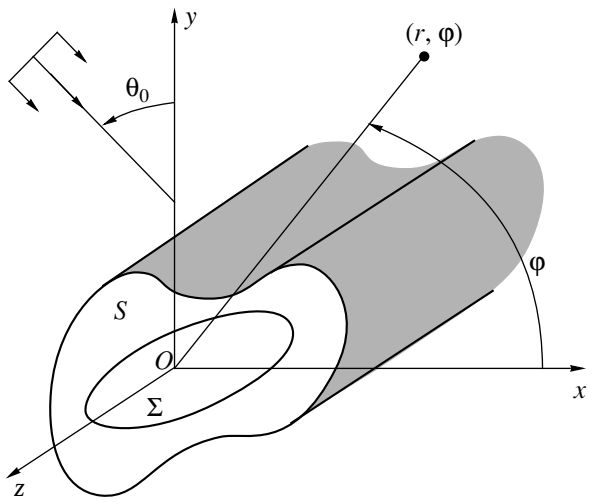

Fig. 1. Geometry for the problem of scattering of a plane electromagnetic wave by an infinite cylinder in realization of the auxiliary-current method.

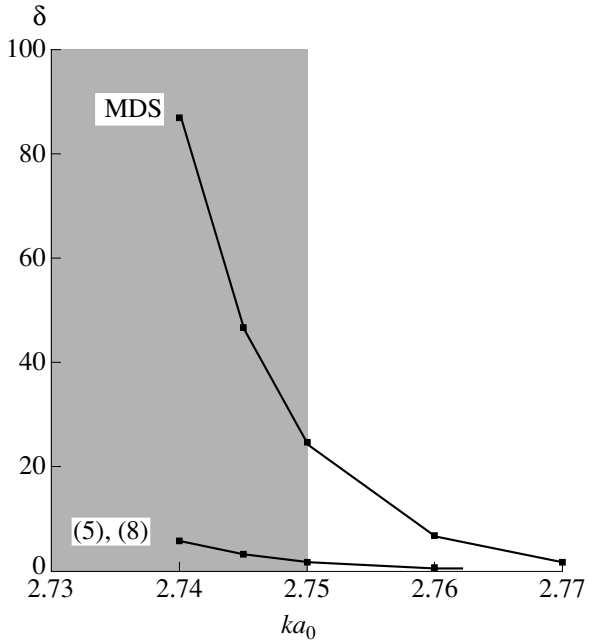

Fig. 2. Residual δ as a function of the parameter ka_0 ($kb_0 = 1.08$) of the auxiliary contour for different realizations of the auxiliary-current method ($N = 90$) in the problem of scattering of a plane electromagnetic wave by a perfectly conducting infinite elliptic cylinder ($\theta_0 = \pi/4$, $ka = 3$, and $kb = 1.2$).

easy to see that the value $ka_0 = kf$ is the threshold one in the sense that for $ka_0 > kf$, the solution is stable, whereas for $ka_0 < kf$ it is unstable. The larger N is, the more pronounced is the threshold effect, the residual corresponding to the discrete-source method being several times larger than that obtained from (5) or (8).

The character of the results shown in Fig. 2 does not vary if another contour enclosing the singularities is chosen: only the value of δ can change.

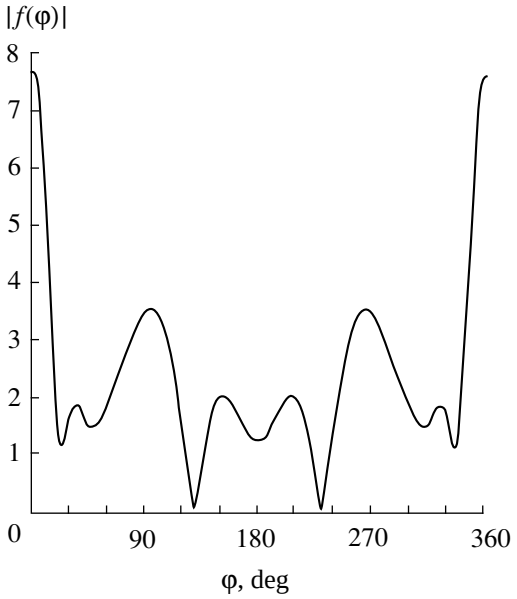

Fig. 3. Amplitude in the scattering diagram $|f(\varphi)|$ for the case of scattering of a plane electromagnetic wave by a perfectly conducting infinite cylinder with a multifoil-shaped cross section ($\theta_0 = \pi/2$, $ka = 6$, $\tau = 0.2$, and $q = 4$).

2. A cylinder with a multifoil-shaped cross section. In this case, it is more convenient to specify the equation for the directrix of S in the polar coordinates

$$r(\varphi) = a(1 + \tau\cos q\varphi),$$

where $a > 0$, $\tau \in (0; 1)$, $q \in N$. As an auxiliary surface, we choose a cylindrical one for which Σ can be represented as

$$r_0(\varphi) = a_0(1 + \tau_0\cos q\varphi)$$

with

$$a_0 = (b_0 + c)/(1 + \tau_0),$$

$$b_0 = \begin{cases} a\tau/2, & q = 1 \\ aq\dfrac{\tau^2(q-1) + A}{(q-1)A}\left[\dfrac{\tau(q-1)}{A}\right]^{1/q}, & q = 2, 3, \ldots, \end{cases}$$

$$A = 1 + [1 + \tau^2(q^2 - 1)]^{1/2}, \quad c = \beta[a(1 + \tau) - b_0].$$

To properly use the auxiliary-current method, the values of the parameter β must belong to the set $[0; 1]$, since for $\beta \geq 1$ the directrix of Σ encloses S. At the same time, at $\beta < 0$, the singularities for the continuation of the wave field do not lie within the inner (with respect to Σ) region [9]. We consider the case with $\theta_0 = \pi/2$, $ka = 6$, $\tau = 0.2$, and $q = 4$ (quarterfoil-shaped cross section). We will vary the value of β assuming $\tau_0 = 0.2$.

The numerical experiments performed for the case $\beta \in [-0.3; 0.3]$ and $N = 90$ have shown that the scattering diagrams corresponding to different approaches to the realization of the auxiliary-current method coincide with the curve shown in Fig. 3 with graphic accuracy. At the same time, the character of the dependence of δ on β is similar to that shown in Fig. 2. This unambiguously implies that positions of the singularities for the analytic continuation of the wave field must be taken into account while choosing an auxiliary surface. As in the case of an elliptic cylinder, the threshold effect is the most pronounced for the realization corresponding to the discrete-source method.

The approach proposed can be extended in an apparent manner to arbitrary boundary conditions, to problems of wave scattering by periodic surfaces and discrete gratings, as well as to three-dimensional and vectorial problems.

ACKNOWLEDGMENTS

This work was supported by the Russian Foundation for Basic Research (project no. 97-02-16722) and the State Program “Integratsiya” (project no. 43).

REFERENCES

1. V. D. Kupradze, Zh. Vychisl. Mat. Mat. Fiz. **4**, 1118 (1964).
2. K. Yasuura and T. Itakura, in *Approximate Method for Wave Function* (Kyushu Univ. Press, Kyushu, 1966), p. 1065.
3. R. S. Popovidi-Zaridze, *Method of Auxiliary Sources*, Preprint No. 14/386, IRÉ AN SSSR (Institute of Radio Engineering and Electronics, Russian Academy of Sciences, Moscow, 1984).
4. Yu. A. Eremin and A. G. Sveshnikov, *Method of Discrete Sources in Electromagnetic-Diffraction Problems* (Mosk. Gos. Univ., Moscow, 1992).
5. A. G. Kyurkchan, Radiotekh. Élektron. (Moscow) **29**, 2129 (1984).
6. A. G. Kyurkchan, Radiotekh. Élektron. (Moscow) **31**, 20 (1986).
7. B. Sternin and V. Shatalov, *Differential Equations on Complex Manifolds* (Academic, Boston, 1994).
8. A. G. Kyurkchan, B. Yu. Sternin, and V. E. Shatalov, Usp. Fiz. Nauk **166**, 1285 (1996) [Phys. Usp. **39**, 1221 (1996)].
9. A. G. Kyurkchan, Radiotekh. Élektron. (Moscow) **31**, 1294 (1986).

Translated by V. Tsarev

Doklady Physics, Vol. 45, No. 6, 2000, pp. 273–276. Translated from Doklady Akademii Nauk, Vol. 372, No. 5, 2000, pp. 615–618.

TECHNICAL PHYSICS

A Distributed Active Semiconductor Structure

V. A. Abdulkadyrov*, E. V. Abdulkadyrova*, V. F. Kravchenko, and Corresponding Member of the RAS V. I. Pustovoĭt*****

Received December 3, 1999

The advances in developing modern microwave devices are associated with the design of functional systems implementing a variety of wave phenomena (both at the surface and in the bulk) occurring in semiconductor structures [1–4], especially taking into account progress in modern precision technologies. A large number of papers deal with the problems of manufacturing active devices based on the long-range (prolonged) interaction of drifting charge carriers in semiconductors with fields generated by structures [1–8].

Formulation of the problem. We consider the electron–wave interactions in the distributed semiconductor structure with reflecting screens. The key element of the electrodynamic model of the system under study is a semiconductor film of thickness h and a periodic structure placed at distance b from the film (l is the period of the structure, and d is the distance between its elements) arranged on substrates between the screens (Fig. 1). The semiconductor is subjected to applied longitudinal electric and magnetic fields. The wave interactions in the system consisting of the semiconductor and the periodic microstructure are described by the set of equations

$$\mathrm{curl}\mathbf{H} = \frac{1}{c}\frac{\partial \mathbf{D}}{\partial t} + \frac{4\pi}{c}\mathbf{I}, \quad \mathrm{div}\mathbf{D} = 4\pi\rho,$$

$$\mathrm{curl}\mathbf{E} = -\frac{1}{c}\frac{\partial \mathbf{H}}{\partial t}, \quad \mathrm{div}\mathbf{H} = 0, \quad \mathrm{div}\mathbf{I} + \frac{\partial \rho}{\partial t} = 0, \quad (1)$$

$$\frac{d\mathbf{V}}{dt} + \nu\mathbf{V} + \frac{V_T^2}{\rho_0}\nabla\rho = \frac{e}{m^\alpha}\left(\mathbf{E} + \frac{1}{c}[\mathbf{V}\mathbf{H}]\right).$$

Here, $\nu = \sum_k \nu_k$, ν_k are the collision frequencies corresponding to the kth scattering mechanism, m^α is the effective mass of conduction electron, V_T is the velocity, and the remaining notation is conventional for electrodynamics. The system is in the nonequilibrium state; therefore, the disturbances of the space charge arising in the semiconductor propagate in the form of electrokinetic waves, which, in turn, are transformed into electromagnetic radiation. A certain part of this radiation reflected from the interfaces interacts with charge carriers, etc. The reflecting screens can be made of a superconductor (a film or a layered composite structure is possible). The superconductor is described within the framework of a two-fluid Gorter–Casimir model [9, 10]. In the electrodynamic structure under study, the fields should meet the following requirements: the Helmholtz equation, the Floquet condition, the finiteness condition for the energy integral, the condition on the ideal metal, the continuity condition for the field at the boundary of dielectric and plasma media [11], and the impedance boundary condition [9, 10, 12]

$$[\mathbf{n}\mathbf{E}] = -Z[\mathbf{n}[\mathbf{n}\mathbf{H}]], \quad (2)$$

where Z is the impedance and $\mathbf{n}$ is the external unit normal to the screen surface.

Solution method. If the fields at the corresponding boundaries meet the aforementioned conditions, we have a system of functional equations with respect to the unknown field amplitude. According to [13], we obtain an infinite system of linear algebraic equations of the second order. The latter system belongs to the Fredholm type. The existence and uniqueness theorems

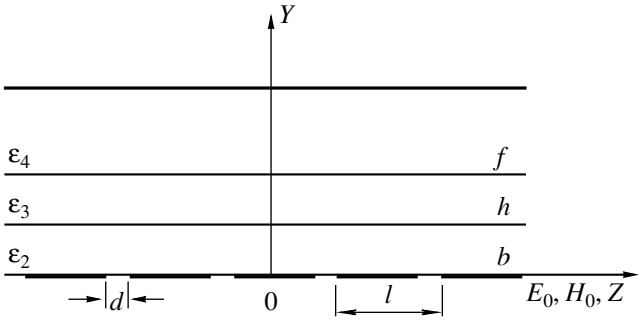

Fig. 1. Electrodynamic model of the distributed semiconductor structure.

* *Institute of Radiophysics and Electronics, National Academy of Sciences of Ukraine, ul. Malo-Belgorodskaya 12, Kharkov, 310085 Ukraine*

** *Institute of Radio Engineering and Electronics, Russian Academy of Sciences, ul. Mokhovaya 11, Moscow, 103907 Russia*

*** *Central Design Bureau of Unique Instrumentation, Russian Academy of Sciences, ul. Butlerova 15, Moscow, 117342 Russia*

1028-3358/00/4506-0273$20.00

are proved in the same way as in [14]. From this system, one can easily derive the characteristic equation

$$\det\left\{\frac{|n|}{n}T_n - \delta_{mn}\right\} = 0, \quad (3)$$

where

$$T_n = \left[1 + i\frac{|n|}{n}\frac{g_{n4}}{K_{nz}}Q_{n1}A_n\right]\Omega_m^n,$$

$$Q_{n1,2} = B_{n1}e^{-ign2b} \pm B_{n2}e^{ign2b},$$

$$g_{nj}^2 = \frac{\omega^2}{c^2}\varepsilon_j - K_n^2, \quad \delta_{mn} = \begin{cases}0, & m \neq n\\ 1, & m = n;\end{cases}$$

$j = 1, 2, 3, 4$ are the numbers of regions;

$$A_n^{-1} = Q_{n2} - \frac{\xi_{n2}e^{2ig_n a} - 1}{\xi_{n2}e^{2ig_{n1}a} + 1}\frac{\varepsilon_2 g_{n2}}{\varepsilon_3 g_{n3}}Q_{n1},$$

$$K_n^2 = g_{n3}^2\frac{\varepsilon_{zz}}{\varepsilon_3}, \quad \varepsilon_{zz} = \varepsilon_3 - \frac{\omega_p^2}{\omega_1(\omega_1 + i\nu) - V_T^2K_{nz}^2},$$

$$B_{n1,2} = \frac{1}{2}[L_{n1}\rho_{n1,2}^2e^{iK_nh} + L_{n2}\rho_{n2,1}^2e^{+iK_nh}],$$

$$u = \cos\frac{\pi d}{l}, \quad \chi = \frac{l}{\lambda},$$

$$L_{n1,2} = \frac{g_{n4}}{2K_ng_{n1}^2}(\xi_{n1}(\varepsilon_1 g_{n4}K_n + g_{n1}^2))e^{ig_{n4}f},$$

$$\Omega_m^n = V_m^n(u) - R_m(u)\frac{V_\delta^n(u, \chi\alpha)}{R_\delta(u, \chi\alpha)}, \text{ and}$$

$$\rho_{n1,2} = \frac{\varepsilon_1 g_{n4} \pm \varepsilon_1 g_{n2}K_n}{g_{n2}^2\varepsilon_3}, \quad \xi_{n1,2} = \frac{Z_{1,2}\frac{\omega}{c} \pm g_{n4,1}}{Z_{1,2}\frac{\omega}{c} \mp g_{n4,1}},$$

$$\omega_1 = \omega - V_dK_{nz}, \quad K_n = \frac{2\pi}{l}(\chi\alpha + n).$$

Here, α is the required dimensionless constant characterizing the wave propagation along the system, V_d is the drift velocity, ω_p is the plasma frequency, Z_1 and Z_2 are the impedances of the "upper" and "lower" screens, and V_m^n, V_δ^n, and $R_m^nR_\delta$ are complicated functions of polynomials and the Legendre functions defined in [13]. Equation (3) is obtained under the assumption that the cyclotron frequency is much larger than all characteristic frequencies of the system. Characteristic equation (3) allows us to analyze the spectrum of bulk and surface waves, which can propagate in the system at any values of its parameters (except those imposed by the aforementioned conditions). The infinite system of algebraic equations is a system of the Fredholm type. Hence, for physical analysis, one can use an approximate solution utilizing the reduction of the system and, consequently, also the reduced form of characteristic equation (3). From the asymptotic solution of (3) for m, $n = 0, -1, -2$, we find (in the first approximation of the perturbation theory) the complex constants characterizing the wave propagation for the cases of plasma ($\omega_p^2 \gg \nu^2$) and relaxation ($\nu^2 \gg \omega_p^2$) mechanisms responsible for generating oscillations for the drift flow of the charge carriers in the semiconductor. Taking into account that the plasma mechanism is more efficient (within the given formulation of the problem), we present below an analytical expression for the complex constant corresponding to the propagation of the leaking space charge wave. In the case of narrow spacing between the electrodes of the periodic microstrip structure ($\varepsilon_1 = \varepsilon_2 = 1$, $Z_2 = 0$), the propagation constant for the leaking space charge wave has the form

$$\chi\alpha = \frac{\chi}{\beta} + \rho\frac{\omega_p}{\omega}M_1 + i\frac{\nu}{2\omega}M_2, \quad (4)$$

where

$$M_1 = \frac{\pi H}{(\rho\pi)^2 + HM_0}, \quad M_2 = \frac{M_0H}{(\rho\pi)^2 + HM_0},$$

$$M_0 = \frac{1}{\varepsilon_3}\left[\frac{1 + \varepsilon_3}{2\varepsilon_3} + 2\ln\frac{\pi\theta}{2} - i\frac{1}{\chi L^*}\right], \quad \theta = \frac{l-d}{l},$$

$$L^* = \frac{(1 - e^{2i\chi A})L_1}{(1 - e^{2i\chi A}) + (1 + e^{2i\chi A})L_1 + i(1 - e^{2i\chi A})L_2},$$

$$A = \frac{2\pi a}{l},$$

$$L_1 = \frac{(Z_1 + 1) + (Z_1 - 1)e^{2i\chi A}}{(Z_1 + 1) - (Z_1 - 1)e^{2i\chi A}} - \frac{i}{\sqrt{\varepsilon_3}}\tan(\sqrt{\varepsilon_3}\chi H),$$

$$H = \frac{2\pi h}{l},$$

$$L_2 = \sqrt{\varepsilon_3}\frac{(Z_1 + 1) + (Z_1 - 1)e^{2i\chi F}}{(Z_1 + 1) - (Z_1 - 1)e^{1i\chi F}}\tan(\sqrt{\varepsilon_3}\chi H),$$

$$F = \frac{2\pi f}{l},$$

$$\beta = \frac{V_d}{c}, \quad \rho = \pm1, \pm2, \pm3, \ldots.$$

Analysis of relationships (3) and (4) demonstrated that each nth space harmonic is put into correspondence with the infinite set of electromagnetic waves driven by the space charge waves with the radiation losses. This set involves the combination of fast and

slow space charge waves. Depending on the parameters (geometric, dynamical, electrical), the propagation of these waves can be accompanied by an increase or decrease of their amplitude. The increasing space charge waves in the semiconductor provide an indication of the modulation of the drifting carriers and the generation of the coherent radiation. Under the effect of the field, the modulation ("bunching") increases alongside the coherent radiation of the system. Since the radiating bunches are formed by the field itself, this is the induced radiation. However, the system supporting the induced radiation has a fundamental property, namely, the possibility of amplifying the radiation. Thus, the system under study is unstable, and it can amplify an input signal. Any feedback mechanism in the system gives rise to self-sustained oscillations.

Excitation of the open resonance system. To support the self-sustained oscillation mode with efficient feedback, we placed a system consisting of a semiconductor and a microstrip structure in the field of the open resonator with superconducting mirrors. The elements of the microstrip structure were also made up of a superconductor. The self-excitation condition for such a resonance system is as follows:

$$P \geq \frac{\omega W}{Q}, \tag{5}$$

where P is the power transferred by the flow of the drifting charge carriers in the semiconductor to the microwave field, W is the field energy stored in the resonator, and Q is the Q factor of the loaded system. It is known that the Q factor of the loaded system under study is inversely proportional to the total losses and has the form

$$Q = \frac{2\pi}{\lambda}\frac{D}{R}, \tag{6}$$

where D is the distance between the mirrors, λ is the wavelength, and R is the parameter characterizing the losses: ohmic losses at the mirrors and the microstructure, diffraction losses, losses in the semiconductor and in the substrate, coupling losses related to the load, etc. Diffraction losses can be reduced by adjusting the aperture of the resonator mirrors. The losses in the substrate can be lowered if we use high-resistivity semiconducting substrate materials with low losses, such as gallium arsenide and silicon. Ohmic losses can be significantly reduced by using large-area high-T_c YBCO film at liquid nitrogen temperature. It is shown in [15] that the tangent of the dielectric loss angle ($\tan\delta$) for the structure with electrodes made of YBCO is less than $\tan\delta$ for the samples with metallic electrodes within the whole temperature range. Thus, the superconducting mirrors, which form the open resonator, and the superconducting electrodes in the periodic microstructure results provide a much larger reduction of ohmic losses in the resonance system than in the case when these elements are made of a metal. Thus, it leads to an enhanced Q factor of the loaded system. The complex power corresponding to interaction of the drifting charge carriers in the semiconductor with the field of the open resonator can be written as

$$P = P_0 \sum_{j=0,1} (-1)^j \int_{-\infty}^{\infty} \frac{|E|^2}{h_j - K} dK. \tag{7}$$

Here,

$$P_0 = \frac{i\omega\theta_n q a_T B_n}{16\pi h_p \rho}, \quad h_p = \frac{\omega_p}{V_d},$$

$$\rho = \left\{ a_T - \frac{\omega^2}{\omega_p^2}\left[a_T\left(1 - i\frac{\nu}{\omega}\right) - b_\nu \right] \right\}^{1/2}, \tag{8}$$

$$q = \frac{2l^2 n_0}{m^* V_d^2}; \quad b_\nu = 1 + i\frac{\nu}{2\omega}, \quad a_T = 1 - \frac{V_T^2}{V_d^2};$$

h_j is the propagation constant of the spatial charge wave, B_n is the field amplitude of the synchronous harmonics averaged over the cross section of the semiconductor film, and θ_n is the coefficient characterizing the flow efficiency. The first and the second terms in (7) determine the efficiency of the energy exchange with the slow and fast space charge waves, respectively. From (5), we find the threshold value of the current needed to promote the self-sustaining mode:

$$I \approx \frac{m^*}{e}\frac{S_0 S_p^2}{\varepsilon_3}\frac{A_0^4}{A_n^4}\left(\frac{D V_d^{3/2} g_n}{L(1 - \exp(-2g_n h))}\right)^2,$$

where

$$S_p = \frac{\nu_p^2}{\nu_p - 1 + \exp(-\nu_p)}, \quad \nu_p = \frac{\nu L}{2V_d},$$

L is the length of the sample where the interaction between the field and charge carriers occurs, A_n is the field harmonic in the spatial spectrum of the resonance system, S_0 is the sample cross section, and D is the distance between the mirrors of the open superconducting resonator.

Numerical simulations. We present here the results of the numerical solution of the reduced (m, n = 0, –1, –2) characteristic equation (3) dependent on the screen positions, i.e., on f and a (Figs. 2 and 3). The real part and imaginary parts of $\chi\alpha$ are plotted by solid and dashed lines, respectively. Note that the periodic microstrip structure with the screen placed above it forms the electromagnetic structure, which is equivalent by its properties to a "comb." The presence of the screen above the semiconductor–microstrip structure provides the formation of the electromagnetic system with characteristics similar to those of an orotron oscillator.

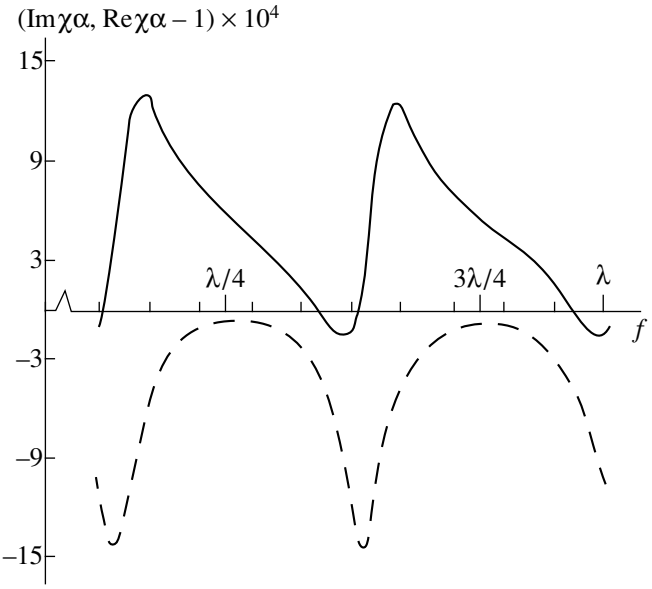

Fig. 2. Real and imaginary parts of the solution to characteristic equation (3) versus position of the "upper" screen for GaAs ($\varepsilon_3 = 12$, $m^* = 0.07m_0$, $n_0 = 10^{14}$ cm^{-3}, $\nu = 10^{11}$ s^{-1}, m_0 is the free electron mass) at $\chi = 5 \times 10^{-3}$, $\beta = 5.05 \times 10^{-3}$, $H = 60$, $a = \frac{\lambda}{4}$, $z_1 = 0.265 - i \times 2.7 \times 10^{-4}$, $\varepsilon_1 = \varepsilon_2 = 1$, $z_2 = 0$, $p = -1$, $\theta = 0.2$.

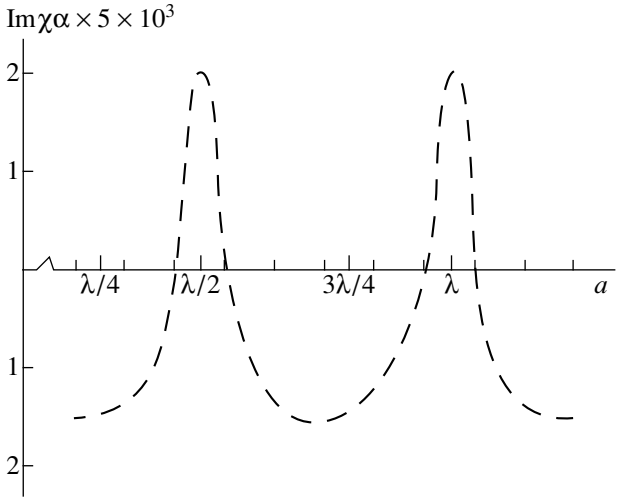

Fig. 3. Imaginary part of the solution to characteristic equation (3) versus position of the "lower" screen for InSb ($\varepsilon_3 = 17.6$, $m^* = 0.013m_0$, $n_0 = 10^{13}$ cm^{-3}, $\nu = 10^{11}$ s^{-1}) at $H = 60$, $\chi = 2 \times 10^{-3}$, $\beta = 2.02 \times 10^{-3}$, $z_1 = 0.265 - i \times 2.7 \times 10^{-4}$, $f = \frac{\lambda}{2}$, $\varepsilon_1 = \varepsilon_2 = 1$, $z_2 = 0$; $p = -1$, $\theta = 0.2$.

In conclusion, electrodynamic analysis of the semiconductor structure presented in this paper demonstrates a principal possibility for exciting microwave oscillations in this structure. The analytical expression for the threshold current necessary for the excitation of the open resonator is found.

REFERENCES

1. M. C. Steele and B. Vural, *Wave Interactions in Solid State Plasmas* (McGraw-Hill, New York, 1969; Atomizdat, Moscow, 1973).
2. Yu. K. Pozhela, *Plasma and Current Instabilities in Semiconductors* (Nauka, Moscow, 1977).
3. N. N. Beletskiĭ, A. A. Bulgakov, S. I. Khankina, and V. M. Yakovenko, *Plasma Instabilities and Nonlinear Phenomena in Semiconductors* (Naukova Dumka, Kiev, 1984).
4. V. I. Pustovoĭt, Usp. Fiz. Nauk **97**, 257 (1969) [Sov. Phys. Usp. **12**, 105 (1969)].
5. Yu. V. Gulyaev, V. V. Proklov, and G. N. Shkerdin, Usp. Fiz. Nauk **124**, 61 (1978) [Sov. Phys. Usp. **21**, 29 (1978)].
6. L. Solumar and A. Ash, Int. J. Electron. **20**, 124 (1966).
7. V. A. Abdulkadyrov, A. M. Andrusenko, and V. F. Kravchenko, in *Proceedings of the V All-Union Seminar on Numerical Methods in the Boundary Problems of Electrodynamics, Minsk, 1975*, pp. 86–89.
8. V. A. Abdulkadyrov, I. D. Revin, and V. P. Shestopalov, Pis'ma Zh. Tekh. Fiz. **19**, 65 (1993) [Tech. Phys. Lett. **19**, 26 (1993)].
9. V. F. Kravchenko and A. B. Kazarov, Zarubezh. Radioélektron. Usp. Sovrem. Radioélektron., No. 11, 59 (1997).
10. M. R. Trunin, Usp. Fiz. Nauk **23**, 931 (1998) [Phys. Usp. **41**, 843 (1998)].
11. V. P. Silin and A. A. Rukhadze, *Electromagnetic Properties of Plasma and Plasmalike Media* (Atomizdat, Moscow, 1961).
12. L. A. Vaĭnshteĭn, *Electromagnetic Waves* (Radio i Svyaz', Moscow, 1988).
13. V. P. Shestopalov, *The Riemann–Hilbert Method in the Theory of Diffraction and Propagation of Electromagnetic Waves* (Kharkov, 1971).
14. V. P. Shestopalov, *Spectral Theory and Excitation of the Open Structures* (Naukova Dumka, Kiev, 1987).
15. B. M. Gol'tsman, V. V. Lemanov, A. I. Dedyk, *et al.*, Pis'ma Zh. Tekh. Fiz. **23** (15), 46 (1997) [Tech. Phys. Lett. **23**, 594 (1997)].

Translated by T. Galkina

Doklady Physics, Vol. 45, No. 6, 2000, pp. 277–280. Translated from Doklady Akademii Nauk, Vol. 372, No. 5, 2000, pp. 619–621.

TECHNICAL PHYSICS

A Mathematical Model for Diffraction on a System of Coupled Resonators

G. L. Sidel'nikov

Presented by Academician Yu.A. Mitropolskiĭ June 5, 1999

Received July 14, 1999

1. Constructing adequate mathematical models for complex resonance systems is an urgent problem in the theory of diffraction. In [1, 2], using an approach based on conjugate integral equations and the method of discrete singularities, the diffraction from two model nonuniformities of planar and cylindrical types was studied. In this paper, a new approach is developed for analyzing the excitation of a resonance system of coupled endovibrators in a cylindrical waveguide structure.

2. We consider a round waveguide with a finite number of rectangular corrugations of arbitrary width and height (see figure). From infinity in the direction of increasing z-values, a bunch of waves uniform in azimuth propagate which are the proper waves of the round waveguide. The time dependence is given by the factor $\exp(-i\omega t)$. It is required to find the fields diffracted and scattered by nonuniformities. We consider a case of excitation with only the components E_φ, H_r, and H_z being nonzero. The initial vectorial problem reduces to the scalar first boundary value problem for the Helmholtz equation with respect to the component $E_\varphi \equiv u(r, z)$ of the electric field. We seek the solution to the problem in the form

$$u(r,z) = \begin{cases} u^0 + u^-, & r < r_0, \quad z \in R \\ u_q^+, & r_0 < r < r_q, \quad a_q < z < b_q, \quad q = 1, 2, \ldots, m, \end{cases}$$

where the incident field is given as

$$u^0 = \sum_{p=1}^{\wp} J_1\left(\frac{\mu_{1p} r}{r_0}\right) e^{ik_\parallel z}.$$

Here, $\wp$ is a fixed positive integer, $k_\parallel^2 = k^2 - \mu_{1p}^2 / r_0^2$, μ_{1p} is the pth zero of the first-order Bessel function, $\mathrm{Re}\, k_\parallel \geq 0$, $\mathrm{Im}\, k_\parallel \geq 0$, $k = \omega/c$, and u^- and u_q^+ are to be determined.

The function u satisfies the boundary conditions

$$(u^0 + u^-)\big|_{r=r_0} = 0, \quad z \in CL, \tag{1}$$

$$L = \bigcup_{q=1}^{m} L_q, \quad L_q \equiv (a_q, b_q), \quad L_k \cap L_q = \varnothing, \quad k \neq q, \; k, q = 1, 2, \ldots, m,$$

$$u_q^+\big|_{r=r_q} = 0, \quad z \in L_q, \quad q = 1, 2, \ldots, m, \tag{2}$$

$$u_q^+\big|_{z=a_q} = u_q^+\big|_{z=b_q}, \quad r_0 < r < r_q, \quad q = 1, 2, \ldots, m, \tag{3}$$

the conjugation conditions

$$(u^0 + u^-)\big|_{r=r_0} = u_q^+\big|_{r=r_0}, \; z \in L_q, \; q = 1, 2, \ldots, m, \tag{4}$$

$$\left(\frac{\partial u^0}{\partial r} + \frac{\partial u^-}{\partial r}\right)\Bigg|_{r=r_0} = \frac{\partial u_q^+}{\partial r}\Bigg|_{r=r_0}, \quad z \in L_q, \quad q = 1, 2, \ldots, m, \tag{5}$$

and the emission condition (which will be stated below).

Since the boundary has breaks, the above conditions should be supplemented with the Meixner condition:

$$\int_V \{|u|^2 + |\nabla u|^2\} dV < \infty. \tag{6}$$

3. In the region $\mathcal{B} = \{(r, z): r < r_0, z \in R\}$, the solu-

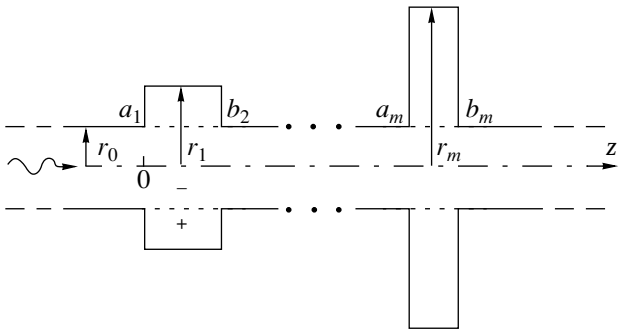

Cross section of a waveguide by a plane passing through the symmetry axis.

Kharkov Institute of Physics and Technology, Ukrainian Scientific Center, Akademicheskaya ul. 1, Kharkov, 310108 Ukraine

1028-3358/00/4506-0277$20.00 © 2000 MAIK "Nauka/Interperiodica"

tion is sought in the form

$$u^-(r, z) = \int_{-\infty}^{\infty} C(\lambda)\frac{I_1(\gamma r)}{I_1(\gamma r_0)}e^{i\lambda z}d\lambda, \quad (7)$$

where $\gamma^2(\lambda) = \lambda^2 - k^2$, and, in accordance with the emission condition, we choose that branch of the function $\gamma(\lambda)$ for which $\mathrm{Re}\,\gamma \geq 0$ and $\mathrm{Im}\,\gamma \leq 0$; $I_1(z)$ is the modified Bessel function of the first-order.

In the region $\mathcal{D}_q = \{(r, z) : r_0 < r < r_q, a_q < z < b_q\}$, $q = 1, 2, \ldots, m$, we present the solution to the problem satisfying boundary conditions (2), (3) in the form

$$u_q^+(r, z) = \sum_{l=1}^{\infty} C_l^q \frac{V(\gamma_l^q r)}{V(\gamma_l^q r_0)}\sin\lambda_l^q(z - a_q), \quad (8)$$

where

$$V(\gamma_l^q r) \equiv \frac{I_1(\gamma_l^q r)}{I_1(\gamma_l^q r_q)} - \frac{K_1(\gamma_l^q r)}{K_1(\gamma_l^q r_q)}, \quad (\gamma_l^q)^2 = (\lambda_l^q)^2 - k^2,$$

$$\lambda_l^q = \frac{\pi l}{\Delta_q}, \quad \Delta_q \equiv b_q - a_q, \quad q = 1, 2, \ldots, m,$$

$$\mathrm{Re}\,\gamma_l^q \geq 0, \quad \mathrm{Im}\,\gamma_l^q \leq 0;$$

$K_1(z)$ is the first-order MacDonald function.

Substituting expressions (7) and (8) into conjugation condition (5), we have

$$\int_{-\infty}^{\infty} \gamma(\lambda)C(\lambda)\frac{I_1'(\gamma r_0)}{I_1(\gamma r_0)}e^{i\lambda z}d\lambda$$

$$-\sum_{l=1}^{\infty}\gamma_l^q C_l^q \frac{V'(\gamma_l^q r_0)}{V(\gamma_l^q r_0)}\sin\lambda_l^q(z - a_q) = -\frac{\partial u^0}{\partial r}(r_0, z), \quad (9)$$

$$z \in L_q, \quad q = 1, 2, \ldots, m.$$

We now rewrite equation (9) in the following equivalent form:

$$\int_{-\infty}^{\infty} |\lambda| C(\lambda)e^{i\lambda z}d\lambda + \sum_{l=1}^{\infty}\lambda_l^q C_l^q \sin\lambda_l^q(z - a_q)$$

$$- \int_{-\infty}^{\infty}\left[|\lambda| - \gamma(\lambda)\frac{I_1'(\gamma r_0)}{I_1(\gamma r_0)}\right]C(\lambda)e^{i\lambda z}d\lambda \quad (10)$$

$$-\sum_{l=1}^{\infty}\left[\lambda_l^q + \gamma_l^q\frac{V'(\gamma_l^q r_0)}{V(\gamma_l^q r_0)}\right]C_l^q \sin\lambda_l^q(z - a_q) = f_q(z),$$

$$z \in L_q, \quad q = 1, 2, \ldots, m.$$

Here, $f_q(z) \equiv -\dfrac{\partial u^0}{\partial r}(r_0, z)\big|_{z \in L_q}$ is the contraction of the function $-\dfrac{\partial u^0}{\partial r}(r_0, z)$ for the interval L_q.

4. Following [3], we introduce the new function

$$F(z) \equiv \frac{\partial}{\partial z}u^-(r_0, z) = \int_{-\infty}^{\infty} i\lambda C(\lambda)e^{i\lambda z}, \quad z \in R.$$

By virtue of condition (4), the representation

$$F_q(z) \equiv \frac{\partial}{\partial z}u_q^+(r_0, z) = \sum_{l=1}^{\infty}\lambda_l^q C_l^q \cos\lambda_l^q(z - a_q),$$

$$z \in L_q, \quad q = 1, 2, \ldots, m$$

holds, where $F_q(z) \equiv F(z)\big|_{z \in L_q}$ is the contraction of the function $F(z)$ for the interval L_q.

The function $F(z)$ possesses the properties

(a) $F(z) = 0, \quad z \in CL,$

(b) $\int_{L_q} F(z)dz = 0, \quad z \in L_q, \quad q = 1, 2, \ldots, m.$

Using the parametric representation for the Hilbert transformation [4], the definition of the function $F(\zeta)$, and its property (a), we find for the first term in the left-hand side of equality (10)

$$\int_{-\infty}^{\infty}|\lambda|C(\lambda)e^{i\lambda z}d\lambda = -\frac{1}{\pi}\int_L \frac{F(\zeta)}{\zeta - z}d\zeta, \quad z \in L. \quad (11)$$

Employing the integral operator with the Hilbert kernel [5], we obtain for the second term in the left-hand side of equality (10)

$$\sum_{l=1}^{\infty}\lambda_l^q C_l^q \sin\lambda_l^q(z - a_q)$$

$$= \frac{\sin\dfrac{\pi}{\Delta_q}(z - a_q)}{\Delta_q}\int_{L_q}\frac{F_q(\zeta)d\zeta}{\cos\dfrac{\pi}{\Delta_q}(\zeta - a_q) - \cos\dfrac{\pi}{\Delta_q}(z - a_q)}. \quad (12)$$

Taking into account (11) and (12), we rearrange equation (10) to the form

$$-\frac{1}{\pi}\int_{L_q}\frac{F_q(\zeta)d\zeta}{\zeta - z} + \frac{\sin\dfrac{\pi}{\Delta_q}(z - a_q)}{\Delta_q}$$

$$\times \int_{L_q} \frac{F_q(\zeta)d\zeta}{\cos\frac{\pi}{\Delta_q}(\zeta - a_q) - \cos\frac{\pi}{\Delta_q}(z - a_q)}$$
$$+ \sum_{k=1}^{m} \int_{L_k} K_{qk}(z, \zeta)F_k(\zeta)d\zeta = f_q(z), \quad (13)$$
$$z \in L_q, \quad q = 1, 2, \ldots, m,$$

where $K_{qk}(z, \zeta)|_{\{z \in L_q, \zeta \in L_k\}}$ is the known continuous function.

Thus, the initial problem of diffraction is reduced mathematically to solving the system of singular integral equations on a set of nonoverlapping segments L_k: $L_k \cap L_q = \varnothing$, $k \neq q$, $k, q = 1, 2, \ldots, m$. The correctness of the rearrangement of equation (10) is provided by the following asymptotic estimates:

$$\frac{1}{r_0} + \gamma(\lambda)\frac{I_1'(\gamma r_0)}{I_1(\gamma r_0)} = |\lambda|\left(1 + O\left(\frac{1}{\lambda}\right)\right), \quad |\lambda| \longrightarrow \infty,$$

$$\frac{1}{r_0} + \gamma_l^q \frac{V'(\gamma_l^q r_0)}{V(\gamma_l^q r_0)} = \lambda_l^q\left(-1 + O\left(\frac{1}{l}\right)\right), \quad l \gg 1.$$

In accordance with the Meixner condition (6) on the edge of the right dihedral angle, the solution to the system of singular integral equations (13) with the additional condition [property (b) for the function $F(z)$, $z \in R$] is sought in the form

$$F_k(\zeta) = \frac{S_k(\zeta)}{\sqrt{(b_k - \zeta)(\zeta - a_k)}},$$

where $S_k(\zeta) = \sqrt[6]{(b_k - \zeta)(\zeta - a_k)}\, U_k(\zeta)$, and $U_k(\zeta)$ is bounded within the interval $[a_k, b_k]$.

5. Using the linear transformation $\zeta = g_q(t)$, $q = 1, 2, \ldots, m$: $(a_q, b_q) \mapsto (-1, 1)$, we can reduce system (13), which is written with respect to an unknown function $F(\zeta)$ given on a set of m intervals, to the form of m unknown functions in a single interval.

The formal discretization procedure is performed according to the method of discrete singularities [6].

The system of linear algebraic equations for approximately solving a system of singular integral equations (13) with additional conditions has the form

$$-\frac{1}{n_q}\sum_{i=1}^{n_q} \frac{\nu_{qi}}{t_i^{(n_q)} - t_{0j}^{(n_q-1)}} + \frac{\pi}{n_q}\frac{\sin\frac{\pi}{\Delta_q}(g_q(t_{0j}^{(n_q-1)}) - a_q)}{2}$$
$$\times \sum_{i=1}^{n_q} \frac{\nu_{qi}}{\cos\frac{\pi}{\Delta_q}(g_q(t_i^{(n_q)}) - a_q) - \cos\frac{\pi}{\Delta_q}(g_q(t_{0j}^{(n_q-1)}) - a_q)} \quad (14)$$
$$+ \sum_{k=1}^{m}\frac{\pi}{n_k}\sum_{i=1}^{n_k} Q_{qk}(t_{0j}^{(n_q-1)}, t_i^{(n_k)})\nu_{ki} = f_{qj},$$

$$f_{qj} \equiv \frac{\Delta_q}{2} f_q(g_q(t_{0j}^{(n_q-1)})), \quad j = 1, 2, \ldots, n_q - 1,$$

$$q = 1, 2, \ldots, m, \quad \frac{1}{n_q}\sum_{i=1}^{n_q} \nu_{qi} = 0, \quad (15)$$

$$j = n_q, \quad q = 1, 2, \ldots, m,$$

where $t_i^{(n_k)} = \cos\frac{2i-1}{2n_k}\pi$, $i = 1, 2, \ldots, n_k$ are zeroes for Chebyshev polynomials of the first-kind; $t_{0j}^{(n_k-1)} = \cos\frac{j}{n_k}\pi$, $j = 1, 2, \ldots, n_k - 1$ are zeroes for Chebyshev polynomials of the second-kind; $\nu_{ki} \equiv \nu_k^{(n_k)}(t_i^{(n_k)})$ are values of the interpolational polynomials approximating the desired functions $S_k(g_k(t))$ at nodes of the network; $i = 1, 2, \ldots, n_k$, $k = 1, 2, \ldots, m$; and n_q is the order of the quadrature formula.

The accuracy of the finite-discrete approximation for the system of singular integral equations and additional conditions can be improved by increasing the power n_q of the interpolational polynomials $\nu_q^{(n_q)}(t)$ under the condition of a corresponding increase in the number of the collocation points $n_q - 1$, $q = 1, 2, \ldots, m$.

The approximate values of the amplitude and Fourier coefficients are directly expressed in terms of the solutions to the system of linear algebraic equations

$$\tilde{C}(\lambda) = \frac{1}{2i}\sum_{q=1}^{m}\frac{1}{n_q}\sum_{k=1}^{n_q}\nu_q(t_k^{n_q})\frac{e^{-i\lambda g_q(t_k^{(n_q)})} - 1}{\lambda}, \quad \lambda \in R,$$

$$\tilde{C}_l^q = \frac{2}{ln_q}\sum_{k=1}^{n_q}\nu_q(t_k^{(n_q)})\cos\left(\pi l\frac{t_k^{(n_q)} + 1}{2}\right),$$
$$l \in N, \quad q = 1, 2, \ldots, m.$$

6. Thus, in this paper, a formal procedure for constructing an exact mathematical model for the diffraction of proper waves on a resonance system of coupled endovibrators in a waveguide cylindrical structure is proposed. The issue of physical substantiation for the choice of points in gaps, in which electromagnetic fields are sewed together, is considered now purely from the standpoint of mathematical advisability for choosing the collocation points and nodes of an interpolational function when discretizing a system of singular integral equations. It is worth reminding that previously, in most cases, this problem was solved empirically (the partial-domain method, the method of integral equations, etc.). The new approach may be

highly profitable for numerically analyzing mechanisms of diffraction scattering by multiple-component structures in various physical situations.

REFERENCES

1. Yu. V. Gandel' and G. L. Sidel'nikov, Zh. Tekh. Fiz. **65**, 143 (1995) [Tech. Phys. **40**, 711 (1995)].
2. V. F. Kravchenko and G. L. Sidel'nikov, Dokl. Akad. Nauk **361**, 185 (1998) [Dokl. Phys. **43**, 408 (1998)].
3. Yu. V. Gandel', *Theory of Functions and Functional Analysis and Their Applications* (Vyshchaya Shkola, Kharkov, 1982), No. 38, pp. 15–18.
4. N. I. Akhiezer, *Lectures on Integral Transforms* (Vyshchaya Shkola, Kharkov, 1984; American Mathematical Society, Providence, R.I., 1988).
5. A. Zygmund, *Trigonometric Series* (Cambridge Univ. Press, Cambridge, 1959; Mir, Moscow, 1965), Vol. 1.
6. I. K. Lifanov, *Method of Singular Integral Equations and Numerical Experiment* (Yanus, Moscow, 1995).

Translated by V. Tsarev

Doklady Physics, Vol. 45, No. 6, 2000, pp. 281–283. Translated from Doklady Akademii Nauk, Vol. 372, No. 5, 2000, pp. 622–624.

POWER ENGINEERING

Determination of the Emissivity in the Course of Cooling and Heating Processes

D. Ya. Svet

Presented by Academician A.I. Leont'ev February 22, 2000

Received February 24, 2000

Measuring the spectral emissivity of a surface whose radiation does not obey the Lambert law presents considerable difficulties when a black body or certain integrating cavities (of spherical or other shapes) are not employed. Until now, only two noncontact methods are known for solving this problem in the on-line mode.

The first one is the Kunz method [1–3] based on determining the ratio of spectral-absorption coefficients for two laser beams with different wavelengths. The method uses thermal effects caused by the action of these beams on a surface, whose emissivity must be measured.

The second is the Svet method [4, 5] based on the optimum employment of the excess information contained in the spectrum of the proper thermal radiation.

It should be noted that only nowadays, i.e., a quarter century after both these methods had been proposed, they, being promoted by the progress of modern microelectronics and laser technique, began to be developed. Recently, the author has suggested [6–8] a new method for the determination of true temperature, which is based on measuring the proper radiation of a body. The method makes it possible to apply the thermodynamic temperature scale without using a black body. Physically, this method exploits changes in properties of a medium under investigation. The changes result in the temperature dependence for spectral components of the emissivity coefficients. The method enables us to eliminate the influence of the emissivity and response function, although it makes it impossible to directly obtain values of desired quantities.

In this paper, we consider the further development of this new method applying directional relative modulation reflectometry. This enables us to considerably reduce the necessary excessiveness of spectral components used and, as a result, to obtain a rather efficient method for measuring the emissivity of a surface, in particular, of that whose radiation does not obey Lambert's law.

Thus, this measurement method is based on the combined employment of radiation pyrometry and relative directional reflectometry of a surface in the process of its cooling or heating.

Here, we consider several variants of implementing this method. The first one is associated with a system measuring the proper radiation, which is calibrated in terms of temperatures, i.e., represents a brightness pyrometer operating at two wavelengths. The second one implies using a noncalibrated system, i.e., a linear system for measuring radiation spectral intensities (for two wavelengths as well).

In the first case, we measure the difference between reciprocal values of two brightness temperatures $T_{b1,1}^{-1}$ and $T_{b2,1}^{-1}$, which correspond to two values of the true temperature:

$$\ln J_1 = T_{b1,1}^{-1} - T_{b2,1}^{-1} = \frac{\lambda_1}{C_2}\ln\varepsilon(\lambda_1, T_1) - \frac{\lambda_2}{C_2}\ln\varepsilon(\lambda_2, T_1),$$

$$\ln J_2 = T_{b1,2}^{-1} - T_{b2,2}^{-1} = \frac{\lambda_1}{C_2}\ln\varepsilon(\lambda_1, T_2) - \frac{\lambda_2}{C_2}\ln\varepsilon(\lambda_2, T_2).$$

On exponentiating both above expressions, we obtain

$$J_1 = \frac{\varepsilon(\lambda_1, T_1)}{\varepsilon(\lambda_2, T_1)^{\lambda_2/\lambda_1}}, \quad (1)$$

$$J_2 = \frac{\varepsilon(\lambda_1, T_2)}{\varepsilon(\lambda_2, T_2)^{\lambda_2/\lambda_1}}. \quad (2)$$

Here, $\varepsilon(\lambda_i, T_j)$ represent the values of the desired emissivity corresponding to the wavelengths λ_i ($i = 1, 2$) and temperatures T_j ($j = 1, 2$).

At the same time, for the same temperatures and wavelengths, the ratio of the directional-reflection

IVTAN (Institute of High Temperatures) Scientific Association, Russian Academy of Sciences, Izhorskaya ul. 13/19, Moscow, 127412 Russia

1028-3358/00/4506-0281$20.00 © 2000 MAIK "Nauka/Interperiodica"

coefficients measured by a reflectometer should satisfy the relations

$$\frac{\rho^*(\lambda_1, T_1)}{\rho^*(\lambda_1, T_2)} = \frac{x_1\rho(\lambda_1, T_1)}{x_1\rho(\lambda_1, T_2)},$$

$$\frac{\rho^*(\lambda_2, T_1)}{\rho^*(\lambda_2, T_2)} = \frac{x_2\rho(\lambda_2, T_1)}{x_2\rho(\lambda_2, T_2)}.$$

Here, $\rho^*(\lambda_i, T_j)$, $(i = 1, 2, j = 1, 2)$ are the directional spectral-reflection coefficients for the wavelengths λ_i and temperature T_j $(j = 1, 2)$; $\rho(\lambda_i, T_j)$ is the coefficient of the normal spectral reflection for the same temperatures and wavelengths; x_1 and x_2 are the coefficients taking into account scattering of the radiation due to the surface roughness. In the case when the emitting surface is smooth, i.e., satisfies the Lambert's law, $x_1 = x_2 = 1$.

Applying Kirchhoff's law for opaque bodies, we obtain

$$\frac{\rho^*(\lambda_1, T_1)}{\rho^*(\lambda_1, T_2)} = \frac{1-\varepsilon(\lambda_1, T_1)}{1-\varepsilon(\lambda_1, T_2)},$$

$$\frac{\rho^*(\lambda_2, T_1)}{\rho^*(\lambda_2, T_2)} = \frac{1-\varepsilon(\lambda_1, T_1)}{1-\varepsilon(\lambda_2, T_2)}.$$

Temperature variation naturally results in a change of the emissivity:

$$\varepsilon(\lambda_i, T_j) = \varepsilon(\lambda_i, T_{j-1}) + \alpha_i(T_1 - T_2) + \beta_i(T_1^2 - T_2^2) + \ldots + \gamma_i(T_1^n - T_2^n),$$

where $\alpha_i, \beta_i, \ldots, \gamma_i$ are the coefficients of a power polynomial approximating the temperature dependence of the emissivity.

Introducing the following notation for the polynomial in the right-hand side of the above-expression,

$$\alpha_i(T_2 - T_1) + \beta_i(T_2^2 - T_1^2) + \ldots + \gamma_i(T_2^n - T_1^n) = \Delta\varepsilon_i,$$

we can write out

$$\frac{\rho^*(\lambda_1, T_1)}{\rho^*(\lambda_1, T_2)} = \frac{1-\varepsilon(\lambda_1, T_2)-\Delta\varepsilon_1}{1-\varepsilon(\lambda_1, T_2)} = \frac{1-\Delta\varepsilon_1}{1-\varepsilon(\lambda_1, T_2)},$$

$$\frac{\rho^*(\lambda_2, T_1)}{\rho^*(\lambda_2, T_2)} = \frac{1-\varepsilon(\lambda_2, T_2)-\Delta\varepsilon_2}{1-\varepsilon(\lambda_2, T_2)} = \frac{1-\Delta\varepsilon_2}{1-\varepsilon(\lambda_2, T_2)}$$

or

$$A = 1 - \frac{\rho^*(\lambda_1, T_1)}{\rho^*(\lambda_1, T_2)} = \frac{\Delta\varepsilon_1}{1-\varepsilon(\lambda_1, T_2)}, \quad (3)$$

$$B = 1 - \frac{\rho^*(\lambda_2, T_1)}{\rho^*(\lambda_2, T_2)} = \frac{\Delta\varepsilon_2}{1-\varepsilon(\lambda_2, T_2)}. \quad (4)$$

Taking into account expressions (1) and (2), we obtain four expressions (1)–(4) for four variables: $\varepsilon(\lambda_1, T_2)$, $\varepsilon(\lambda_2, T_2)$, $\Delta\varepsilon_1$, and $\Delta\varepsilon_2$. Simultaneous solving of these equations does provide all desired values of the emissivity. It is natural that in doing so, for various wavelength ratios λ_2/λ_1, we need to perform computer calculations. However, for reasonable and sufficiently efficient (from the technical standpoint) ratios $\lambda_2/\lambda_1 = 2$, we obtain an analytical solution featuring the form of a quadratic-equation.

Indeed, for $\lambda_2/\lambda_1 = 2$,

$$J_1 = \frac{A + [(1-A)\varepsilon(\lambda_1, T_2)]}{\{B + [(1-B)\varepsilon(\lambda_2, T_2)]\}^2}, \quad (5)$$

$$J_2 = \frac{\varepsilon(\lambda_1, T_2)^2}{\varepsilon(\lambda_2, T_2)}. \quad (6)$$

Using (3), (4) and (5), (6), we obtain the regular quadratic equation for $\varepsilon(\lambda_2, T_2)$

$$\varepsilon(\lambda_2, T_2)^2[J_1(1-B)^2 - J_2(1-A)] + \varepsilon(\lambda_2, T_2)J_1 \times 2B(1-B) + [J_1B^2 - A] = 0.$$

The roots of this equation can be simply evaluated since $0 < \varepsilon(\lambda_2, T_2) \le 1$.

The second variant of the method under consideration enables us to find the unknown values of the emissivity without using the pyrometer calibration. For this purpose, it is necessary to measure only spectral radiation intensities. However, it is necessary to execute these measurements for three (not two) thermal states of the surface, i.e., for three unknown values of temperatures T_1, T_2, and T_3.

Indeed, having measured the ratios of the directional-reflection coefficients for two wavelengths at three different temperatures, we can write out as before

$$A_1 = 1 - \frac{\rho^*(\lambda_1, T_1)}{\rho^*(\lambda_1, T_2)} = \frac{\Delta\varepsilon_{1,1}}{1-\varepsilon(\lambda_2, T_2)}, \quad (7)$$

$$A_2 = 1 - \frac{\rho^*(\lambda_1, T_3)}{\rho^*(\lambda_1, T_2)} = \frac{\Delta\varepsilon_{1,2}}{1-\varepsilon(\lambda_2, T_2)}, \quad (8)$$

$$B_1 = 1 - \frac{\rho^*(\lambda_2, T_1)}{\rho^*(\lambda_2, T_2)} = \frac{\Delta\varepsilon_{2,1}}{1-\varepsilon(\lambda_2, T_2)}, \quad (9)$$

$$B_2 = 1 - \frac{\rho^*(\lambda_2, T_3)}{\rho^*(\lambda_2, T_2)} = \frac{\Delta\varepsilon_{2,2}}{1-\varepsilon(\lambda_2, T_2)}. \quad (10)$$

Hence, it follows that

$$\Delta\varepsilon_{1,1} = A_1[1-\varepsilon(\lambda_1, T_2)],$$

$$\Delta\varepsilon_{1,2} = A_2[1-\varepsilon(\lambda_1, T_2)],$$

$$\Delta\varepsilon_{2,1} = B_1[1-\varepsilon(\lambda_2, T_2)],$$

$$\Delta\varepsilon_{2,1} = B_2[1-\varepsilon(\lambda_2 - T_2)].$$

On the other hand, measuring not temperature, but spectral intensities of the radiation for three unknown

temperatures and two wavelengths λ_1 and λ_2, we can write out

$$J_1 = \frac{[U(\lambda_1, T_1)/U(\lambda_1, T_2)]^{\lambda_1}}{[U(\lambda_2, T_1)/U(\lambda_2, T_2)]^{\lambda_2}} = \frac{1 + \Delta\varepsilon_{1,1}/\varepsilon(\lambda_1, T_2)}{[1 + \Delta\varepsilon_{2,1}/\varepsilon(\lambda_2, T_2)]^{\lambda_2/\lambda_1}}, \quad (11)$$

$$J_2 = \frac{[U(\lambda_1, T_3)/U(\lambda_1, T_2)]^{\lambda_1}}{[U(\lambda_2, T_3)/U(\lambda_2, T_2)]^{\lambda_2}} = \frac{1 + \Delta\varepsilon_{1,2}/\varepsilon(\lambda_1, T_2)}{[1 + \Delta\varepsilon_{2,2}/\varepsilon(\lambda_2, T_2)]^{\lambda_2/\lambda_1}}. \quad (12)$$

The spectral intensities are described by the expression

$$U(\lambda_i, T_j) = \xi_i C_1 \lambda_i^{-5} \varepsilon(\lambda_i, T_j) \exp\left(-\frac{C_2}{\lambda_i T_j}\right), \quad (13)$$

where $i = 1, 2$ and $j = 1, 2, 3$; ξ_i is the response function; C_1 and C_2 are the pyrometric constants.

Thus, we obtain six equations (7)–(12) with 11 unknown variables: $\varepsilon(\lambda_1, T_2)$, $\varepsilon(\lambda_2, T_2)$; $\Delta\varepsilon_{1,1}$, $\Delta\varepsilon_{1,2}$, $\Delta\varepsilon_{2,1}$, $\Delta\varepsilon_{2,2}$; ξ_1, ξ_2; T_1, T_2, and T_3.

As is seen from equations (11) and (12), the unknown values of the response functions ξ_1 and ξ_2, as well as temperatures T_1, T_2, and T_3, are eliminated.

Hence, in this variant, the method under consideration enables us to find the desired values of the emissivity, but not the values of temperature and response functions.

In the case when the wavelength ratio is $\lambda_2/\lambda_1 = 2$, the value of $\varepsilon(\lambda_2, T_2)$, as before, is evaluated analytically from the quadratic equation

$$\varepsilon(\lambda_2, T_2)^2[I_1(1 - B_1)^2 + I_2A_1/A_2(1 + B_2)^2 - (1 + A_1/A_2)] + \varepsilon(\lambda_2, T_2)[2I_1B_1(1 - B_1) - 2I_2A_1/A_2B_2(1 + B_2)] + (I_1B_1^2 + I_2A_1/A_2B_2) = 0. \quad (14)$$

Owing to weak temperature dependence of the emissivity, it is reasonable to extend the temperature intervals T_1–T_2 and T_2–T_3.

In the case of insufficient monochromaticity, we should allow for the variation of the effective values of wavelengths with temperature [9, 10] and use lasers in the reflectometer.

REFERENCES

1. H. Kunz and D. de Witt, in *Temperature: Its Measurement and Control in Science and Industry* (ISA, Pittsburg, 1972), Vol. 5, pp. 599–610.
2. E. Schreiber and G. Neuer, in *Proceedings of TEMPMEKO'96, Turin, 1996*, p. 365.
3. G. J. Edward and A. L. Levick, in *Proceedings of TEMPMEKO'96, Turin, 1996*, pp. 383–388.
4. D. Ya. Svet, Dokl. Akad. Nauk SSSR **221**, 81 (1975) [Sov. Phys.–Dokl. **20**, 214 (1975)].
5. D. Ya. Svet, Yu. N. Pyrkov, and V. G. Plotnichenko, Dokl. Akad. Nauk **361**, 626 (1998) [Dokl. Phys. **43**, 498 (1998)].
6. D. Ya. Svet, Dokl. Akad. Nauk **366**, 759 (1999) [Dokl. Phys. **44**, 362 (1999)].
7. D. Ya. Svet, in *Proceedings of the XV World Congress IMEKO, Osaka, 1999*, Vol. 7, pp. 167–169.
8. D. Ya. Svet, Dokl. Akad. Nauk **362**, 760 (1999) [Dokl. Phys. **44**, 552 (1999)].
9. P. B. Coates, Metrologia **13**, 1 (1977).
10. D. Ya. Svet and O. R. Popova, Metrologia, No. 3, 56 (1986).

Translated by O. Chernavskaya

Doklady Physics, Vol. 45, No. 6, 2000, pp. 284–287. Translated from Doklady Akademii Nauk, Vol. 372, No. 4, 2000, pp. 484–486.

MECHANICS

A Method of Asymptotic Homogenization in the Mechanics of Rocky Grounds

A. N. Vlasov, V. P. Merzlyakov*, and S. B. Ukhov***

Presented by Academician E.I. Shemyakin June 21, 1999

Received July 9, 19999

The anisotropy of deformability is inherent to layered and fractured rocks (varved clays, schists, and stratifications of limestone, sandstone, and other rocks and semirocks), which results in a complicated behavior of rocky solids under loading. In particular, the inclined position of layers with respect to the plane of the building basement results in lower stability owing to the nonuniformity of its displacements. The anisotropy is often taken into account by representing the mountain mass as a transversally isotropic body.

In this case, the elastic stressed-deformable state is well determined by the Young and shear moduli and the Poisson coefficients $E_{\|}$, $E_{\perp}$, $G_{\perp}$, $\nu_{\|,\perp}$, $G_{\|}$ (or $\nu_{\|,\|}$), where subscripts $\|$ and $\perp$ define the direction along and across the bedding.

Here, we discuss the conventional (so-called effective) characteristics of deformability, i.e., the parameters generally characterizing the deformability of a certain virtual material. The latter is assumed to be uniform and transversally isotropic, situated within the bulk of the rock under study, and similar in deformability to the actual rock massif. The effective characteristics of deformability critically depend on the correctness of averaging over the actual characteristics of the rock layers.

Historically, the first formulas allowing one to estimate the effective values of deformation moduli of layered rocks along and across the bedding were suggested by Tarkhov [1]. Subsequent work in this direction (described in the comprehensive review [2]) generalized, in fact, the Tarkhov formulas, supplementing them by formulas for the shear modulus and the Poisson coefficients. The substantial difference in conditions under which the characteristics were determined does not allow us to consider them as belonging to one and the same rigidity tensor. The correct solution of the problem demands finding the invariant characteristics of the deformability for the equivalent uniform medium, which would provide the exact determination of average displacements and stresses in the nonuniform massif at any boundary conditions. One such method, namely, the method of asymptotic homogenization, was proposed in [3, 4], based on the substitution of exact equations with fast-oscillating coefficients following from the elasticity theory by averaged equations. The effective characteristics determined in the framework of this method ensure meeting the aforementioned condition. The method allows us to determine the values of displacements and stresses with any given accuracy and does not require the weakening conditions of the type discussed in [1, 2].

The essence of the method is the following. The displacement vector is presented in the form of the series expansion in terms of small parameter $\varepsilon = \delta/L$, where δ is the size of the typical structure element (unit cell) and L is the characteristic size of the domain. This allows us to replace the system of elasticity theory equations in terms of displacements by a system of recurrent relationships providing an opportunity to determine subsequent terms of the series. One of these relationships generates the system of averaged equations with respect to the zero-approximation term (the initial term of a series) $\mathbf{u}^{(0)}$; the other relationships allow us to subsequently determine $\mathbf{u}^{(i)}$, $i = 1, 2, \ldots$. The asymptotic conditions result in equations with respect to auxiliary matrix functions $N_i(\xi_1, \xi_2, \xi_3)$, $i = 1, 2, 3$, which allow us to obtain effective rigidity tensor $\hat{A}_{ij}$ and to study the structure of the displacement and stress fields (for a structureless material).[1] Here, $A_{ik} = \|C_{ijkl}\|$ are the matrices, the elements of which correspond to Hook's law in the form $\sigma_{ij} = C_{ijkl}\varepsilon_{kl}$ ($i, j, k, l = 1, 2, 3$; the summation over repeated indices is implied); $\xi_i = x_i/\varepsilon$ are the "fast" variables describing the local properties; and x_i are the conventional coordinates used to describe the average properties.

* *Moscow State University of Civil Engineering, Yaroslavskoe sh. 26, Moscow, 129337 Russia*

** *Institute of Applied Mechanics, Russian Academy of Sciences, Leninskiĭ pr. 32a, Moscow, 117334 Russia*

[1] Another way to determine the function with a "structure" is suggested by Revuzhenko [5]. To meet the above conditions, it is necessary to make the averaged function (displacement) approximately equal to the actual one together with its derivatives.

1028-3358/00/4506-0284$20.00

Solving these equations, we get the formula for the effective rigidity tensor,

$$\hat{A}_{ij} = \left\langle A_{ij} + A_{ik}\frac{\partial N_j}{\partial \xi_k}\right\rangle. \quad (1)$$

In the case of a layered material, (1) can be written in the form

$$\hat{A}_{ij} = \langle A_{ij}\rangle + \langle A_{i1}A_{11}^{-1}\rangle\langle A_{11}^{-1}\rangle\langle A_{11}^{-1}A_{1j}\rangle - \langle A_{i1}A_{11}^{-1}A_{1j}\rangle, \quad (2)$$

where we define $\langle f(\xi)\rangle = \int_Q f(\xi)dv$, Q is the region occupied by a typical structure element, $\boldsymbol{\xi} = (\xi_1, \xi_2, \xi_3)$, and axis x_1 is directed across the bedding.

The discussed formulas provide the solution to the averaged problem with an accuracy $\|\mathbf{u} - \mathbf{u}^{(0)}\| \sim O(\varepsilon^m)$, where $m = 1$ for the one-dimensional problem and $m = 1/2$ in the other cases [4]. The plots of the bulk and shear moduli and the Poisson coefficients versus relative thickness $\alpha = \delta_n/\delta$ ($n = 2$) of the intermediate layer are shown in Fig. 1, where the parameters used in calculations are also presented. It was assumed in the calculations that $E_1 = 2.6 \times 10^3$ MPa for the rock under study.

The fracture is caused by local physical processes, i.e., by processes at the microscopic level. Consequently, accurate description of the stress (strain) field is required. The concentration of stresses (strains) plays the essential role here. It is natural to formulate such a description based on the method of asymptotic homogenization, which takes into account the structure of nonuniformity elements and their interrelation. Let $u_i^{(0)}$, $\varepsilon_{ij}^{(0)}$, $\sigma_{ij}^{(0)}$ be the displacements, strains, and stresses obtained from the solution of the averaged (homogenized) problem. The stresses (including stresses at the microscopic level [4]) can be written in the following form:

$$\sigma_{ij}^{(0)} = \tilde{c}_{ijkl}\varepsilon_{kl}^{(0)} = \tilde{c}_{ijkl}\frac{\partial u_k^{(0)}}{\partial x_l} = \tilde{c}_{ijkl}\hat{c}_{klmn}^{-1}\sigma_{mn}^{(0)}, \quad (3)$$

where $\tilde{c}_{ijkl} = c_{ijkl} + c_{ijmn}\dfrac{\partial n_k^{nl}}{\partial \xi_m}$ and $\hat{c}_{klmn}^{-1}$ are the components of the effective tensor of compliance, which is inverse with respect to the effective rigidity tensor.

A tensor with components defined by the relationship

$$\zeta_{ijkl} = \tilde{c}_{ijmn}\hat{c}_{mnkl}^{-1} \quad (4)$$

will be referred to as the stress concentration tensor.

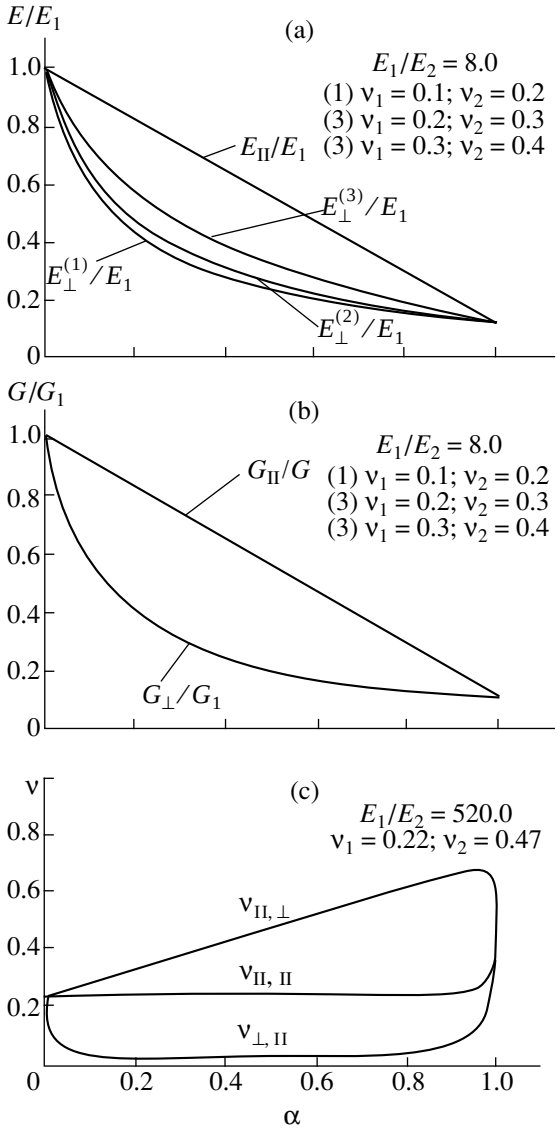

Fig. 1. Dependence of the effective characteristics of deformability of layered rocks on the relative thickness of the intermediate layer: (a) the Young moduli, (b) shear moduli, and (c) the Poisson coefficients.

Taking into account relationships $u_i^{(1)} = u_i^{(0)} + \varepsilon n_k^{ij}\dfrac{\partial u_j^{(0)}}{\partial x_k}$ ($i, j, k = 1, 2, 3$) [4] for the displacements, which describe their local behavior, and neglecting the second order terms, we get the following expressions for strains:

$$\varepsilon_{ij}^{(1)} = \left[\Delta_{ijkp} + \frac{1}{2}\left(\frac{\partial n_k^{ip}}{\partial \xi_j} + \frac{\partial n_k^{jp}}{\partial \xi_i}\right)\right]\varepsilon_{kp}^{(0)}, \quad (5)$$

where $\Delta_{ijkp} = \dfrac{1}{2}(\delta_{ik}\delta_{jp} + \delta_{ip}\delta_{jk})$ is the unit tensor of the fourth rank. Here, we used the symmetry conditions

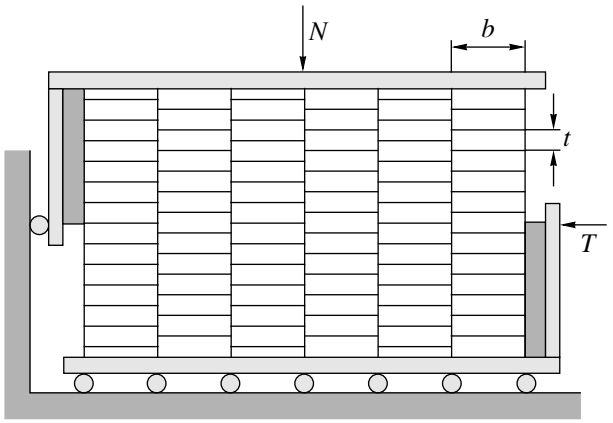

Fig. 2. Schematic diagram illustrating loading of the columnar brickwork sample, which models the behavior of the fractured rocky grounds.

$n_k^{ip} = n_k^{jp}$ and $\varepsilon_{kp}^{(0)} = \varepsilon_{pk}^{(0)}$. Note that the second term in (5) takes into account the microscopic strains.

Let us define the expression in brackets in (5) as the strain concentration tensor and denote it as ξ_{ijkp}. Using (3), we can find that stresses and strains involving those related to the microscopic distortion obey the following relationship:

$$\sigma_{ij}^{(1)} = c_{ijkl}\varepsilon_{kl}^{(1)}. \tag{6}$$

This relationship proves the correctness of the introduced definition of the concentration tensors.

Further on, the strength criteria for the geological materials will be represented as tensor polynomials [6]:

$$\begin{aligned} F &= F_0 + F_{ij}\sigma_{ij} + F_{ijkl}\sigma_{ij}\sigma_{kl} \\ &+ F_{ijklmn}\sigma_{ij}\sigma_{kl}\sigma_{mn} + \ldots = 0, \end{aligned} \tag{7}$$

where F_{ij}, F_{ijkl}, and F_{ijklmn}, … are the components of the strength tensors of the corresponding ranks and σ_{ij} are the components of the stress tensor.

If criterion (7) is known for each *s*th component of the rock ground, then, substituting (3) in it and taking into account (4), we get

$$\begin{aligned} \tilde{F}^{(s)} &= \tilde{F}_0^{(s)} + \tilde{F}_{ij}^{(s)}\sigma_{ij}^{(0)} + \tilde{F}_{ijkl}^{(s)}\sigma_{ij}^{(0)}\sigma_{kl}^{(0)} \\ &+ \tilde{F}_{ijklmn}^{(s)}\sigma_{ij}^{(0)}\sigma_{kl}^{(0)}\sigma_{mn}^{(0)} + \ldots = 0, \end{aligned} \tag{8}$$

where

$$\begin{aligned} \tilde{F}_0^{(s)} &= F_0^{(s)}, \quad \tilde{F}_{ij}^{(s)} = F_{kl}^{(s)}\zeta_{klij}, \\ \tilde{F}_{ijkl}^{(s)} &= F_{mnpr}^{(s)}\zeta_{prij}\zeta_{mnkl}\ldots. \end{aligned} \tag{9}$$

We assume below that the stress field $\sigma_{ij}^{(0)}$ is uniform for the typical structure element. Then, the "true" stresses $\sigma_{ij}^{(1)}$ at it are determined by relationship (3). We will assume that the typical structure element corresponds to the limiting state if there exists a connected domain [defined by (8) and (9)] in the limiting state which "cuts" it. For example, in the case of layered rocks, this domain either crosses the layer as a whole, or passes the layers from one to another edge of the typical structure element.

Relationships (7)–(9) determine, in general, the anisotropy in the strength characteristics of rocky grounds, as well as their dependence on the strength and deformation characteristics of its components, on the volumetric fraction, and on the mutual arrangement and shape of the components forming the rock. It can be shown that the fracture can also occur at hydrostatic uniform compression, even if this compression does not destroy each individual component.

As an example, we compare the strength characteristics calculated in the framework of the asymptotic homogenization method with the results of laboratory studies of the shear resistance [7]. Planar model samples 0.04 m thick had a brickwork structure containing bricks $0.04 \times 0.015 \times 0.005$ m in size. The strength of blocks with respect to uniaxial compression and to the tension was $R_c = 0.6$ MPa and $R_p = 0.07$ MPa, respectively, the bulk modulus was $E = 10$–80 MPa, and the parameters characterizing shear resistance to a shear along the horizontal cracks within the same brick were $\tan\varphi = 0.5$ and $c = 0$. Tests of the combined samples were performed according to a torqueless loading scheme (Fig. 2) under normally directed loads in the 0- to 1.2-MPa range. As a result of shear tests, the following values of strength characteristics of a combined model were obtained: $c = 0.2$–0.028 MPa and $\varphi = 35°$–$39°$.

In calculating the strength characteristics according the brickwork model of the rock base, the bulk modulus was taken equal to 60 MPa, and the level of normal stresses was assumed to be 0.08 MPa. The cracks were modeled by a continuous medium with mechanical characteristics determined according to [8, 9]. As a result of calculations, we obtained the following values: $c = 0.03$ MPa and $\varphi = 38°$, which agree well with the available experimental data.

REFERENCES

1. A. G. Tarkhov, Mater. VSEGEI, Obshch. Ser., No. 5, 209 (1940).
2. K. V. Ruppeneĭt, *Deformability of Cracked Rock Massifs* (Nedra, Moscow, 1975).
3. N. S. Bakhvalov, Dokl. Akad. Nauk SSSR **221**, 516 (1975).

4. N. S. Bakhvalov and G. P. Panasenko, *Averaging of the Processes in Periodic Media* (Nauka, Moscow, 1984).
5. A. F. Revuzhenko, Fiz.-Tekh. Probl. Razrab. Polezn. Iskop., No. 4, 14 (1990).
6. E. M. Wu, in *Mechanics of Composite Materials*, Ed. by J. Sendecky (Academic, New York, 1974; Mir, Moscow, 1978), Vol. 2.
7. D. D. Sapegin, R. A. Shiryaev, N. M. Karpov, *et al.*, Izv. VNIIG im. B.E. Vedeneeva **193**, 36 (1986).
8. A. N. Vlasov, V. P. Merzlyakov, and Van-Chzhen, in *Proceedings of the IV Russia Conference "Nonlinear Mechanics of Grounds," St. Petersburg, 1993*, Vol. 1, pp. 19–25.
9. A. N. Vlasov and V. P. Merzlyakov, in *Proceedings of the ISRM International Symposium on Safety and Environmental Issues in Rock Engineering, Eurock 93, Lisboa, Portugal, 1995* (Balkema, Rotterdam, 1995), pp. 975–981.

Translated by T. Galkina

Doklady Physics, Vol. 45, No. 6, 2000, pp. 288–290. Translated from Doklady Akademii Nauk, Vol. 372, No. 4, 2000, pp. 487–489.

MECHANICS

Application of the *R*-Function Theory to Diffraction of Thermoelastic Waves by Complex Objects

V. F. Kravchenko*, Corresponding Member of the RAS V. I. Pustovoĭt, V. L. Rvachev***, and N. D. Sizova*****

Received November 5, 1999

Introduction. It is well known that complex design elements in industrial facilities can be affected by thermal and mechanical stresses. In the temperature field, a design element playing the role of a mechanical unit can be affected by an incident wave with arbitrary profile and wavefront. As a result, we observe the diffraction of thermoelastic waves by complex objects. These diffraction problems are studied in mechanics of deformable solids, physics, seismology, etc.

Formulation of the problem and the method of its solving. Mathematical formulation of such problems is reduced to analyzing the following system of differential equations [1]:

$$\mu\nabla^2\mathbf{U} + (\lambda+\mu)\mathrm{grad}\,\mathrm{div}\mathbf{U} = \rho\frac{\partial^2\mathbf{U}}{\partial t^2} + (3\lambda+2\mu)\mathrm{grad}\,\alpha_T T - \mathbf{F}(x), \quad x \in (x_1, x_2, x_3). \tag{1}$$

Here, $\mathbf{U}$ is the displacement vector with components u_1, u_2, and u_3; α_T is the thermal expansion coefficient of the material; $T(x_1, x_2, x_3)$ is the temperature of an elastic body; λ and μ are the Lamè coefficients; ρ is the density of the material; and $\mathbf{F}(x_1, x_2, x_3)$ are the volume forces acting upon the elastic body. Without any loss of generality, we assume for simplicity that $\mathbf{F}(x_1, x_2, x_3) = 0$.

The following conditions are specified at the boundary of the elastic body:

$$N(\mathbf{U}) = \left[2\mu\frac{\partial\mathbf{U}}{\partial\nu} + \lambda(\boldsymbol{\nu}\mathrm{div}\mathbf{U}) + \mu(\boldsymbol{\nu}\times\mathrm{rot}\mathbf{U})\right]\Big|_S = \boldsymbol{\psi}(x). \tag{2}$$

Here, $\boldsymbol{\nu}$ is the unit vector of the outer normal to the boundary surface S, and $\boldsymbol{\psi}(x)$ is the stress vector at S, which is a sum of the mechanical and thermal contribution to the total stress acting upon body Ω. In this case, we assume that solvability conditions for equations (1) and (2) are met. In addition to equation (1) and boundary condition (2), a complete system of the equations describing the diffraction of thermoelastic waves involves the heat conduction relations [2, 3]

$$AT = \sum_{k,l=1}^{3}\frac{\partial}{\partial x_l}\left(a_{kl}\frac{\partial T}{\partial x_k}\right) = f(x) + a^2\frac{\partial T}{\partial t}, \quad (x = x_1, x_2, x_3) \in \Omega, \tag{3}$$

$$T(x,t) \in H^1(\Omega, A) \equiv \{T/T \in H^1(\Omega), AT(x,t) \in L^2(\Omega)\},$$

$$B^m T = \sum_{k=1}^{3} b_{kl}^m\frac{\partial T}{\partial x_k}\cos(\nu_l, x_k) - b_0^m T = g^m(x), \quad x \in S, \quad S = \bigcup_p S_p, \quad m = 1, 2, 3, 4, \tag{4}$$

$$T|_{t=0} = \psi(x). \tag{5}$$

Equation (3) is a linear differential equation with variable coefficients a_{kl}, $a^2 = c\rho/\bar{\lambda}$, c is the coefficient of heat transfer, and $\bar{\lambda}$ is the heat conduction. Relationship (4) is a general boundary condition, which can be reduced to mixed boundary conditions, as well as to boundary conditions of the first, second, and third kinds depending on the choice of coefficients b_{kl}^m, b_0^m, and g^m. In (4), B^m is a differential operator of boundary conditions; $T(x, t)$ is the temperature at point x within domain Ω bounded by piecewise smooth surface S, with $S = \bigcup_{p=1}^{r} S_p$ at time point t; and ν_k is a component of the inner normal to the surface element S_k of the boundary surface S.

Methods of solving problem (3)–(5) are adequately covered, for example, in [2–4].

* *Institute of Radio Engineering and Electronics, Russian Academy of Sciences, ul. Mokhovaya 11, Moscow, 103907 Russia*

** *Central Design Bureau of Unique Instrumentation, Russian Academy of Sciences, ul. Butlerova 15, Moscow, 117342 Russia*

*** *Institute of Mechanical Engineering Problems, National Academy of Sciences of Ukraine, ul. Dm. Pozharskogo 2/10, Kharkov, 310046 Ukraine*

1028-3358/00/4506-0288$20.00

By using the *R*-function theory, analytical solutions to heat conduction problems can be written in the form [4]

$$T(x, t) = g(t)B(T),$$

where $g(t)$ is a function meeting initial condition (5) and operator $B(T)$ is an analytical solution to problem (3), (4) constructed using the *R*-function theory [4] and exactly meeting boundary conditions (4). According to [1], the system of equations (1) can be transformed into that for potentials corresponding to longitudinal Φ and transverse Ψ waves:

$$\Delta\Phi - c_1^2\frac{\partial^2\Phi}{\partial t^2} = \frac{\gamma_1}{c_1^2\rho}T, \quad \Delta\Psi = \gamma^2\frac{\partial^2\Psi}{\partial t^2}. \qquad (6)$$

Here, $t = c_1 t_1$; $\gamma = c_1/c_2$; c_1 and c_2 are the propagation velocities of longitudinal and transverse waves, respectively; and $\gamma_1 = (3\lambda + 2\mu)\mathrm{grad}\,\alpha_T$.

Let us write in the following form boundary conditions related to the effect of the wave with an arbitrary profile on an elastic medium weakened by the hole with a complex shape (having the boundary contour Γ):

$$\sigma_n|_\Gamma = f_1(x, t), \tau_n|_\Gamma = f_2(x, t), \qquad (7)$$

where n and τ are the vectors along normal and tangent to the boundary contour Γ, respectively.

We will solve problem (6) and (7) using a method based on the *R*-function theory [4]. Let us represent the analytical solutions for potentials Φ and Ψ in the form of relationships discussed in [5], omitting factor $\exp(-i\omega t)$ in the case of steady-state motions:

$$\Phi = \frac{\partial}{\partial x_1}[\Phi_1 + \Psi_2] - \frac{\partial}{\partial x_2}[\Phi_2 + \Psi_1] + \Phi_0,$$

$$\Psi = \frac{\partial}{\partial x_2}[\Phi_1 - \Psi_2] - \frac{\partial}{\partial x_1}[\Phi_2 - \Psi_1] + \Psi_0,$$

$$\Phi_1 = \Phi_{i1} + \omega D_1\Phi_{i1} + \omega T_1\Phi_{i1}\frac{\partial\omega}{\partial x_1}\frac{\partial\omega}{\partial x_2}\frac{2(\lambda + \mu)}{\lambda + 2\mu},$$

$$\Psi_i = \omega T_1\Phi_{i1}\left[\frac{\lambda}{\lambda + 2\mu}\left[\frac{\partial\omega}{\partial x_1}\right]^2 + \left[\frac{\partial\omega}{\partial x_2}\right]^2\right], \quad i = 1, 2; \qquad (8)$$

$$\Phi_0 = \frac{\partial}{\partial x_1}\tilde{\Phi}_0 + \frac{\partial}{\partial x_2}\tilde{\Psi}_0, \Psi_0 = \frac{\partial}{\partial x_2}\tilde{\Phi}_0 - \frac{\partial}{\partial x_1}\tilde{\Psi}_0,$$

$$\tilde{\Phi}_0 = \frac{1}{\lambda + \mu}\omega\frac{\partial\omega}{\partial x_1}\bar{f}_1(x) + \frac{1}{\mu}\omega\frac{\partial\omega}{\partial x_2}\bar{f}_2(x),$$

$$\tilde{\Psi}_0 = \frac{1}{\lambda + \mu}\omega\frac{\partial\omega}{\partial x_2}\bar{f}_1(x) - \frac{1}{\mu}\omega\frac{\partial\omega}{\partial x_1}\bar{f}_2(x).$$

Here, $\omega = \omega(x)$ are functions describing the equation for contour Γ, T_1 and D_1 are differential operators defined in [4], and Φ_{i1} are special functions, conventional polynomials, or polynomials with local supports.

Solutions (8) take the form of functional relationships involving either elementary functions or superpositions of elementary and special functions. Both boundary conditions (7) and the configuration of the domain, in which problem (6) and (7) is considered, are treated analytically. Moreover, due to an arbitrary choice of functions Φ_{i1} ($i = 1, 2$), we can take into account certain *a priori* information on exact solutions (if they exist) and approximate them in the metrics of a corresponding functional space. To account for the conditions at infinity, we introduce pseudodifferential operators

$$S_1(\Phi) = \frac{\partial\Phi}{\partial n}, \quad S_2(\Phi) = \frac{\partial\Psi}{\partial n},$$

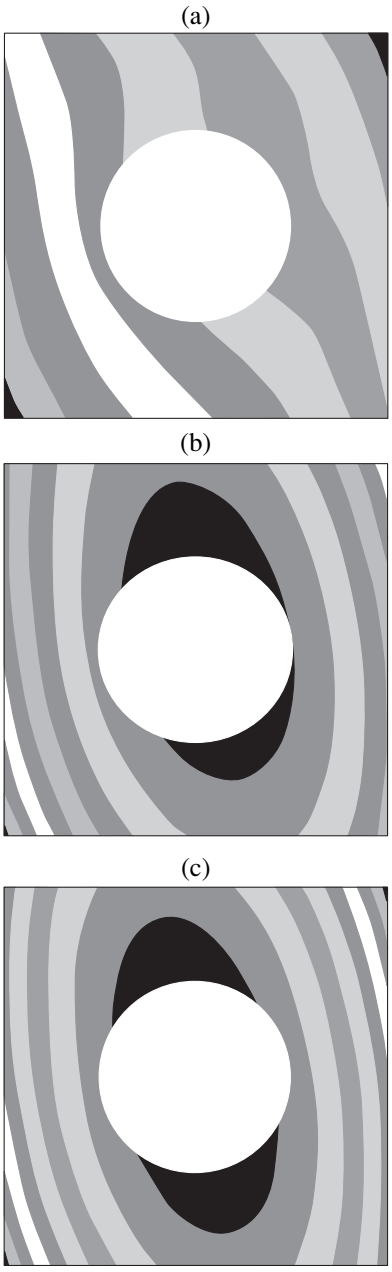

Fig. 1.

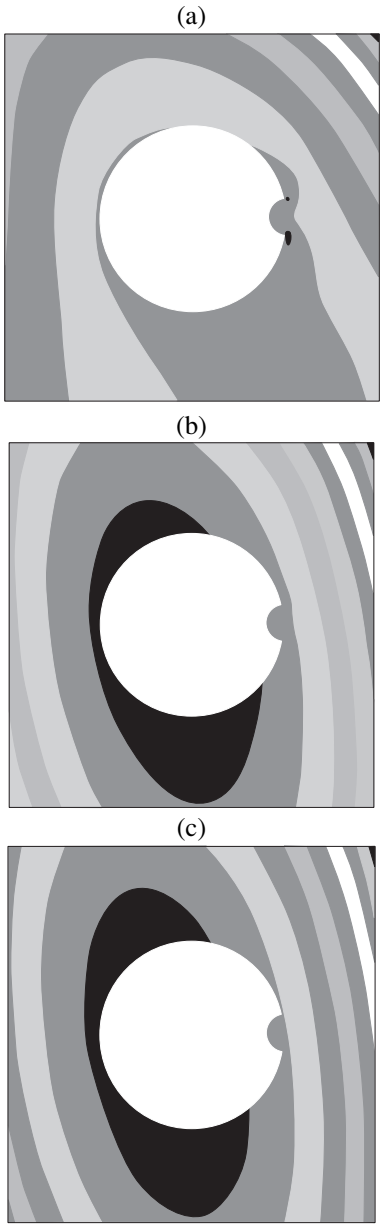

Fig. 2.

which are defined in a bounded domain $\Omega_0 \in \Omega$ with boundary Γ_0.

Provided that function $\omega(x)$ is chosen in the form

$$\omega = \frac{\omega_0 r}{\omega_0 + r}, \quad r = (x_1^2 + x_2^2)^{1/2},$$

with ω_0 being the equation for boundary Γ_0 of domain Ω_0, structural formula (8) describes fairly well wave processes in various zones of incident and reflected waves. From the relationships found for potentials Φ and Ψ, the components of the strain and stress tensors are determined by the formulas [1]

$$2\varepsilon = \nabla \mathbf{U} + (\nabla \mathbf{U})^*, \quad \sigma = \lambda \varepsilon E + 2\mu\varepsilon,$$

where the asterisk stands for transposition and E is the unit matrix. Displacement vector $\mathbf{U}$ can be presented in the form

$$\mathbf{U} = \mathbf{U}_p + \mathbf{U}_s,$$

where $\mathbf{U}_p$ and $\mathbf{U}_s$ correspond to the potential and solenoidal fields, respectively,

$$\mathbf{U}_p = \nabla \Phi, \quad \mathbf{U} = \nabla \Psi, \quad \nabla \Psi = 0.$$

Numerical simulations. We analyzed the steady-state diffraction of thermoelastic waves in an elastic medium weakened by a circular hole of radius r (Fig. 1) and by the same hole with an additional segment (Fig. 2). Temperature T_0 was kept constant at the cavity boundary Γ, and the elastic medium was exposed to an incident wave.

In Figs. 1 and 2, we present stress distributions σ_θ in elastic media weakened either by a circular hole or the same hole with an additional segment for the cases of (a) short, (b) medium, and (c) long incident wave. The effect of the temperature field is the most pronounced if this field is accompanied by a short-incident wave, and it is much weaker for long-incident waves.

Thus, we proposed and substantiated a method of solving boundary value problems for the diffraction of thermoelastic waves by complex objects based on the *R*-function theory. Our numerical simulations for the diffraction of thermoelastic waves either by a circular hole in an elastic medium or by the same hole with a segment demonstrated that the method is rather efficient. The effect of the temperature field was shown to be more (less) pronounced provided this field is accompanied by a short (long) incident wave. This method can be used for studying thermoelastic waves in objects subjected simultaneously to complicated thermal and wave stresses.

REFERENCES

1. W. Nowacki, *Teoria sprézystósci* (PWN, Warszawa, 1970; Mir, Moscow, 1975).
2. A. V. Lykov, *Theory of Thermal Conductivity* (Vysshaya Shkola, Moscow, 1967).
3. H. S. Carslaw and J. C. Jaeger, *Conduction of Heat in Solids* (Clarendon Press, Oxford, 1959; Nauka, Moscow, 1964).
4. V. L. Rvachev, *Theory of R-Functions and Its Selected Applications* (Naukova Dumka, Kiev, 1982).
5. Yu. V. Gulyaev, V. F. Kravchenko, V. L. Rvachev, *et al.*, Dokl. Akad. Nauk **343**, 163 (1995).

Translated by V. Chechin

Doklady Physics, Vol. 45, No. 6, 2000, pp. 291–293. Translated from Doklady Akademii Nauk, Vol. 372, No. 6, 2000, pp. 759–761.

MECHANICS

Mechanical Aspects of Hydrogen Enhanced Fatigue-Crack Growth

Academician V. V. Bolotin

Received February 17, 2000

It is well known [1] that absorption of hydrogen results in substantial degradation of mechanical properties for many metals and alloys, most structural steels included. The most significant effect is the reduction of the resistance to fracturing. In particular, reduction of the critical-stress intensity under monotonous loading is observed. In cyclical loading, reduction of the crack-growth threshold and increase of the crack-growth rate takes place. A similar effect is observed under slowly varied loading.

Hydrogen embrittlement includes several mechanisms developing at various levels of material structure. Among them are penetration of atomic hydrogen into the metal lattice, interaction between atomic hydrogen and dislocations, hydrogen accumulation in micropores and microcracks, and formation of hydrides and decarburization as a result of chemical reactions. Frequently, common electrochemical corrosion occurs along with hydrogenization. All these effects are closely associated with atomic-hydrogen transport in the solid phase. Along with classical diffusion, hydrogen transport controlled by stress-strain and distributed-damage fields takes place. In addition, the transport of gaseous hydrogen or a hydrogen-carrying agent to the crack tip should also be analyzed. In the case of cyclical loading, the cyclical convective motion of gaseous or liquid media within the crack hollow should be also taken into account.

Until now, hydrogen embrittlement was studied mostly by specialists in materials science, electrochemistry, and those branches of industry for which this effect is important. The suggested models included one or two possible mechanisms and resulted in estimates of qualitative character. The most important quantitative parameter is the crack growth rate enhanced by hydrogen embrittlement. This parameter is assessed as the ratio of a characteristic length used in fracture mechanics, such as the crack-tip opening displacement, and a characteristic time of hydrogen diffusion in the solid phase. A detailed analysis of works published before 1977 was given in paper [2]. Since then, no substantial progress has been observed [3]. However, mechanical aspects of hydrogen embrittlement are important in evaluating the safe service life for pressure vessels, pipelines, and other highly stressed structural components subjected to contact with molecular hydrogen or its carrier. As many interacting and partially competing mechanisms enter the picture, phenomenological models seem more realistic from the practical viewpoint. The number of model parameters should be minimal, and the methods for assessing these parameters from direct macroscopic experiments should be indicated.

From the viewpoint of mechanics of deformable solids, crack initiation and growth is a result of the interaction of two mechanisms: damage accumulation near the crack tip and the general balance of forces and energy in the system involving the cracked body, loading, and environment [4, 5]. Due to irreversibility of cracks in common materials, the constraints put on the crack dimensions are treated as unilateral. As applied to a single-parameter crack with depth a, the crack behavior depends on the relationship between generalized (in the meaning of analytical mechanics) forces: the generalized driving force G and the generalized resistance force Γ. The former can be associated with the energy release rate in linear fracture mechanics, and the latter, with the critical magnitudes of this rate. A crack does not grow at $G < \Gamma$. The crack front propagates continuously at $G = \Gamma$, $\frac{\partial G}{\partial a} < \frac{\partial \Gamma}{\partial a}$, and as a jump (until the next arrest or until the final failure) at $G = \Gamma$, $\frac{\partial G}{\partial a} > \frac{\partial \Gamma}{\partial a}$. In the case of $G > \Gamma$, the state of the system is unstable. This approach is valid at both long cyclical and slowly varied loading. Then, the generalized forces depend on the damage accumulated in the tip zone and, sometimes, in the far-field zone. The crack growth is frequently accompanied by environmental effects; then, the corrosion, hydrogen, etc. modes of damage should be included.

Blagonravov Institute of Machine Science, Russian Academy of Sciences, Malyĭ Khariton'evskiĭ per. 4, Moscow, 101830 Russia

E-mail: bolotin@deans.mpei.ac.ru

1028-3358/00/4506-0291$20.00

It is natural to model dispersed damage accumulation in the framework of damage continuum mechanics. In general, damages are described in terms having a tensorial nature. However, when the crack trajectory is known beforehand, e.g., from symmetry considerations, the damage level may be characterized by a scalar Rabotnov–Kachanov quantity ω ($0 \le \omega \le 1$).

In the presence of several different mechanisms, corresponding damage measures should be introduced. We distinguish mechanical damage produced by cyclical loading ω_f, and that by sustained loading, ω_s. Corrosion damage is characterized by the measure ω_c. Hydrogenization effects are introduced by two measures ω_a and ω_b. The first one takes into account the material degradation due to the direct action of atomic hydrogen; the second one corresponds to the degradation due to chemical actions. Kinetic equations are to be formulated for each measure to connect the damage rate with the corresponding damaging factor such as the tensile stress range or the concentration of atomic hydrogen. The set of all introduced damage measures as functions of time t are denoted by $\omega(t)$.

The conditions of stability and growth of a single-parameter crack given by the depth a may be formulated in terms of the function $H(N)$ of the cycle number N:

$$H(N) = \sup_{t_{N-1} < t \le t_N} \{G[a(t), \mathbf{s}(t), \boldsymbol{\omega}(t)] - \Gamma[a(t), \mathbf{s}(t), \boldsymbol{\omega}(t)]\}. \quad (1)$$

Here $a(t)$ is the crack size; $\mathbf{s}(t)$ is the set of load and environment parameters. Let the transport of the agent from the crack mouth to the crack tip and of atomic hydrogen in the solid phase be described in the one-dimensional approximation. Let $c_e(t)$ and $c(x, t)$ be the concentrations of molecular or chemically bounded hydrogen in the environment and in the crack hollow, respectively. The equation of diffusion should be supplemented with a convection term, as well as with a term taking into account hydrogen adsorption on crack faces:

$$\frac{\partial c}{\partial t} + v\frac{\partial c}{\partial x} = \frac{\partial}{\partial x}\left(D\frac{\partial c}{\partial x}\right) - \frac{2kf(c)}{h}. \quad (2)$$

Here, D is the diffusion coefficient, v is the agent's convective velocity, $kf(c)$ is the adsorption rate, and h is the crack opening displacement. For the hydrogen transport in the solid phase, we have the equations

$$\frac{\partial c_a}{\partial t} = \frac{\partial}{\partial x}\left(D_s\frac{\partial c_a}{\partial x}\right) - \frac{\partial}{\partial x}\left(B_s c_a\frac{\partial \sigma}{\partial x}\right) - \frac{\partial c_b}{\partial t},$$

$$\frac{\partial c_b}{\partial t} = g(c_a, c_b).$$

The first equation describes the diffusion process with the coefficient D_s and the transport controlled by the stress gradient $\frac{\partial \sigma}{\partial x}$ with the coefficient B_s. The last term in this equation takes into account trapping of atomic hydrogen, e.g., because of the formation of hydrides. The rate of the latter process is given in the second equation of (3). We can assume that

$$g(c_a, c_b) = k_b(c_a - c_{at})(c_{bt} - c_b)$$

with two threshold-concentration values c_{at} and c_{bt} and rate parameter k_b. All material parameters depend, in the general case, on temperature and local damage measures. The boundary conditions for equations (2) and (3) are $c = c_e$ at $x = 0$; $D\frac{\partial c}{\partial x} = kf(c)$ and $D\frac{\partial c}{\partial x} = D_s\left(\frac{\partial c_a}{\partial x} + \frac{\partial c_b}{\partial x}\right)$ at $x = a$. The thickness of the surface embrittlement film is small. Therefore, we may assume that $c_a \longrightarrow c_\infty$ and $c_b \longrightarrow c_\infty$ as $x \longrightarrow \infty$. The initial conditions depend on that whether the crack hollow is "dry" at $t = 0$ or filled with the carrying agent, whether the solid phase is initially hydrogenized or not, etc.

The crack hollow volume under cyclical loading varies cyclically. A part of the agent leaves the hollow while downloading, and the fresh agent enters the hollow while uploading. This is the so-called pumping effect of fatigue cracks. Due to this effect, the concentration of the agent at the crack tip approaches a certain quasi-steady level that depends on the hydrogen adsorption and corrosion rates. In any case, at the crack tip, we have an estimate for the film thickness of the hydrogen embrittlement: $\frac{\partial c}{\partial x} \sim \frac{c_e}{a_0}$ and less. Here a_0 is the initial crack depth. The estimate for the thickness of the corrosion and hydrogenization film is $\lambda_h \sim \frac{D_s/D_0}{a_0}$ and less. As D_s is two–three orders of magnitude smaller than D, the film thickness is small compared to the size of the zone corresponding to a cyclical process.

The proposed model includes, along with the partial differential equations (2) and (3), the ordinary differential equations of damage accumulation and the functional relationships with respect to the function $H(N)$ entering into equation (1). Obviously, the realization of equation (1) requires solving the problem of continuum mechanics for a body with a crack, whose size is subjected to isochronic variation [5]. The corresponding computational algorithm is rather complicated. It contains several iteration loops as well as special means to provide computational stability. Some details are presented in paper [7] as applied to corrosion fatigue cracks.

The estimation of model parameters meets certain difficulties. The direct identification of these parameters leads to ill-posed problems. However, a number of the parameters can be estimated from direct macro-

scopic experiments. For example, the damage measures can be found by analyzing the reduction of the specific work for destruction of samples subjected to the corresponding action. In turn, this makes it possible to evaluate parameters for right-hand sides in equations describing the accumulation of damages.

Numerical simulation, parameter assessment, and comparison with available experimental data show that the proposed model gives a satisfactory presentation of hydrogen-enhanced cracking in metals and alloys. Among these effects are the following: first, the decrease of the crack-growth threshold under cyclical and/or sustained loading; second, the tendency to the formation of a plateau on the crack-growth diagrams in the domain of low mechanical loads and/or short cracks; third, the influence of the mean applied stress, the applied-stress range, and load frequency on the crack growth rate and the summed cycle number (summed time) until the final failure. In addition, a deeper insight becomes possible into the internal mechanisms that are difficult to observe and measure directly. In particular, the following phenomena can be described within the framework of the proposed model: the effect of crack closure under cyclical loading on the agent concentration at the tip, the intermittent blunting and sharpening of the tip, and the change of the ratio between the mechanical, corrosion, and hydrogen-induced damages during all stages of the crack growth.

ACKNOWLEDGMENTS

This work was supported in part by the Russian Foundation for Basic Research (project no. 99-01-0282).

REFERENCES

1. *Structural Materials for Nuclear-Power Plants*, Ed. by Yu. F. Balandin, I. V. Gorynin, Yu. I. Zvezdin, *et al.* (Énergoatomizdat, Moscow, 1984).
2. A. E. Andreĭkin, V. V. Panasyuk, and V. S. Kharin, Fiz.-Khim. Mekh. Mater. **13** (2), 3 (1977).
3. R. A. Oriani, *Hydrogen Degradation of Ferrous Alloys* (Noyes, Park Ridge, 1985).
4. V. V. Bolotin, Eng. Fract. Mech. **22**, 387 (1985).
5. V. V. Bolotin, *Stability Problems in Fracture Mechanics* (Wiley, New York, 1996).
6. V. V. Bolotin and A. A. Shipkov, Prikl. Mat. Mekh. **62**, 313 (1998).
7. W. W. Gerberich, P. G. March, and W. Hoech, in *Hydrogen Effects in Materials* (TMS Publ., Wyoming, 1994), pp. 539–553.

Translated by V. Bolotin

Doklady Physics, Vol. 45, No. 6, 2000, pp. 294–297. Translated from Doklady Akademii Nauk, Vol. 372, No. 6, 2000, pp. 762–765.

MECHANICS

On the Dynamics of a Small Body in a Nonuniform Flow

O. V. Voinov

Presented by Academician V.P. Myasnikov September 1, 1999

Received September 6, 1999

We consider the dynamics of a small body in a nonuniform potential flow of incompressible fluid. An asymptotic analysis of both the flow interaction with a body and stability of its equilibrium is developed. Studying the dynamics of a body in a nonuniform flow is of interest as far as this is associated with hydrodynamic interaction of bodies moving in a fluid. Certain basic methods for solving this problem are described in [1–9].

Let, being free of a body, a potential flow of a perfect fluid have the velocity $\mathbf{v}(\mathbf{x}, t)$ and the pressure $p(\mathbf{x}, t)$. The distance r_0 between the geometric center of the body ($\mathbf{x} = \mathbf{q}$) and external boundaries of the flow is large compared to the body diameter D; i.e., the parameter D/r_0 is small [6, 7]. Other possible small parameters are introduced below. Dynamics of the surface of the body in the fluid is described by the Lagrange function L [6, 7]:

$$L = \frac{\rho}{2}\int_{\Omega}|\mathbf{v}' - \mathbf{v}|^2 d\tau - \int_{V} p d\tau, \qquad (1)$$

which takes into account the perturbance of the fluid velocity $\mathbf{v}' - \mathbf{v}$ caused by the body. Here, Ω and V are the domains occupied by the fluid and the small body, respectively, while ρ is the fluid density. The Lagrange function (1) forms the basis for an effective method of calculating the response of a body subjected to straining due to the hydrodynamic effect of nonuniform flow [6, 7]. In the case of a rigid body, dynamic equations include the Lagrange function L_b describing the body's dynamics:

$$\frac{d}{dt}\frac{\partial L'}{\partial \dot{q}_\alpha} - \frac{\partial L'}{\partial q_\alpha} = 0, \quad L' = L + L_b. \qquad (2)$$

Here and below, $\alpha, \beta = 1, 2, \ldots, 6$. The coordinates $q_{3+i} = \varphi_i$ ($i = 1, 2, 3$) represent the angles determining the orientation of the axes z_i. These axes are tied to the body, and their origin is located in the body center $\mathbf{q}$.

In the vicinity of a small body, we define the unperturbed fluid velocity $\mathbf{v}$ by the first terms of the expansion into the Taylor series at the point $\mathbf{x} = \mathbf{q}$ [6, 7]. We make use of the notation $\nabla_i v_j = v_{ij}(\mathbf{q}, t)$, $\nabla_i \nabla_j v_k = v_{ijk}(\mathbf{q}, t)$ and assume that the derivatives having an order of magnitude, which exceeds the second one, are zero. Due to the harmonic properties of the velocity potential ($\mathbf{v} = \nabla\Phi$), only 12 quantities v_{ij} and v_{ijk} out of 36 are independent.

The velocity perturbation $\mathbf{v}' - \mathbf{v}$ is expressed in terms of the potential perturbation $\Phi' - \Phi$, which depends linearly on the relative velocity $\mathbf{u} = \dot{\mathbf{q}} - \mathbf{v}(\mathbf{q})$, the angular velocity $\boldsymbol{\omega}$, as well as the derivatives v_{ij} and v_{ijk}. The coefficients of the linear form $\Phi' - \Phi$ depend on the body orientation and the difference $\mathbf{x} - \mathbf{q}$. At a large distance from the body, they decrease no slower than $|\mathbf{x} - \mathbf{q}|^{-2}$. Therefore, similarly to [6, 7], calculating integrals in (1) yields

$$\begin{aligned} L &= T(\mathbf{u}, \boldsymbol{\omega}) - pV + \Gamma_{\alpha jk} U_\alpha v_{jk} + A_{ijkl} u_i v_{jkl} \\ &\quad + \Theta_{ijkl}\omega_i v_{jkl} + B_{ijkl} v_{ij} v_{kl} - \frac{1}{2} I_{ij} \nabla_i \nabla_j p, \\ 2T &= \lambda_{\alpha\beta} U_\alpha U_\beta, \quad U_i = u_i, \\ U_{3+i} &= \omega_i, \quad I_{ij} = \int_V z_i z_j d\tau. \end{aligned} \qquad (3)$$

(Summation is implied over identical indices.) The first three terms of expressions (3) are indicated in [6, 7]. The coefficients occurring in (3) are constant in the coordinate system z_i and depend on the body's shape and diameter D: $\Gamma_{ijk} \sim D^4$, $\Gamma_{3+ijk} \sim D^5$ [6, 7]; $\mathbf{A}, \mathbf{B}, \mathbf{I} \sim D^5$; $\boldsymbol{\Theta} \sim D^6$. The apparent-mass coefficients ($\lambda_{ij} \sim D^3$, $\lambda_{3+ij} \sim D^4$, $\lambda_{3+i\,3+j} \sim D^5$) are determined by solving the problem for the motion of a rigid body in an unbounded uniform flow [2, 3]. It is convenient to calculate (3) in the z_i-axes. To do this, we express both the velocity components u_i and derivatives of v_i in terms of the corresponding quantities by using the x_i-axes. The contri-

Institute of Theoretical and Applied Mechanics, Tyumen' Branch, Siberian Division, Russian Academy of Sciences, Tyumen', 625600 Russia

1028-3358/00/4506-0294$20.00

bution of different terms in (3) is estimated with allowance for the possible validity of the relation $\omega \sim u/D$. At large values of r_0, the effect of a weak flow perturbance caused by a small body on the velocity field ν can attain the maximum value on the order of uD^3/r_0^3. Therefore, it is useless to retain those terms in (3) whose order of magnitude exceeds D^5. In the case of a variable body volume, the other estimate is valid [6–8].

For a spherical body, $\mathbf{\Gamma}$, $\mathbf{A}$, and $\mathbf{\Theta}$ are equal to zero. However, the values of

$$\lambda_{ij} = \frac{\rho}{4}V\delta_{ij},\ B_{ijkl} = \frac{\rho}{15}R^2V\delta_{ik}\delta_{jl},\ I_{ij} = \frac{1}{5}R^2V\delta_{ij} \quad (4)$$

are nonzero, where δ_{ij} is the Kronecker delta and $R = D/2$. Relations (2)–(4) lead to the following formula for a force acting on a spherical body in a nonuniform flow:

$$\mathbf{F} = \rho V\left[\frac{3}{2}\frac{d\mathbf{v}}{dt} + \frac{1}{3}R^2\nabla^2\frac{d\mathbf{v}}{dt} - \frac{1}{2}\mathbf{q}^{\cdot\cdot} - \mathbf{g}\right], \quad (5)$$

where $\mathbf{g}$ is the mass force. Compared to the formula known from [6–8], relation (5) contains the new term $\nabla^2\frac{d\mathbf{v}}{dt}$. According to (5), gas-bubble acceleration in a nonuniform flow can differ noticeably from the previously known value and equals the threefold accelerations of the fluid. For the first time, the first term occurring in (5) was written out by N.E. Joukowski for the case of an immovable sphere.

Small parameters in the problem of dynamics for a body placed in a flow. It is well known that the description of the dynamics for a body in a nonuniform flow is based on the dependence of the Lagrange function on the velocity $\mathbf{v}(\mathbf{q})$ with allowance for the term $T - pV$, where the kinetic energy T of the relative motion includes coefficients of apparent masses [6, 7]. This description is adequate when flow around the body is determined mainly by the relative velocity [7]. It is of interest to find small parameters corresponding to an approximately uniform flow around a rigid body and their possible role in describing the dynamics of the process. Below, we consider the general case when the apparent-mass tensor is not spherical.

The contribution of different terms to the perturbance of the velocity $\mathbf{v}' - \mathbf{v}$, which occurs near the body, is estimated taking into account the properties of the solutions to the corresponding Neumann problems of the Laplace equation. If $u^2 \gg D^2\nu_{ij}\nu_{ij}$, the contribution of terms (the maximum of their moduli) determined by the quantity ν_{ij} is small compared to that for terms depending on the velocity $\mathbf{u}$. If $u_2 \gg D^4\nu_{ijk}\nu_{ijk}$, the contribution of terms determined by ν_{ijk} is small. Under these conditions, a flow around a small body is close to uniform. At the same time, the contributions to (3) of terms containing $\mathbf{\Gamma}$, $\mathbf{A}$, $\mathbf{\Theta}$, and $\mathbf{B}$ are small compared to those of $T(\mathbf{u}, \boldsymbol{\omega})$. The contribution of the mentioned terms to $\frac{\partial L}{\partial\varphi_i}$ is small as well. We now introduce the parameter

$$\varepsilon = \frac{DG}{u},\quad G^2 = \nu_{ij}\nu_{ij} + u\sqrt{\nu_{ijk}\nu_{ijk}},\ G > 0. \quad (6)$$

The small parameter ε combines the two above-mentioned conditions into a single one for an approximately uniform flow around a body, which is uniform at $\varepsilon = 0$. If ε is not small, it is necessary to take into account all terms in (3). The parameter ε is similar to D/r_0 and represents also one of the definitions for the dimensionless diameter of a small body. Therefore, expansion in terms of the small parameter D/r_0 [6, 7] coincides with that in terms of small ε. The parameter ε allows us to refine the limits on the applicability of the equations for each approximation. We note that the velocity u occurring in the definition of ε is known *a priori*, e.g., in problems of calculating the hydrodynamic response or the stability of the equilibrium.

We introduce a parameter determining the role of the second integral occurring in (1) and in the dynamic equations (2) with respect to angular variables:

$$\varepsilon_2 = D(p_{ij}p_{ij})^{1/4}(\rho u^2)^{-1/2},\quad p_{ij} = \nabla_i\nabla_j p. \quad (7)$$

If ε_2 is small ($\varepsilon_2 \longrightarrow 0$), the term $-\frac{1}{2}\mathbf{I}\nabla\nabla p$ in (3) is also small as compared to $T(\mathbf{u}, \boldsymbol{\omega})$, and the second integral in (1) is insignificant for calculating the hydrodynamic angular momentum. In the case when ε_2 is on the order of unity, the contribution of the mentioned term to equations of the body rotation is not small. When we deal with the steady-state flow and when the magnitude of the velocity u is on the order of ν, then the order of magnitude for (7) does not exceed that for (6), and the parameter ε_2 differs insignificantly from ε (by a factor on the order of unity). In the limit of a weakly nonuniform flow (small values of ε and ε_2), the interaction of the body and flow is determined by the Lagrange function $T - pV$ [6, 7].

We assume that the coordinate system z_i coincides with the main axes of the apparent-mass tensor. The velocity $\mathbf{v}$ is given in the inertial system x_i, which is related to the system z_i by the transformation

$$z_i = e_{ij}(x_j - q_j), \quad (8)$$

where e_{ij} depend on the angles φ_k. The angles φ_1, φ_2, and φ_3 represent those for successive rotations about the axes 1, 2, and 3, respectively, of the movable trihedron. As a result, the trihedron axes transform from $x_i - q_i$ to the z_i-axes.

The equilibrium of a body in a steady-state flow is described by the equations $\nabla L = 0$ and $\frac{\partial L}{\partial\varphi_i} = 0$ ($i = 1$, 2, 3). We assume that $q_i = 0$, $\varphi_i = 0$, mass forces are absent, and the parameter ε is small. Then, taking into

account (3), we can conclude that the direction of the velocity **v** is almost collinear to the first axis:

$$v_i = vO(\varepsilon^N) \text{ at } i = 2, 3. \quad (9)$$

As for the exponent in (9), $N = 1$ for $\mathbf{\Gamma} \neq 0$ and $N = 2$ for $\mathbf{\Gamma} = 0$ (the latter case is possible for a symmetric body). The first angle $\varphi_1 = O(1)$ is determined only with allowance for those terms in (3) which are small with respect to ε, because at $\varepsilon = 0$ this angle is arbitrary. Using $\frac{\partial L}{\partial \varphi_1} = 0$ at $\varphi_1 = 0$, we impose restrictions on v_{ij} and v_{ijk}. We admit that $\lambda_{11} > 0$. Then, the three equations of equilibrium $\nabla_i L = 0$ yield $v_{1j} = GO(\varepsilon^N)$ $(j = 1, 2, 3)$.

Symmetry in perturbation dynamics. We consider a case with a body being not spherical but symmetric with respect to three mutually perpendicular planes. Then, $\lambda_{\alpha\beta} = 0$ at $\alpha \neq \beta$, $\mathbf{\Gamma} = 0$, and $N = 2$. The dynamic equations are written out in the linear approximation with respect to small perturbances q_α. The functions $e_{ij}(\varphi_k)$ occurring in (8) are calculated with an accuracy to small quantities of the second order, $\varphi_k\varphi_l$, inclusively. The following equations with respect to the coordinates q_i result from (2), (3), (8), and (9):

$$\begin{aligned}(m + \lambda_{33})\ddot{q}_3 + (\lambda_{11} - \lambda_{33})v_1(\dot{\varphi}_2 + v_{33}\varphi_2 - v_{23}\varphi_3) \\ - (\lambda_{33} - \lambda_{22})v_{23}(v_1\varphi_3 + \dot{q}_2) \\ - (\lambda_{11} + \rho V)v_1 v_{13j}q_j \\ - (\lambda_{22} + \rho V)v_{23}v_{2j}q_j - (\lambda_{33} + \rho V)v_{33}v_{3j}q_j = 0,\end{aligned} \quad (10)$$

$$(m + \lambda_{11})\ddot{q}_1 - (\lambda_{11} + \rho V)v_1 v_{11j}q_j = 0. \quad (11)$$

Here, m is the body mass, and the quantities v_i, v_{ij}, and v_{ijk} are calculated at the point $\mathbf{x} = 0$ at which $v_2 = v_3 = 0$ and $v_{1j} = 0$ $(j = 1, 2, 3)$. The equations are valid within an accuracy to ε^2. The equation with respect to q_2 is similar to (10). We introduce the new notation

$$\begin{gathered}\bar{t} = tG, \ \bar{q}_i = \frac{q_i}{D}, \ \bar{v}_{ij} = \frac{v_{ij}}{G}, \\ \tilde{v}_{ij} = \frac{u_k v_{kij}}{G^2}, \ \bar{\varphi}_i = \frac{\varphi_i}{\varepsilon}\end{gathered} \quad (12)$$

and normalize the quantities λ_{ij}, ρV, and m to λ_{11}. With the notation of (12), the equations with respect to the variables q_i contain neither dimensional quantities nor the parameter ε. By virtue of $|\bar{v}_{ij}| \leq 1$ and $|\tilde{v}_{ij}| \leq 1$, the coefficients of these equations that depend on the nonuniformity of the velocity field are bounded. With the notation of (12), equation (2) with respect to the coordinate φ_2 takes the form

$$\varepsilon^2 a_2 \ddot{\bar{\varphi}}_2 + \bar{\varphi}_2 - \dot{\bar{q}}_3 + \bar{v}_{3j}\bar{q}_j = 0, \quad (13)$$

where the quantity $a_2 = (\lambda_{55} + J_2)(\lambda_{11} - \lambda_{33})^{-1}D^{-2}$ includes the body moment of inertia J_2 with respect to the z_2-axis, and the dot denotes differentiation with respect to $\bar{t}$.

Equation (2) with respect to the coordinate $\bar{\varphi}_3$ is similar to (13). The equation with respect to φ_1 proves to be independent of the other five equations of small-perturbation dynamics.

Amplitudes of the perturbations have the form $\bar{q}_\alpha = c_\alpha \exp(\bar{\Lambda}\bar{t})$. For certain motions, the first term in (13) need not necessarily be small despite a small value of ε. With the notation of (12), the solution to the system depends on ε in a specific manner, in particular, $|\dot{\varphi}_2| \sim (1/\varepsilon)|\bar{\varphi}_2|$. Values of the characteristic exponent $\bar{\Lambda}$ are large: $|\bar{\Lambda}| \sim 1/\varepsilon$ as $\varepsilon \longrightarrow 0$. To exclude instability with a high increment, it is necessary to accept that $\lambda_{11} > \lambda_{33}$ and $\lambda_{11} \geq \lambda_{22}$. The mentioned "rapid" motions correspond to the solution of the problem, which concerns small perturbances of equilibrium for a body placed into a uniform flow [3]. The derived system of equations allows two values of $\bar{\Lambda}$, which correspond to the next approximation in the small ε, to be obtained.

To solve the problem of stability, it is sufficient to consider other solutions, which, in the limit $\varepsilon \longrightarrow 0$, are independent of ε. For them, in particular, $|\ddot{\bar{\varphi}}_2| \sim |\bar{\varphi}_2|$, and the first term in (13) is small, so that $|\bar{\Lambda}| \sim 1$. We now derive the asymptotic equations for such "slow" motions. It follows from relation (13) and a similar equation for $\alpha = 6$ written in the initial notation that

$$\begin{aligned}v_1\varphi_2 - \dot{q}_3 + v_{3j}q_j = 0, \\ v_1\varphi_3 + \dot{q}_2 - v_{2j}q_j = 0.\end{aligned} \quad (14)$$

If two apparent-mass coefficients coincide with each other, then $(\lambda_{11} = \lambda_{22})$, and only the first equation of (14) remains. Substituting (14) into both (9) and a similar equation with respect to q_2 yields the equation for the slow-perturbation dynamics

$$\begin{gathered}(m + \lambda_{11})\ddot{q}_i - (\lambda_{11} + \rho V)q_j\nabla_j\nabla_i(v^2/2) = 0, \\ i = 1, 2, 3.\end{gathered} \quad (15)$$

Here, ∇_i are calculated at the point $\mathbf{x} = 0$. In contrast to (10), relation (15) is free from contributions of both velocities and the apparent-mass coefficients λ_{22} and λ_{33}. As in the case of a mass point, the inertial term occurring in (15) is symmetric. This symmetry (isotropy) is unexpected, because the apparent-mass tensor is not spherical. Regularity (15) is valid, for example, in the case of a disk, a thin symmetric body, and ellipsoids. Symmetry of equations describing small perturbances occurs in another problem as well, namely,

when a body moves in a fluid under the effect of a constant (at $t > 0$) external force. If initial conditions are appropriate, there exists the solution to this problem, which, for short times, is described by an equation similar to (15).

The effective potential energy entering into (15) has no minimum in the equilibrium position (because $\Delta(v^2) \geq 0$), and this is similar to the known case of the sphere [9]. This behavior agrees with the fact that the condition $L \geq 0$ indicates instability [9]. With only one exception, relation (15) corresponds to the exponential instability of equilibrium for a body placed into flow. We now show that (15) can describe the neutral stability of the equilibrium. We assume that $\nabla\mathbf{v} = 0$ and consider two cases. In the first of them, except for $v_{122} = \gamma \neq 0$ and $v_{111} = -\gamma$, the quantities $v_{ijk} = 0$ for all ijk (permutation of the indices is insignificant). Based on (15), we can express the characteristic exponent in the form

$$\Lambda_1 = (v_1|\gamma|)^{1/2}(\lambda_{11} + \rho V)^{1/2}(\lambda_{11} + m)^{-1/2}.$$

In the second case, among all v_{ijk}, only $v_{233} = \gamma$ and $v_{222} = -\gamma$ are nonzero. In contrast to the first case, $v_i v_{ijk} = 0$ for all jk. As a result, according to (15), the exponent $\Lambda = 0$; i.e., the equilibrium is neutrally stable in the framework of (15). The same result is obtained by solving the system of equations (10), (11), (13) and the similar equations with respect to the variables q_2 and φ_3. It is noteworthy that these results are valid for small ε. Therefore, we may conclude that in the second case, $\Lambda = \Lambda_1 O(\varepsilon)$. Thus, the effect of an abnormally strong (by a factor of ε^{-1}) decrease in the perturbance amplitude for the equilibrium state of the body in the flow is possible. This effect is caused by a variation of the orientation of the coordinate system under the condition of a given nonuniformity of the velocity field with respect to the vector **u**.

When a body is in equilibrium, and its center is situated at the critical point ($\mathbf{v} = 0$) of a steady-state flow, the parameter ε is unlimitedly large. The corresponding linear problem of the equilibrium stability has been considered in the case of $\nabla\mathbf{v} \neq 0$ and $\nabla\nabla\mathbf{v} = 0$. The exponential instability is proven to occur for an arbitrary symmetric body [10]. If the center of the body is immovable, its stable orientation in the steady-state flow can be determined with the use of formulas (2) and (3).

REFERENCES

1. N. E. Joukowski, *Collection of Papers*, Vol. 2: *Hydrodynamics* (Gostekhizdat, Moscow, 1949).
2. L. I. Sedov, *A Course in Continuum Mechanics* (Nauka, Moscow, 1970; Wolters-Noordhoff, Groningen, 1971), Vol. 2.
3. H. Lamb, *Hydrodynamics* (Cambridge Univ. Press, Cambridge, 1932; Gostekhizdat, Moscow, 1947).
4. M. I. Gurevich, Izv. Akad. Nauk SSSR, Mekh. Zhidk. Gaza, No. 3 (1968).
5. O. V. Voinov and M. I. Gurevich, Izv. Akad. Nauk SSSR, Mekh. Zhidk. Gaza, No. 2, 169 (1974).
6. O. V. Voinov and A. G. Petrov, Dokl. Akad. Nauk SSSR **210**, 1036 (1973) [Sov. Phys.–Dokl. **18**, 372 (1973)].
7. V. V. Voinov, O. V. Voinov, and A. G. Petrov, Prikl. Mat. Mekh. **37**, 680 (1973).
8. O. V. Voinov, Prikl. Mekh. Tekh. Fiz., No. 4, 182 (1973).
9. O. V. Voinov and A. G. Petrov, Dokl. Akad. Nauk SSSR **237**, 1303 (1977) [Sov. Phys.–Dokl. **22**, 722 (1977)].
10. O. V. Voinov, Available from VINITI, No. 2769-V99 (Moscow, 1999).

Translated by Yu. Verevochkin

Doklady Physics, Vol. 45, No. 6, 2000, pp. 298–301. Translated from Doklady Akademii Nauk, Vol. 372, No. 6, 2000, pp. 766–769.

MECHANICS

A Model for Filtration in an Aperiodic Medium with Double Porosity

M. V. Goncharenko*, L. S. Pankratov*, and M. B. Panfilov**

Presented by Academician V.P. Myasnikov April 18, 1999

Received August 27, 1999

In this paper, the time-dependent equation for diffusion in an aperiodic porous medium with weakly penetrable inclusions is considered. The asymptotic behavior of its solutions is described by an averaged equation with memory. Effective parameters are calculated with the help of solutions to local problems. The general model obtained is shown to describe three qualitatively distinguished cases differing by the degree of inhomogeneity of a medium.

1. Introduction. We consider here transport processes in a porous medium representing the spatial alternation of two types of rocks with contrast transport properties. In this case, we cannot ignore the existence of a weakly conducting subsystem since, even being virtually impenetrable, it can contain a considerable quantity of a fluid. Objects of this type are widely met in hydrology or oil engineering, where natural porous strata are composed of rocks with sharply different petrographic properties or are dissected by nets of cracks. For the description of such objects, a model of media with double porosity is used. In the framework of this model, a medium is represented as a unified highly penetrable system (matrix) Ω^ε having weakly penetrable inclusions (blocks) F^ε. The porosity of blocks is considered to be not lower than that of the matrix. If the scale of an inhomogeneity ε is small, the averaged behavior of the system is of interest. This behavior is complicated due to the fact that the medium involves the second substantial parameter $\omega \ll 1$ equal to the ratio between the conductivity of blocks and that of the matrix, so that the asymptotic degeneracy of coefficients of the equations occurs on the inclusions as $\omega \longrightarrow 0$.

The classical model of flow through a medium with double porosity [1] was based on the hypothesis of a quasisteady exchange process between the blocks and the matrix. In the general case, the exchange process is unsteady, and, by virtue of the Duhamel principle, the appearance of operators of the time-convolution type can be expected. A similar model with memory was proposed in [2, 3] for a particular relation between the medium parameters when $\omega \sim \varepsilon^2$ (ε^2-model). In the more general case, media with double porosity correspond to all situations when $\omega \sim \varepsilon^2$. Four classes of such media [4] can be distinguished. For $\omega \ll \varepsilon^2$, weakly penetrable blocks can be ignored; for $\omega \sim \varepsilon^2$, the transport is described by the above model with a long-term memory; for $\omega \sim \varepsilon^2$, the medium has a short-term memory; and, for $\varepsilon \ll \omega \ll 1$, the medium behavior is moderately inhomogeneous without memory.

Similar objects were studied in [5, 6].

In this paper, we derive a mathematically rigorous general macroscopic model for the zero-order transport. The generalization concerns three aspects: (a) the heterogeneity can be aperiodic; (b) the ratio between conductivities is arbitrary, so that $\omega \ll 1$; (c) the degree of connectedness of the block system is arbitrary. To derive the model, we have used the variational method developed in [7–9]. The periodic cases, for which the effective coefficients can be calculated explicitly, are considered as examples.

2. Formulation of the problem. Let Ω be a bounded region in $\mathbf{R}^3$ with a piecewise-smooth boundary $\partial\Omega$. The following initial boundary value problem is considered:

$$\frac{\partial u^\varepsilon}{\partial t} - \operatorname{div}(a^\varepsilon(x)\nabla u^\varepsilon) = f^\varepsilon(x), \quad x \in \Omega, \quad t \in (0, T); \quad (1)$$

$$\begin{gathered} \frac{\partial u^\varepsilon}{\partial \nu}(x, t) = 0, \quad x \in \partial\Omega, \quad t \in (0, T), \\ u^\varepsilon(x, 0) = u_0^\varepsilon(x), \quad x \in \Omega, \end{gathered} \quad (2)$$

where $a^\varepsilon(x)$, $f^\varepsilon(x)$, and $u_0^\varepsilon(x)$ are given. We assume that $f^\varepsilon(x) \in L^2(\Omega)$, $u_0^\varepsilon(x) \in H^1(\Omega)$, and $a^\varepsilon(x)$ is the positive limited function in Ω for an arbitrary $\varepsilon > 0$.

It is known that for an arbitrary $\varepsilon > 0$, there exists a unique solution $u^\varepsilon(x, t)$ to problem (1), (2), which belongs to the class $C[0, T; H^1(\Omega)]$.

* *Institute of Low-Temperature Physics, National Academy of Sciences of Ukraine, Kharkov, Ukraine*

** *Institute of Oil and Gas Problems, Russian Academy of Sciences, Moscow, Russia*

1028-3358/00/4506-0298$20.00

We assume that there exists a set $F^{(\varepsilon)} \subset \Omega$, which satisfies the following conditions:

(i) $F^{(\varepsilon)}$ becomes progressively denser in Ω, so that, in the case of an arbitrary ball $V(x, \rho)$ with the center at the point $x \in \Omega$ and radius ρ, we have $V(x, \rho) \cap F^{\varepsilon} \neq 0$, $V(x, \rho) \cap (\Omega \backslash F^{(\varepsilon)}) \neq 0$ for a reasonably small $\varepsilon > 0$;

(ii) $\sup_{x \in F^{(\varepsilon)}} a^{\varepsilon}(x) \longrightarrow 0$ as $\varepsilon \longrightarrow 0$;

(iii) the region $\Omega^{(\varepsilon)} = \Omega 0 F^{(\varepsilon)}$ is strongly connected [8] with respect to the region Ω, and, moreover, $a^{\varepsilon}(x) \geq a_0 > 0$ for $x \in \Omega^{(\varepsilon)}$.

We denote the norms in the spaces $L^2(Q)$ and $H^1(Q)$ as $\|\cdot\|_Q$ and $\|\cdot\|_{1, Q}$, respectively, and investigate the asymptotic behavior of the solution $u^{\varepsilon}(x, t)$ as $\varepsilon \longrightarrow 0$.

To do this, we introduce a local description of the penetrability for the sets $\Omega^{(\varepsilon)}$.

Let $K(z, k) = K_h^z$ be a cube with its center at the point $z \in \Omega$ and an edge of length $h > 0$. We define the functional for the vectors $\mathbf{l} = (l_1, l_2, l_3) \in \mathbf{R}^3$ assuming

$$A(z, \varepsilon, h; \mathbf{l}) = \inf_{v^{\varepsilon}} \int_{\Omega^{(\varepsilon)} \cap K_h^z} \left\{ a^{\varepsilon}(x) \left| \nabla v^{\varepsilon} \right|^2 + h^{-2-\gamma} \left| v^{\varepsilon} - (x - z, \mathbf{l}) \right|^2 \right\} dx. \quad (3)$$

Here, $(\cdot, \cdot)$ is the scalar product in $\mathbf{R}^3$ and $0 < \gamma < 2$. The lower bound in (3) is taken according to the class of functions $v^{\varepsilon}(x) \in H^1(\Omega^{(\varepsilon)} \cap K_h^z)$. Functional (3) is quadratic with respect to the vector $\mathbf{l} \in \mathbf{R}^3$. The following representation is also true:

$$A(z, \varepsilon, h; \mathbf{l}) = \sum_{i, j = 1}^{3} a_{ij}(z, \varepsilon, h) l_i l_j,$$

if

$$a_{ij}(z, \varepsilon, h) = \int_{\Omega^{(\varepsilon)} \cap K_h^z} \{ a^{\varepsilon}(x) (\nabla v_i^{\varepsilon}, \nabla v_j^{\varepsilon}) + h^{-2-\gamma} \left\lfloor (v_i^{\varepsilon} - (x_i - z_i))(v_j^{\varepsilon} - (x_j - z_j)) \right\rfloor \} dx,$$

where, $v_j^{\varepsilon}(x)$ is the function minimizing (3) and $\mathbf{l}$ is the unit vector along the x_j-axis.

We consider also the functional

$$\Gamma_{\lambda}(z, \varepsilon, h; s) = \inf_{w^{\varepsilon}} \int_{K_h^z} \left\{ a^{\varepsilon}(x) \left| \nabla w^{\varepsilon} \right|^2 + \lambda \left| w^{\varepsilon} \right|^2 \chi_{F^{(\varepsilon)}}(x) + h^{-2-\gamma} \left| w^{\varepsilon} - s \right|^2 \chi_{\Omega^{(\varepsilon)}}(x) \right\} dx, \quad (4)$$

where $\chi_{F^{(\varepsilon)}}(x)$ and $\chi_{\Omega^{(\varepsilon)}}(x)$ are the indicators of the sets $F^{(\varepsilon)}$ and $\Omega^{(\varepsilon)}$, respectively; $\lambda > 0$, $s \in \mathbf{R}$. The lower bound in (4) is taken according to the class of functions $w^{\varepsilon}(x) \in H^1(K_h^z)$.

The functional $\Gamma_{\lambda}(z, \varepsilon, h; s) = b_{\lambda}(z, \varepsilon, h) s^2$ satisfies the equality

$$\Gamma_{\lambda}(z, \varepsilon, h; s) = b_{\lambda}(z, \varepsilon, h) s^2,$$

where

$$b_{\lambda}(z, \varepsilon, h) = \inf_{w^{\varepsilon}} \int_{K_h^z} \left\{ a^{\varepsilon}(x) \left| \nabla w^{\varepsilon} \right|^2 + \lambda \left| w^{\varepsilon} \right|^2 \chi_{F^{(\varepsilon)}}(x) + h^{-2-\gamma} \left| w^{\varepsilon} - 1 \right|^2 \chi_{\Omega^{(\varepsilon)}}(x) \right\} dx.$$

This function is the local quantitative characteristic of the set $F^{(\varepsilon)}$ as an "accumulator" of particles.

3. The generalized model of filtration in an aperiodic medium with double porosity.

Theorem 1. *Let the following conditions be fulfilled*:

(i) *the continuous functions $a_{ij}(x)$; $i, j = 1, 2, 3$ exist such that*

$$\lim_{h \to 0} \underline{\lim_{\varepsilon \to 0}} \frac{a_{ij}(x, \varepsilon, h)}{h^3} = \lim_{h \to 0} \overline{\lim_{\varepsilon \to 0}} \frac{a_{ij}(x, \varepsilon, h)}{h^3} = a_{ij}(x),$$

where the tensor $\{a_{ij}(x)\}_{i, j = 1}^3$ is positive definite for $x \in \Omega$;

(ii) *there exists the continuous function $b_{\lambda}(x)$ such that*

$$\lim_{h \to 0} \underline{\lim_{\varepsilon \to 0}} \frac{b_{ij}(x, \varepsilon, h)}{h^3} = \lim_{h \to 0} \overline{\lim_{\varepsilon \to 0}} \frac{b_{ij}(x, \varepsilon, h)}{h^3} = b_{ij}(x);$$

$b_{\lambda}(x)$ can be analytically extended to the complex plane with a cut $\arg \lambda(x) = \pi$. We admit that the function $b_{\lambda}(x)$ can be presented in the form $b_{\lambda}(x) = b_1(x)\lambda + b_2(x, \lambda)$, where $b_1(x)$ and $b_2(x, \lambda)$ are the nonnegative continuous functions and $b_{\lambda}(x, \lambda) = O(|\lambda|^{\delta})$, $\delta < 1$ as $|\lambda| \longrightarrow \infty$, and $|\arg \lambda - \pi| \geq \theta_0 0$;

(iii) *there exists the continuous function $m(x) > 0$ such that*

$$\lim_{h \to 0} \lim_{\varepsilon \to 0} \frac{\operatorname{mes} \left\lfloor K_h^x \cap \Omega^{(\varepsilon)} \right\rfloor}{h^3} = m(x);$$

(iv) *the functions $f^{\varepsilon}(x)$ and $u_0^{\varepsilon}(x)$ are uniformly limited in $L^2(\Omega)$ with respect to ε. They are zero for $x \in F^{(\varepsilon)}$ and converge in $L^2(\Omega^{(\varepsilon)})$ to the functions $f(x)$ and $u_0(x)$, respectively.*

Then, the solution to problem (1), (2) *converges in* $L^2(\Omega_T^{(\varepsilon)})$, *where* $\Omega_T^{(\varepsilon)} = \Omega^{(\varepsilon)} \times (0, T)$, *to the solution* $u(x, t)$ *of the following problem*:

$$(m(x) + b_1(x))\frac{\partial u}{\partial t} - \sum_{i,j=1}^{3} \frac{\partial}{\partial x_i}\left(a_{ij}(x)\frac{\partial u}{\partial x_j}\right) + \frac{\partial}{\partial t}\int_0^t B(x, t-\tau)u(x, \tau)d\tau = m(x) f(x),$$

$$x \in \Omega, \quad t \in (0, T);$$

$$\frac{\partial u}{\partial \nu_a}(x, t) = 0, \quad x \in \partial\Omega,$$

$$t \in (0, T); \quad u(x, 0) = u_0(x), \quad x \in \Omega,$$

where

$$\frac{\partial}{\partial \nu_a} = \sum_{ij=1}^{3} a_{ij}(x)\cos(\nu, x_i)\frac{\partial}{\partial x_j}.$$

Moreover, $u^\varepsilon(x, t)\chi_{F^{(\varepsilon)}}(x)$ *converges weakly in* $L^2(\Omega_T)$ *to the function*

$$\omega(x, t) = \int_0^t B(x, t-\tau)u(x, \tau)d\tau + b_1(x)u(x, t).$$

The proof of Theorem 1 is based on the Laplacian transformation of problem (1), (2) to the time-independent boundary value problem:

$$-\mathrm{div}(a^\varepsilon(x)\nabla u^\varepsilon) + \lambda u^\varepsilon = g^\varepsilon(x), \quad x \in \Omega;$$
$$\frac{\partial u^\varepsilon}{\partial \nu} = 0, \quad x \in \Omega, \tag{5}$$

where $g^\varepsilon(x) = \lambda^{-1}f^\varepsilon(x) + u_0^\varepsilon(x)$, the functions $a^\varepsilon(x)$, $f^\varepsilon(x)$, and $u_0^\varepsilon(x)$ are defined previously and $\lambda > 0$. It is known that the unique solution to problem (5) exists in the $H^1(\Omega)$ class for an arbitrary $\varepsilon > 0$.

We now consider the time-independent variant of Theorem 1.

Theorem 2. *Let the conditions of Theorem* 1 *be fulfilled. Then, the sequence of the solutions* $\{u^\varepsilon(x)\}$ *to problem* (5) *strictly converges in* $L^2(\Omega^{(\varepsilon)})$ *as* $\varepsilon \longrightarrow 0$ *to the solution* $u(x)$ *of the following boundary value problem*:

$$-\sum_{i,j=1}^{3} \frac{\partial}{\partial x_i}\left(a_{ij}(x)\frac{\partial u}{\partial x_j}\right) + \lambda m(x)u(x) + b_\lambda(x)u(x) = m(x)g(x), \quad x \in \Omega;$$
$$\frac{\partial u}{\partial \nu_a} = 0, \quad x \in \Omega. \tag{6}$$

Here, $g(x) = \lambda^{-1}f(x) + u_0(x)$, *and the functions* $a_{ij}(x)$, $b_\lambda(x)$, $m(x)$, $f(x)$, *and* $u_0(x)$ *are defined in Theorem* 1.

Moreover, the functions $u^\varepsilon(x)\chi_{F^{(\varepsilon)}}(x)$ *weakly converge in* $L^2(\Omega)$ *to the function*

$$\omega_0(x) = \left\{b_1(x) + \frac{b_2(x, \lambda)}{\lambda}\right\}u(x). \tag{7}$$

Theorem 2 is proved by the variational method for $\lambda > 0$. Namely, the "coordinate" functions are obtained, making it possible to construct on this basis an approximation appropriate for solving variational problems.

4. Penetrability of inclusions ~ε^2: A periodic medium. The well-known model with memory, which was derived for the case $a^\varepsilon \sim \varepsilon^2$ for $x \in F^{(\varepsilon)}$ [2, 3], is developed for a disconnected system of blocks. Theorem 1 makes it possible to obtain the generalization of this model for the case of the connected set $F^{(\varepsilon)}$.

Let Ω be a bounded region in $\mathbf{R}^3$, and $F^{(\varepsilon)}$ is a set in Ω. We assume that $F^{(\varepsilon)}$ is the periodic lattice with the period ε, which is composed of cylinders with a radius $r_\varepsilon = r\varepsilon$ ($r < 1/2$). We put $\Omega^{(\varepsilon)} = \Omega\backslash F^{(\varepsilon)}$. In the region Ω, we consider initial boundary value problem (1), (2) for the following definition of $a^\varepsilon(x)$:

$$a^\varepsilon(x) = \begin{cases} a\varepsilon^\theta, & x \in F^{(\varepsilon)} \\ 1, & x \in \Omega^{(\varepsilon)}, \end{cases} \tag{8}$$

where $\theta = 2$.

It is easy to show that conditions (i)–(iii) are fulfilled.

Let Π be a unit cube in $\mathbf{R}^3$: $\Pi = \{x \in \mathbf{R}^3: |x_i| < 1/2\}$, $F \subset \Pi$, $P = \Pi\backslash\bar{F}$.

Using Theorem 1, we conclude that the solutions $\{u^\varepsilon(x, t)\}$ to problem (1), (2), with the coefficient $a^\varepsilon(x)$ defined as (8), converge in $L^2(\Omega_T^{(\varepsilon)})$ to the solution of the following initial boundary value problem:

$$m\frac{\partial u}{\partial t} - \sum_{i,j=1}^{3} a_{ij}\frac{\partial^2 u}{\partial x_i \partial x_j} + \frac{\partial}{\partial t}\int_0^t B(t-\tau)u(x, \tau)d\tau = m f(x),$$
$$(x, t) \in \Omega_T;$$

$$\frac{\partial u}{\partial \nu_a}(x, t) = 0, \quad x \in \partial\Omega, \quad t \in (0, T);$$

$$u(x, 0) = u_0(x), \quad x \in \Omega,$$

where $m = \mathrm{mes}F$, $\{a_{ij}\}_{i,j=1}^3$ are defined as $a_{ij}(x) = \int_P (\nabla u_i, \nabla u_j)dx$, while u_k is the solution to the boundary value problem

$$\Delta u_k = 0, \quad x \in P;$$

$$\frac{\partial u_k}{\partial \nu} = 0, \quad x \in \partial P \backslash \{x: x_k = \pm 1/2\}; \tag{10}$$

$$u_k = (\pm 1/2), \quad x \in \partial P \cap \{x: x_k = \pm 1/2\}.$$

$$B(t) = \frac{1}{2\pi i}\int\limits_{\sigma - i\infty}^{\sigma + i\infty} \frac{b-\lambda}{\lambda} e^{\lambda t} d\lambda \quad (\sigma > 0), \tag{11}$$

$$b_\lambda = \lambda \int\limits_F w(x)dx.$$

The function $w(x)$ is the solution to the boundary value problem

$$a\Delta w - \lambda w = 0, \quad x \in F;$$

$$\frac{\partial w}{\partial \nu}(x) = 0, \ x \in \partial F \cap \{x: x_k = \pm 1/2, k = 1, 2, 3\}; \tag{12}$$

$$w(x) = 1, \ x \in \partial F \backslash \{x: x_k = \pm 1/2, k = 1, 2, 3\}.$$

It is known that a unique solution $w(x, \lambda)$ to problem (12) exists for $\lambda \in \mathbf{C}\backslash\{\lambda: \arg\lambda = \pi\}$, $w(x, \lambda)$ being the analytical function in the λ-complex plane. Therefore, representation (11) for the function $b_\lambda(x)$ is true for an arbitrary $\lambda \in \mathbf{C}\backslash\{\lambda: \arg\lambda = \pi\}$.

The sequence of the functions $\{u^\varepsilon(x, t)\chi_{F^{(\varepsilon)}}(x)\}$ weakly converges in $L^2(\Omega_T)$:

$$\omega(x, t) = \int\limits_0^t B(t-\tau)u(x, \tau)d\tau.$$

5. Penetrability of inclusions higher than ε^2: A periodic medium. For simplicity, we consider the case of a disconnected set of blocks, for example, in the form of a periodic system of balls. Let Ω be a bounded region in $\mathbf{R}^3$, and $F^{(\varepsilon)}$ be the $F_\alpha^{(\varepsilon)}$ set of balls disposed periodically along the coordinate axes with the period ε. We assume that $\Omega^{(\varepsilon)} = \Omega \backslash F^{(\varepsilon)}$. In the region Ω, we consider initial boundary value problem (1), (2), in which $a^\varepsilon(x)$ is defined as (8) for $0 < \theta < 2$. In this case, $b_\lambda(x) = b_\lambda = \lambda(1-m)$, where $m = \mathrm{mes}\Pi\backslash F$, by virtue of which the kernel $B(x, t)$ turns out to be constant.

From Theorem 1, it follows that the solutions $\{u^\varepsilon(x, t)\}$ to problem (1), (2) converge in $L^2(\Omega^{(\varepsilon)})$ to the solution of the following initial boundary value problem:

$$\frac{\partial u}{\partial t} - \beta\Delta u = m f(x), \quad (x, t) \in \Omega_T;$$

$$\frac{\partial u}{\partial \nu}, \ x \in \partial\Omega, \ t \in (0, T); \ u(x, 0) = u_0(x), \ x \in \Omega,$$

where $\beta = \|\nabla \nu_1\|_p^2$ for $\nu_1(x)$, which is the solution to problem (10).

The sequence $\{u^\varepsilon(x, t)\chi_{F^{(\varepsilon)}}(x)\}$ converges weakly in $L^2(\Omega_T)$ to the function $(1-m)u(x, t)$.

6. Penetrability of inclusions smaller than ε^2: A periodic medium. Let Ω, $F^{(\varepsilon)}$, and $\Omega^{(\varepsilon)}$ be the sets defined in Section 4. We consider initial boundary value problem (1), (2), where $a^\varepsilon(x)$ is defined as (8) for $\theta > 2$. In this case, $b_\lambda(z, \varepsilon, h) = O(\varepsilon^{\theta/2+1})$ as $\varepsilon \longrightarrow 0$. This implies that $b_\lambda(x) = 0$.

According to Theorem 1, we find that the solutions $\{u^\varepsilon(x, t)\}$ to problems (1), (2), for $\theta > 2$ converge in $L^2(\Omega_T^{(\varepsilon)})$ to the solution of the following initial boundary value problem:

$$m\frac{\partial u}{\partial t} - \beta\Delta u = mf, \ (x, t) \in \Omega_T;$$

$$\frac{\partial u}{\partial \nu} = 0, \ x \in \partial\Omega, \ t \in (0, T);$$

$$u(x, 0) = u_0(x), \ x \in \Omega.$$

Here, $m = \mathrm{mes}F$, $\beta = \|\nabla \nu_1\|_P^2$, and the function $\nu_1(x)$ is the solution to problem (10).

The sequence $\{u^\varepsilon(x, t)\chi_{F^{(\varepsilon)}}(x)\}$ weakly converges to zero in $L^2(\Omega_T)$.

ACKNOWLEDGMENTS

This work was supported by the Russian Foundation for Basic Research, project no. 98-01-00460.

REFERENCES

1. G. I. Barenblatt, Yu. P. Zheltov, and I. N. Kochina, Prikl. Mat. Mekh. **24**, 852 (1960).
2. T. Arbogast, J. Douglas, and U. Hornung, SIAM J. Appl. Math. **21**, 823 (1990).
3. M. B. Panfilov, Dokl. Akad. Nauk SSSR **311**, 313 (1990) [Sov. Phys. Dokl. **35**, 225 (1990)].
4. M. B. Panfilov and I. V. Panfilova, *Averaged Models of Filtration Processes for Inhomogeneous Internal Medium* (Nauka, Moscow, 1996).
5. E. Ya. Khruslov, Usp. Mat. Nauk **45**, 197 (1990).
6. A. Bourgeat and L. S. Pankratov, Appl. Anal. **64**, 303 (1997).
7. M. V. Goncharenko and L. V. Berlyand, Teor. Funk., Funk. Analiz. Prilozh. (Kharkov) **52**, 112 (1989).
8. E. Ya. Khruslov, *Theory of Operators in Functional Spaces and Its Applications* (Naukova Dumka, Kiev, 1981), pp. 129–173.
9. L. S. Pankratov and E. Ya. Khruslov, in *Advances in Soviet Mathematics*, Vol. 19: *Spectral Operator Theory and Related Topics* (Am. Math. Soc., Providence, Rhode Island, 1994), pp. 233–268.

Translated by V. Bukhanov